Development of SNAP tag and horseradish peroxidase-based nanobodies as secondary antibody mimics for indirect immunoassays

Inauguraldissertation
eingereicht im Fachbereich Medizin
in Erfüllung der Anforderungen
zur Erlangung des akademischen Grades eines Ph.D.
der Fachbereiche Veterinärmedizin und Medizin
der Justus-Liebig-Universität Gießen

vorgelegt von Wenjie Sheng
aus Hubei, China

Gießen 2025

Aus dem Fachbereich Medizin der Justus-Liebig-Universität Gießen

Zentrum für Frauenheilkunde und Geburtsmedizin

Molekulare Gynäkologie

1. Gutachter und Mitglied der Prüfungskommission:

   Prof. Dr. med. Ivo Meinhold Heerlein

2. Gutachter und Mitglied der Prüfungskommission:

   Prof. Dr. med. Holger Bronger

3. Gutachter und Mitglied der Prüfungskommission:

   Prof. Dr. rer. nat. Franco Harald Falcone

4. Gutachter und Mitglied der Prüfungskommission:

   Prof. Dr. Ross Douglas

Tag der Disputation:
19.01.2026

Abstract

Immunoassays are widely used in diagnosis and biomedical research for the detecting and quantifying specific biomolecules. Based on antigen-antibody interaction system, immunoassays enable the localization, qualitative analysis and quantification of target proteins. Among these, indirect immunoassays offer enhanced signal amplification and flexibility by using fluorescence-conjugated secondary antibodies. However, conventional secondary antibodies, predominantly immunoglobulin (IgG), present challenges due to their large size (150 kDa). Moreover, most animal-derived antibodies raise ethical concerns and exhibit batch-to batch variability. In contrast, small antibody fragments such as nanobodies (Nbs), which are derived from camelids and consist of only a single variable domain, are significantly smaller size (15 kDa) and can be efficiently produced using mammalian cell expression system. In this study, five previously established anti-mouse and anti-rabbit IgG secondary Nbs were selected and incorporated with a self-labeling SNAP-tag. The SNAP-tag (20 kDa) catalyzes the covalent, site-specific attachment of O6-benzylguanine (BG)-modified fluorophores to recombinant Nbs anti-IgG-SNAP proteins. These Nbs anti-IgG-SNAP were expressed in HEK293T cells. Following a rapid and straightforward conjugation protocol involving the SNAP-tag and BG-modified Alexa Fluor dyes, the specific detection capability of Nbs anti-IgG-SNAP for mouse- or rabbit-derived primary antibodies was validated using flow cytometry and multi-color fluorescence microscopy. Additionally, these secondary nanobodies were further developed to be combined with horseradish peroxidase (HRP) and the recombinant Nbs anti-IgG-HRP proteins were expressed in HEK293T cells. Their functionality was validated as secondary antibodies in Western blot (WB) and tyramide signal amplification (TSA)-based multiplex immunofluorescence (mIF) assays. The results demonstrated that Nbs anti-IgG-SNAP and Nbs anti-IgG-HRP specifically bound to mouse or rabbit antibodies, exhibiting fluorescence intensities, quantitative validity and specificity comparable to conventional anti-mouse or anti-rabbit secondary antibodies. Moreover, their cost-effectiveness, scalable expression, easy of purification and simple site-specific conjugation procedures present an innovation alternative to traditional animal-derived antibody production, ensuring greater standardization and reproducibility in research applications. Taking together, these findings suggest that recombinant anti-mouse and anti-rabbit IgG secondary nanobodies present a promising and

reliable alternative to traditional secondary antibodies in various indirect immunoassays.

Zusammenfassung

Der Einsatz von Immunoassays ist in der Diagnostik und der biomedizinischen Forschung weit verbreitet, um spezifische Biomoleküle zu detektieren und zu quantifizieren. Auf der Grundlage des Antigen-Antikörper-Interaktionssystems ermöglichen Immunoassays die Lokalisierung, qualitative Analyse und Quantifizierung von Zielproteinen. Darunter bieten indirekte Immunoassays durch die Verwendung von fluoreszenzmarkierten Sekundärantikörpern eine verbesserte Signalverstärkung und Flexibilität. Dennoch stellen herkömmliche Sekundärantikörper, hauptsächlich Immunglobuline (IgG), aufgrund ihrer Größe (150 kDa) Herausforderungen dar. Darüber hinaus werfen die meisten tierabgeleiteten Antikörper ethische Bedenken auf und weisen Chargenunterschiede auf. Im Gegensatz dazu sind kleine Antikörperfragmente wie Nanobodies (Nbs), die von Kameliden stammen und nur aus einer einzigen variablen Domäne bestehen, deutlich kleiner (15 kDa) und können mithilfe eines Säugerzell-Expressionssystems effizient hergestellt werden. In dieser Studie wurden fünf zuvor etablierte sekundäre Nanobodies (Nbs) gegen Maus- und Kaninchen-IgG ausgewählt und mit einem selbstmarkierenden Tag, dem SNAP-Tag, kombiniert. Der SNAP-Tag (20 kDa) katalysiert die kovalente, ortspezifische Anbindung von O6-Benzylguanin (BG)-modifizierten Fluorophoren an rekombinante anti-IgG-SNAP-Proteine auf Basis von Nbs. Diese anti-IgG-SNAP-Nanobodies wurden in HEK293T-Zellen exprimiert. Nach einem schnellen und einfachen Konjugationsprotokoll, das SNAP-Tag und BG-modifizierte Alexa Fluor-Färbemittel umfasst, wurde die spezifische Nachweisfähigkeit der anti-IgG-SNAP-Nanobodies für primäre Antikörper, die von Mäusen oder Kaninchen stammen, mittels Durchflusszytometrie und mehrfarbiger Fluoreszenzmikroskopie validiert. Zusätzlich wurden diese sekundären Nanobodies weiter entwickelt, um sie mit Hefe-Rettich-Peroxidase (HRP) zu kombinieren, und die rekombinanten anti-IgG-HRP-Proteine auf Basis von Nbs wurden in HEK293T-Zellen exprimiert. Ihre Funktionsfähigkeit als Sekundärantikörper in Western Blot (WB)- und auf Tyramid-Signalverstärkung (TSA) basierenden Multiplex-Immunfluoreszenz (mIF)-Assays wurde validiert. Die Ergebnisse haben gezeigt, dass die anti-IgG-SNAP-Nanobodies und die anti-IgG-HRP-Nanobodies spezifisch an Maus- oder Kaninchenantikörpern binden und Fluoreszenzintensitäten, quantitative Zuverlässigkeit und Spezifität aufweisen, die mit denen herkömmlicher anti-Maus- oder anti-Kaninchen-Sekundärantikörper vergleichbar sind. Darüber

hinaus bieten ihre Kosteneffizienz, die skalierbare Expression, die einfache Reinigung und die einfachen ortspezifischen Konjugationsverfahren eine innovative Alternative zur Herstellung herkömmlicher tierabgeleiteter Antikörper und gewährleisten eine höhere Standardisierung und Reproduzierbarkeit in Forschungsszenarien. Zusammenfassen belegen die Ergebnisse, dass rekombinante sekundäre Nanobodies gegen Maus- und Kaninchen-IgG in verschiedenen indirekten Immunoassays eine vielversprechende und zuverlässige Alternative zu herkömmlichen Sekundärantikörpern darstellen.

Contents

1. Introduction

1.1 Immunoassays

Immunoassay is a method for quantifying analytes based on the reaction between antibodies and antigens (analytes). Since its introduction in the 1960s [1, 2], immunoassay technology has become widely used in drug discovery, clinical diagnosis, food safety, and environmental monitoring [3-6]. Common types of immunoassays include Western blotting (WB), enzyme-linked immunosorbent assay (ELISA), immunofluorescence (IF), immunocytochemistry (ICC), immunohistochemistry (IHC) and immunoprecipitation (IP) (**Table 1.1**).

Table 1.1 Comparison of different immunoassays

Immunoassay	Labels	Advantages	Disadvantages	Reference
ELISA	Enzyme-linked antibodies	high sensitivity and efficiency, easy to perform, low cost.	high cost for sample preparation, high occurrence of false positives or negatives, high storage requirement of antibody.	[7]
WB	Enzyme- or fluorophore-linked antibodies	analysis with colorimetric, chemiluminescent or fluorescent detection, The ability to detect picogram levels of protein.	time-consumption; reproductivity problem, measurement of relative concentrations of proteins.	[8]

IF	Fluorescence probes labeled antibodies	visualization of proteins on cells, tissue or entire organisms, a variety of fluorophores available.	low stain intensity in direct method, high background for indirect method.	[9]
ICC/IHC	Enzyme-link antibodies	long-term storage of samples, the preservation for morphology and structures of samples, various tissues and cells can be prepared for detection.	time-consumption, the quality of sample for ICC is unstable; the activity of endogenous peroxidase and alkaline phosphatase contributes to the high background, some carcinogenic effects for IHC.	[10, 11]
IP	No requirement for labeled antibodies	native antigens can be applied for detection, high concentrated ability.	radiolabeled proteins should be prepared to enhance their detection.	[12]

In immunoassays, a variety of labels, such as enzymes, fluorescence dyes, tags, and radiation, are employed [13-16]. Based on labeling primary or secondary antibody, immunoassays can be classified into two types: direct and indirect methods (**Figure 1.1**). A direct immunoassay is a one-step detection method that uses a labeled primary antibody that specifically detects the target molecule and its epitope. In contrast, an indirect immunoassay is a two-step method, in which the detection system consists of a primary antibody and a labeled secondary antibody. Unlike the direct method, the primary antibody in the indirect method is unconjugated, while the labeled secondary antibody binds specifically to the primary antibody, using it as a bridge to detect the target molecule. Compared to the direct method, an indirect immunoassay can use a single labeled secondary antibody to detect various primary antibodies derived from the same species (**Table 1.2**). For example, if the primary antibodies are generated in mice, a single labeled anti-mouse secondary antibody is sufficient to detect all mouse-derived primary

antibodies. Therefore, the indirect method offers a flexible staining strategy and significantly reduces costs. Moreover, it provides a strong signal due to its signal amplification system.

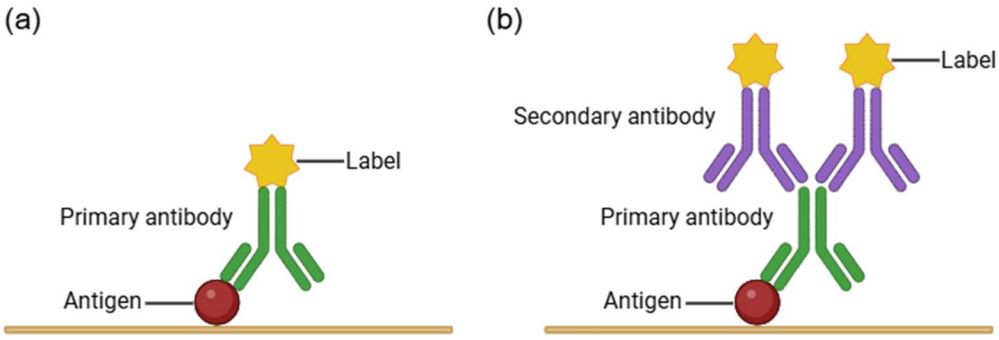

Figure 1.1 Schematic diagram of immunoassays. (a) Direct immunoassays. (b) Indirect immunoassays. Created in https://BioRender.com.

Table 1.2 Comparison of direct and indirect immunoassays

	Direct	**Indirect**
Antibody conjugation method	Primary antibody conjugated with a label	Secondary antibody conjugated with a label
The number of antibodies used	one	two
Time	Processing time is shorter because of only one incubation step.	An extra incubation and washing steps are required to use secondary antibody.
Flexibility	Conjugated primary antibody limits the flexibility.	One conjugated secondary antibody could bind to several primary antibodies from same species and isotypes.
Sensitivity	The signal from direct method is relatively weak.	Several secondary antibodies bind to individual primary antibody, leading to signal amplification.
Cost	Each target antigen needs labeled primary antibody to be detected, this increases the assay cost.	Less secondary antibodies are needed to detect a wide range of antigens through using unlabeled

primary antibodies. This reduces the assay cost.

1.2 Antibodies

Antibodies are secreted by plasma cells in response to foreign invaders or antigens, which stimulate the immune system. These antibodies subsequently activate immune responses. There are five immunoglobulin isotypes of antibodies in the blood or serum: IgG, IgM, IgE, IgA, IgD. As the most abundant immunoglobulin in the blood, IgG accounts for 70-75% of human immunoglobulins. Herein, this project mainly focuses on working with the IgG, and the term "antibody" refers to IgG.

While certain IgG subclasses, such as IgG4, can undergo Fab-arm exchange (FAE) resulting in bispecific antibody structures, IgG is generally composed of two identical heavy chains and two identical light chains linked by disulfide bonds. Additionally, disulfide bonds connect the two heavy chains (**Figure 1.2a**). The molecular weight (MW) of each heavy chain is 50 kDa, while the light chain MW is 25 kDa. Due to its symmetric structure, the MW of IgG is approximately 150 kDa. Furthermore, antibodies possess two types of light chains, lambda (λ) and kappa (κ) chains. Immunoglobulins can have either λ chains or κ chains, with a typical κ to λ chain ratio of 2:1 in humans. The analysis of the amino acid sequences of heavy and light chains reveals that the first 110 amino acids in the N-terminal domain have high variability and are therefore termed the variable region. In contrast, the remaining sequences toward the C-terminal domain are relatively conserved and are referred to as the constant region. The heavy chain consists of four domains, including one variable heavy chain domain (VH) and three constant domains (CH1, CH2 and CH3). The light chain contains two domains: one variable light chain domain (VL) and one constant light chain domain (CL). Upon digestion with the protease papain, the IgG is cleaved into three fragments. Two identical fragments, known as "fragment of antigen binding" (Fab), each consist of a complete light chain paired with the VH and CH1 domains of the heavy chain, therefore retaining the ability to bind antigen. The third fragment, called "fragment crystallizable" (Fc), contains the paired CH2 and CH3 domains of the heavy chains. While the Fc lacks antigen-binding sites, it interacts with effector molecules and immune cells, mediating the functional

diversity of different heavy chain isotypes. Within the variable region, six complementarity-determining regions (CDRs) form the antigen-binding sites of conventional IgG molecules. Typically, three CDRs (CDR1, CDR2 and CDR3) from the VH domain and three from the VL domain form a paratope that specifically recognizes the epitope on the antigen [17]. CDR3 is more variable than other CDRs, making it extremely difficult to predict the structure of the CDRs [18]. The CDRs are surrounded by frame regions (FRs), which are relatively conserved and include four FRs (FR1, FR2, FR3, and FR4) in either VH or VL domains.

As described before, primary and secondary antibodies are essential components of indirect immunoassays and are generally full-length IgG molecules. The identification of primary antibodies typically requires the use of animal species such as mice, rabbits, goats, rats, or chickens and involves several key steps, including immunogen preparation, animal immunization, hybridoma generation, antibody collection, screening and purification. There are two main types of primary antibodies: monoclonal antibodies (mAbs) and polyclonal antibodies (pAbs). The mAbs are derived from a single clone of B cells and therefore consist of an identical IgG that recognizes a single specific epitope. In contrast, pAbs are derived from multiple clones of B cells, resulting in a heterologous mixture of IgGs that bind to different epitopes on the same antigen. The mAbs are commonly produced in mice and, less frequently in rabbits or rats. The pAbs, however, are almost exclusively raised in rabbits. Given the widespread use of mice and rabbits as host species for primary antibody production, secondary antibodies that specifically recognize mouse and rabbit IgGs—such as anti-mouse IgG and anti-rabbit IgG—are in high demand. These secondary antibodies are typically produced in other species, including goats, chickens and donkeys [19].

The key principle of selecting an appropriate secondary antibody is that it must specifically react with the host species of the primary antibodies. For example, if the primary antibody is generated in mice, an anti-mouse IgG is required; if produced in rabbits, an anti-rabbit IgG should be used. However, the production of these secondary antibodies often involves sacrificing large numbers of animals, raising animal welfare and ethical concerns. Additionally, most secondary antibodies are polyclonal, which can result in batch-to-batch variability, followed by irreproducible experimental results, which cannot be overlooked [20, 21]. Another critical aspect of indirect immunoassays is that secondary antibodies

must be pre-labeled with other molecules, such as enzymes (e.g., alkaline phosphatase or HRP), fluorescence dyes, or biotin. Commercially available labeled secondary antibodies are typically conjugated with approximately five fluorophore molecules to enhance signal detection. However, while this multi-labeling approach increases sensitivity and facilitates the detection of low-abundance targets, it may also introduce measurement errors in quantifying protein expression. Furthermore, fluorophores are conventionally conjugated to secondary antibodies via random-conjugation methods [22]. These methods yield heterogeneous products, consisting of a mixture in which fluorophores are attached to different sites and numbers. This variability leads to a broad range of antibody-to fluorophore-molar ratios, resulting in inconsistent detection properties and compromised assay performance.

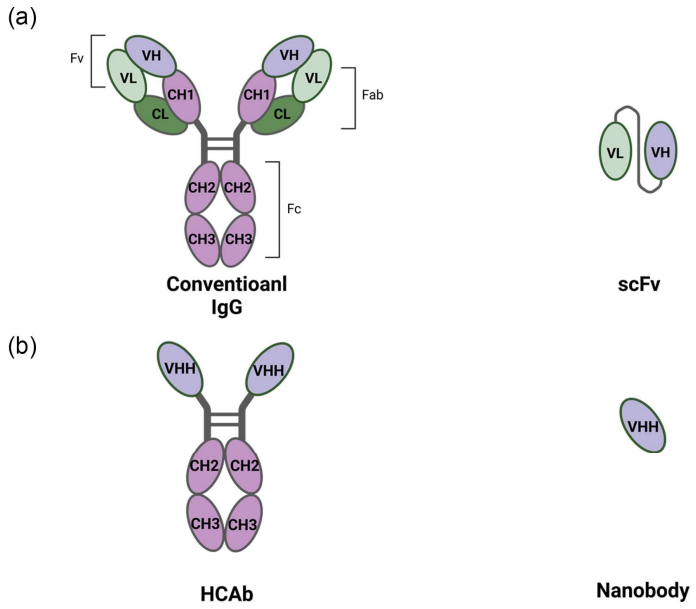

Figure 1.2 Structures of antibodies. (a) The structures of human IgG and scFv. (b) The structures of camelid antibody and nanobody. VH: variable heavy chain; VL: variable light chain; CH: constant heavy chain; CL: constant light chain; VHH: variable of a single heavy-chain; HCAb: heavy chain antibody; Fab: fragment of antigen binding; Fv: variable fragment; Fc: fragment crystallizable; scFv: single-chain variable fragment. Created in https://BioRender.com.

1.3 Small fragment antibodies

IgGs (150 kDa) can be efficiently in mammalian systems, however, their large size and complex quaternary structure can hinder modifications needed, particularly when site-specific or labeling are

required, thereby limiting their application in laboratory diagnostics [23]. Furthermore, the lack of rigorous validation for some commercial mAbs and pAbs can contribute to inconsistent data and poor reproducible experimental results [24]. To address these limitations, smaller fragment antibodies—such as Fab and scFv—have been developed. These fragments can be generated either by enzymatic cleavage of full-length antibodies using proteases like papain or pepsin [25], or through recombinant engineering to produce formats such as Fab, variable fragment (Fv) and single-chain variable fragment (scFv). Among these, scFv is one of the most widely used recombinant antibody formats in immunoassays due to its ease of construction, stable expression and high affinity for target antigens [26]. As shown in **Figure 1.2a**, scFv consists of a VH and a VL linked by a flexible peptide linker, and this linker can be engineered to enhance the stability and affinity of the scFv [27]. With a small molecular weight of approximately 25 kDa and retain the antigen-binding properties of natural antibody. Several studies have reported the successful generation of scFv from various species, including mice, rabbits and chickens, indicating that scFvs are a viable alternative to full-length antibodies [28-30]. Moreover, scFv can be cloned and expressed in bacterial or mammalian expression systems [31, 32], enabling high-yield and cost-effective production.

However, several challenges remain in the use of scFv in immunoassay, including limitations in stability, solubility, thermostability, antigen-binding ability and potential immunogenicity [33, 34]. To overcome these challenges, a natural antibody called the heavy-chain antibody (HCAb) has been explored in camelids in the last decades.

1.4 Nanobody

In 1993, Hamers-Casterman and colleagues first described a natural antibody that was found in serum of camelids [35]. This novel antibody, known as HCAb, is only composed of CH2, CH3 and a variable heavy chain (VHH), lacking both light chains and CH1. As a result, HCAb is smaller (~90 kDa) than the conventional full-length antibody (~150 kDa) (**Figure 1.2b**). HCAbs are naturally found in members of the *Camelidae* family, including camels (*Camelus dromedarius* and *Camelus bactrianus*), llamas (*Lama glama* and *Lama guanicoe*) and vicugnas (*Vicugna vicugna* and *Vicugna pacos*). Similarly, another class of light chain-lacking antibodies immunoglobulin new antigen receptors

(IgNARs), were later discovered in sharks such as *Ginglymostoma cirratum* [36-38]. Due to this unique structure, VHH from HCAbs exhibit minimal interaction with constant domains, distinguishing them structurally and functionally from conventional antibodies [39]. These specific VHH domains have been harnessed to develop a class of recombinant antibody fragments known as nanobodies (Nbs) [40].

1.4.1 Structural hallmarks of nanobodies

Compared with the MW of the camelid HCAbs (~90 kDa), Nbs, which are derived from the VHH of HCAbs, are much smaller, with a MW of about 15 kDa and dimensions of approximately 2.5 × 4.0 nm, making them the smallest intact antigen-binding fragment (**Figure 1.2b**) [41]. Like conventional VH domains, the folded VHH structure is composed of nine β-strands, arranged into two β-sheet—one with four-stranded and the other with five. While VHHs share this overall framework, they exhibit distinct differences from conventional VH domains due to specific amino acid substitutions in the FRs and structural adaptations that compensate for the absence of the light chain. [36].

One key structural hallmark is observed the FR2 region. In conventional VH domains, FR2 contains highly conserved hydrophobic residues (Val47, Gly49, Leu50, Trp52) that facilitate interaction with the VL domain. In contrast, Nb features smaller and/or more hydrophilic residues at these positions—typically Tyr or Phe37, Glu44, Arg or Cys45, and Gly47—due to the absence of a light chain in VHH. This substitution enhances the solubility of nanobodies [42]. A second hallmark is observed in the CDRs. While conventional antibodies rely on VH paired with the VL, which require six CDRs to achieve complete antigen binding, Nbs utilize only three CDRs from the VHH domain [43]. Although this could suggest a reduced binding capacity, Nbs compensate through structural adaptations. Their CDRs form an expanded paratope with an antigen-interacting surface area of 600–800Å^2. Structural studies revealed that CDR1 and CDR2 in Nbs deviate from the canonical structures seen in conventional antibodies [44, 45]. Additionally, the long CDR3 loop plays a dominant role in specificity, and antigen recognition, contributing approximately 46% of the antigen-contacting residues in the Nb (**Figure 1.3**) [46].

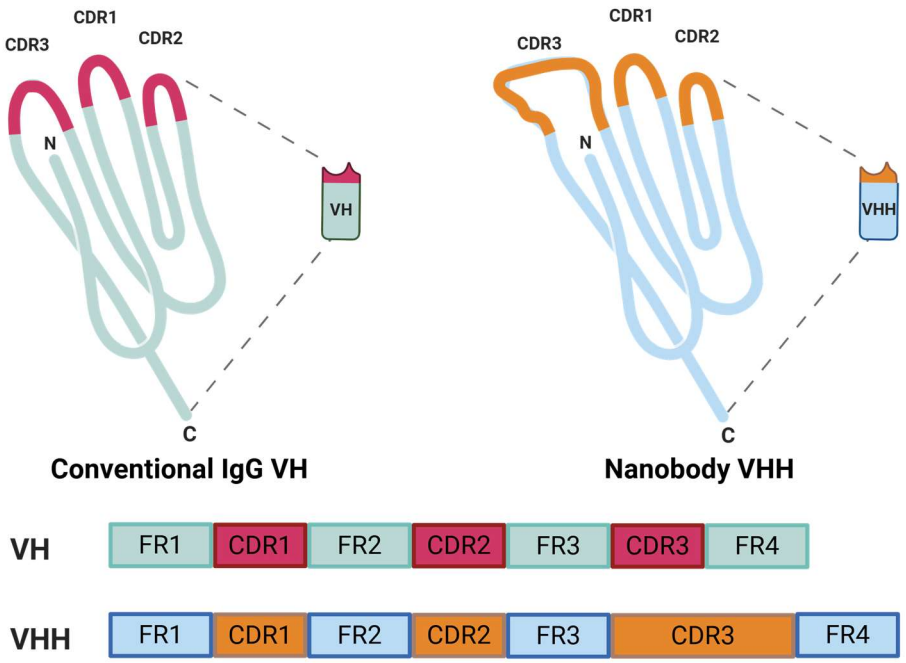

Figure 1.3 Structural differences between conventional IgG VH domain and nanobody VHH domain. The three complementarity-determining regions (CDRs) of the antigen-binding paratope are indicated red and orange respectively. The CDR3 of nanobody VHH is typically much longer than that of conventional IgG VH. Created in https://BioRender.com.

1.4.2 Advantages of nanobodies in immunoassays

Benefiting from their unique structures, Nbs offer significant advantages over conventional antibodies. As the smallest natural antigen-binding fragments, Nbs can achieve equilibrium dissociation constants in the nano- to picomolar range. While conventional IgGs also develop high affinity through affinity maturation [47], Nbs often exhibit comparable binding ability despite their simpler structure. Their longer CDR3 loops and dense framework enable access to concave epitopes that may be inaccessible to full-sized antibodies [36, 48]. In addition, their smaller size allows for superior tissue penetration, which facilitates the development Nb conjugates for both diagnostic and therapeutic purposes [49].

Beyond size, Nbs possess outstanding biochemical properties. As mentioned above, their high solubility arises from hydrophilic residues in FR2, which lacks the hydrophobic interface typically used for paring with VL domains. In addition FR3 contains charged residues that further enhance solubility [50]. These hydrophilic residues contribute to the remarkable thermal and chemical stability of Nbs, making them resistant to denaturants by extreme temperature, acidic, pH conditions, proteases

or ionic strength chemical agents [51] [52]. The presence of additional disulfide bonds within the VHH domain further reinforces their thermal and conformational stability with minimal impact on antigen binding affinity [51, 53]. Notably, Nbs also exhibit low immunogenicity, attributed to their high sequence homology with human VH domains and their robust structural stability [54, 55]. This low immunogenic potential has encouraged the development of Nbs in clinical settings, such as the therapeutic applications for solid tumors or *in vivo* diagnostics [56, 57]. To further minimize immunogenic responses in human therapy, strategies have been developed to humanize camelid Nbs by modifying key residues while preserving antigen-binding capabilities [58].

1.4.3 Nanobody generation

For Nb generation, selecting the most suitable method is one of the main challenges. There are three commonly used approaches for screening antigen-specific Nbs: immune, naïve and synthetic libraries (**Figure 1.4**). A comprehensive guide published in 2021 offered detailed recommendations for Nbs generation and design across various applications [59]. The immune library approach involves immunizing camelids, such as Bactrian camels, dromedaries, llamas or alpacas. This process typically requires two months and involves four to eight rounds of antigen injections. Soluble recombinant proteins are considered ideal for immunization, although DNA vaccines can also be employed [60, 61]. In cases where camelid antigens are difficult to obtain, transgenic mice engineered to produce heavy-chain-only antibodies can serve as a viable alternative [62, 63]. Following immunization, lymphocytes are isolated from the blood. Their mRNA is extracted and reversed-transcribed into complementary DNA (cDNA). Subsequently, a two-step polymerase chain reaction (PCR) is performed to amplify the VHH gene regions. Finally, the PCR products are digested, ligated and typically transformed in *Escherichia coli*. A high-quality immune library should contain more than 10^7 individual transformants [59].

Once the Nbs library has been established, antigen-specific Nbs are selected and retrieved using various screening methods [64]. The most established and widely used method is phage display technology [65, 66], wherein library DNA with M13 bacteriophages that express Nb-encoding sequences on their surface. These phage particles are then incubated with immobilized antigens and

washed to remove excess or unbound phage particles. Bound phages are eluted, typically with a low-pH buffer, and used to infect new bacteria. Through multiple iterative rounds of binding and enrichment, high affinity candidates are identified, often using ELISA [67]. To obtain the highest affinity binders and remove the weakest binders, surface plasmon resonance (SPR) or biolayer interferometry can be employed. Using a SPR, the k_{off} (disassociation rate) value of nanobody with an immobilized antigen can be measured. Due to a k_{on} of the bound Nb (10^5 – 10^6 $M^{-1}s^{-1}$), the Nb candidates with a k_{off} rate of 10^{-3} s^{-1} are classified as a low-binding affinity event [59]. Additionally, a novel technology called NestLink, which bypasses the need for handling individual clones, has been developed to enable the direct selection of binders with desired characteristics in tissues and living organisms [68].

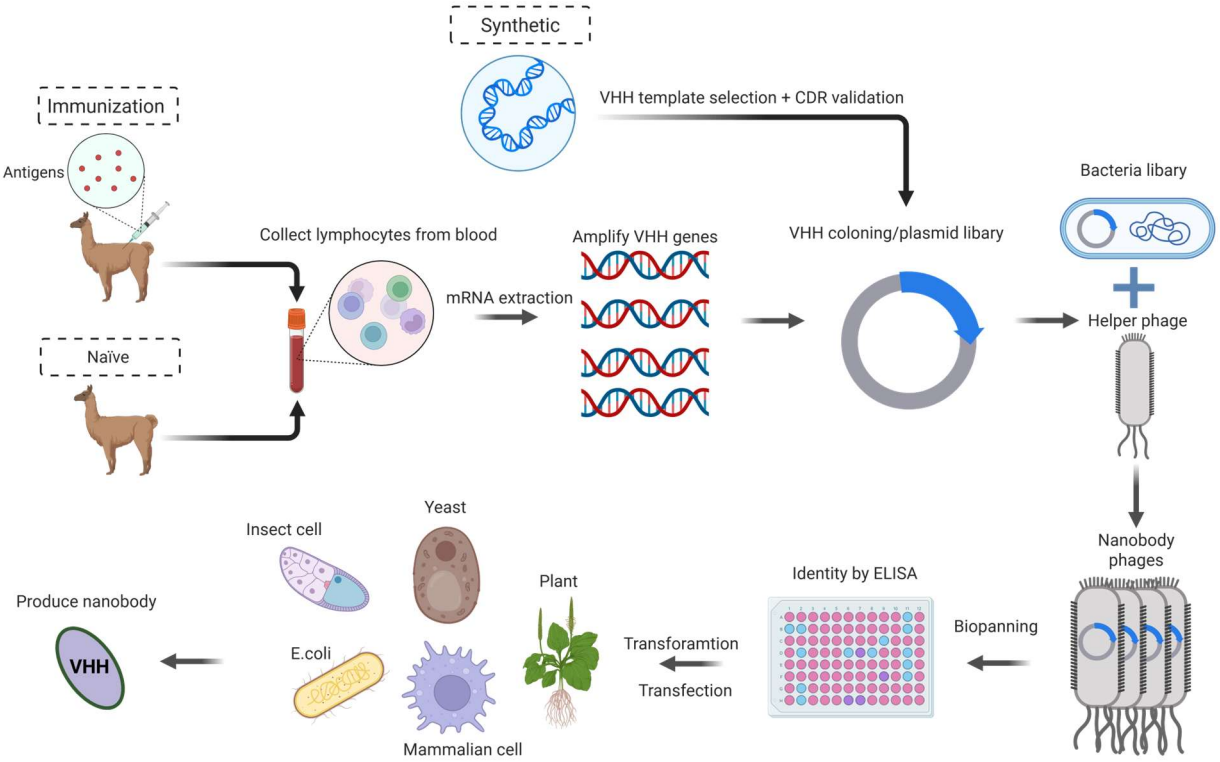

Figure 1.4 The process of nanobody generation. A schematic diagram of three common approaches including immune, naïve and synthetic libraries. Created in https://BioRender.com.

1.4.4 Nanobody expression and purification

Nbs, or recombinant Nbs, can be successfully expressed in a variety of expression systems such as bacteria, yeast, insect cells, mammalian cell lines and plants [69, 70]. Among these, bacteria are the most popular expression systems due to their ease of use, cost-effectiveness and rapid growth.

However, the yield of functional Nbs can be sometimes suboptimal, even when using oxidizing strains to design to enhance proper disulfide bond formation. Yeast, such as *Pichia pastoris*, is a powerful alternative, capable of producing high level of soluble, and correctly folded Nbs. However, yeast N-glycosylation, particularly the presence of high mannose glycans can lead to immunogenicity concerns, which may limit their suitability for therapeutic applications. Plants are also good hosts for protein expression due to some advantages such as simple genetic transformation, scalability, safety, and ability to perform post-translational modifications (PTMs). A unique feature of plant expression is that antibodies can be delivered orally when expressed in *Arabidopsis thaliana* seeds [71]. However, instability of the transgene in chloroplast stroma may lead to failed Nbs production [72]. Insect cell expression systems can produce proteins efficiently while maintaining biosafety standards. They offer a relatively low-cost and simplified process for producing functional Nbs, particularly when using baculovirus-based system. To date, mammalian cell expression remains the most effective method for producing therapeutic antibodies, including Nbs. Their ability to carry out precise and complex PTMs makes them especially suitable for recombinant proteins expression [73]. Currently, Chinese hamster ovary (CHO) cells, human embryonic kidney (HEK) 293 cells, and mouse B cells are the most commonly applied for Nbs production [61, 74, 75].

The most used method for purifying nanobody proteins involves incorporating a 6×histidine (His) tag, which enables efficient purification via immobilized metal affinity chromatography (IMAC). In this technique, the His-tag binds specifically to immobilized metal such as nickel or cobalt on the solid support, facilitating selective enrichment of the target protein with high efficiency and yield [76]. To achieve higher levels of purity, size-exclusion chromatography is often employed as a secondary purification step [77]. On the other hand, Nbs without a tag can be effectively purified using alternative methods. These include protein A chromatography, which utilizes specific Fc binding, or ion exchange chromatography, which separates proteins based on their charge properties [78, 79]. These methods provide flexibility in purification strategies, depending on the Nb's expression format and intended application.

1.5 Methods for conjugating fluorescence dyes to Nbs

Fluorescent proteins (FPs), derived from the green fluorescent protein (GFP) family, are a widely used method for biological imaging. FPs can be genetically fused to a protein of interest (POI), allowing researchers to visually monitor the localization and biochemical activities in living cells and tissues [80-82]. Although newer-generation FPs, such as mScarlet, offers enhanced brightness and photostability compared to earlier variants [83], small organic dyes still provide significant advantages for high-performance imaging applications. These dyes are typically much smaller in size (~1kDa vs. ~25kDa for FPs) which minimize steric hindrance and reduce the possibility of interfering with the native structure or function of the target protein [84]. In contrast, the relatively large size of FPs can disrupt protein folding, localization or interaction dynamics, especially when they are performed in sensitive systems. For example, studies have shown that FPs can significantly change protein oligomerization and activity[85]. Moreover, small organic dyes exhibit higher quantum yields, sharper spectral definition and improved photostability under imaging conditions. These characteristics make them particularly suitable for advanced imaging techniques requiring high resolution, multiplexing or long-term fluorescence stability [86-88]. To address these limitations, various methods have been developed to conjugate fluorescence dyes to antibodies. These methods include N-hydroxysuccinimide (NHS) ester-mediated conjugation [89] [90], which involves the reaction with primary amines, predominantly located on the lysine residues within antibody structures; maleimide-thiol conjugation, which targets thiol groups on cysteine residues using maleimide-activated dyes [91]; click chemistry, which employs biorthogonal reactions such as azide-alkyne cycloaddition to conjugate fluorescent probes to antibodies [92]; affinity-based labeling, which relies on high-affinity interactions—such as biotin-streptavidin or Protein A/G—to non-covalently link fluorescent tags to antibodies [93, 94]; and enzymatic labeling, which uses enzymes capable of recognizing specific amino acid sequences or functional groups to facilitate covalent bonding between fluorescence dyes and antibodies (e.g., sortase A, SNAP-tag, Halo-tag, CLIP-tag) [95-98].

1.6 SNAP-tag

To address the limitations associated with traditional conjugation methods, self-labeling protein tags have been developed over the last few decades. These tags specifically react with synthetic substrates, enabling efficient and site-specific labeling of POIs with organic dyes or other small molecules. The most commonly used self-labeling tags are SNAP-tag [99], CLIP-tag [97] and Halo-tag [100]. Of these, the SNAP-tag is particularly favored for both extracellular and intracellular labeling in living cells due to its high specificity and versatility.

SNAP-tag technology based on an engineered version of the human repair protein O6-alkylguanine-DNA alkyltransferase (hAGT). It is a 20 kDa protein composed of 207 amino acids that rapidly and specifically reacts with O6-benzylguanine (BG) derivatives. The reaction involves transferring a benzyl group to its active site through a nucleophilic substitution reaction and simultaneously releasing free guanine (**Figure 1.5**) [101]. This reaction generates an irreversible thioether bond between the SNAP-tag and the probe [102, 103]. The SNAP-tag can be genetically fused to either the N-terminus or C-terminus of target proteins without affecting their function [103, 104]. As a self-labeling tag, SNAP-tag has demonstrated high reaction efficiency and specific labeling making it ideal for various imaging and biochemical applications. A wide range of BG substrates are commercially available, including BG-GLA-NHS, BG-biotin, BG-fluorophores and others, for synthesizing different probes. In this work, BG-fluorophores substrates were used.

Since the SNAP-tag reaction yields stable and quantifiable fluorescent labeling, it enables the detection and quantification of the labeled protein by sodium dodecyl-sulfate polyacrylamide gel electrophoresis (SDS-PAGE) using fluorescent scanning. Moreover, the labeling process requires no auxiliary enzymes or activation steps. This simplicity allows for the use of both cell-permeable substrates (suitable for intracellular and cell-surface labeling) and non-cell-permeable substrates (restricted to cell-surface labeling), depending on the experimental design. For example, SNAP-tag fusion proteins expressed in mammalian cells can be labeled intracellularly with the commercially available substrate red-emitting dye tetramethylrhodamine (TMR). This approach enhances imaging resolution of stimulated emission depletion (STED) microscopy to 40 nm in living cells [105]. Maurel et al., developed a technology that combines time-resolved fluorescence resonance energy transfer (FRET)

with SNAP-tag in living cells, enabling the study of cell-surface protein interactions in real time [106]. Other fluorescent applications, such as flow cytometry, immunofluorescence, and single-molecule labeling, further highlight the advantages of SNAP-tag technology [107-109]. Currently, SNAP-tag and the BG-fluorophores substrates are commercially available from New England Biolabs (NEB).

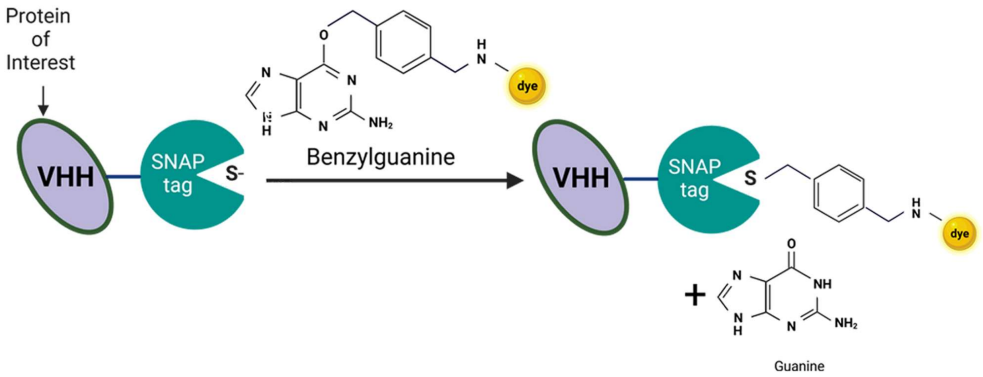

Figure 1.5 Labeling mechanism of SNAP-tag fusion proteins. Created in https://BioRender.com.

1.7 Tyramide signal amplification

Tyramide signal amplification (TSA), also known as catalytic reporter deposit (CARD), is an immunoassay that catalyzes the deposition of tyramide to detect target molecules. In this method, HRP converts tyramide into highly reactive radicals in the presence of a low concentration of hydrogen peroxide. The activate tyramide radicals then covalently bind to tyrosine residues on proteins at or near the site of HRP activity (**Figure 1.6**). Consequently, HRP functions as a catalyst that facilitates fluorophore-tyramide complexity, leading to signal amplification of up to 100-fold [110]. In TSA, the detection relies on either an HRP-conjugated secondary antibody, or biotinylated secondary antibody followed by avidin-biotin complex (ABC) techniques [111]. Due to the simplicity and time efficiency of the detection step, the use of HRP-labeled secondary antibodies has become the most common approach in TSA-based detection protocols.

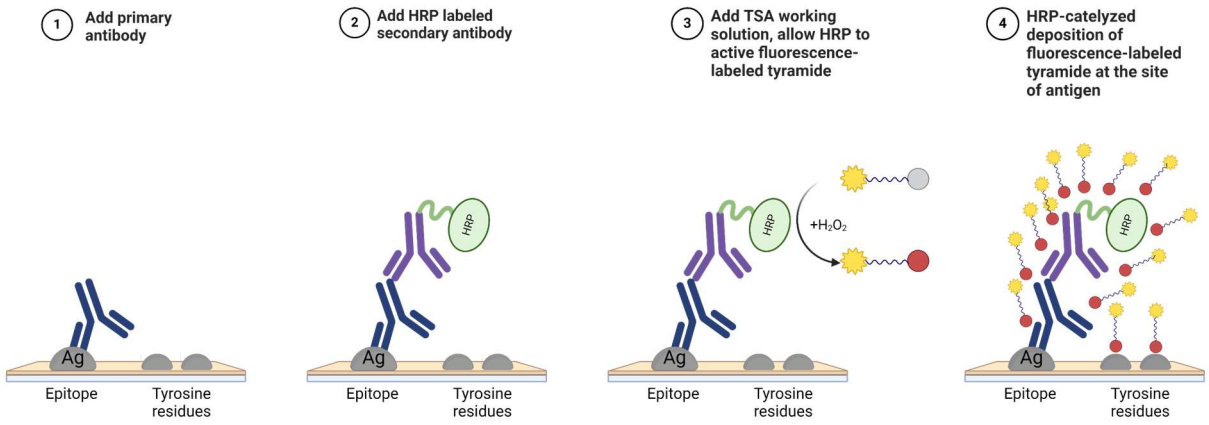

Figure 1.6 Illustration of the tyramide signal amplification system. Created in https://BioRender.com.

Based on TSA technology, multiplex immunofluorescence (mIF) assays have been subsequently developed to address the limitations of traditional immunochemistry, which typically allows only single-marker staining per slide using brightfield imaging. TSA-based mIF enables the simultaneous detection of multiple biological markers on a single slide using fluorescence dyes with distinct emission spectra. This approach provides spatial information about cells, cell-cell interactions and cell-tissue relationships in diseases contexts, offering valuable insights for therapeutic development. The general workflow of TSA is illustrated in **Figure 1.7**. A critical step in this process involves the use of microwave heating to strip primary and secondary antibodies before initiating the next staining cycle. This step preserves the antigen-tyramide-fluorophore complexes, while removing unbound antibodies and any residual horseradish peroxidase (HRP). This ensures minimal cross-reactivity between antibody species and prevents interference during subsequent staining cycle [112]. TSA-based mIF has been successfully applied to more than 4,000 formalin-fixed paraffin-embedded tissues (FFPE) tumor samples for protein-level translational research, aiding in the identification of therapeutic target biomarkers [113]. Later advancements have enabled TSA-based mIF to stain up to eight markers on a single slide. This capability allows researchers to design tailored marker panels for their research goals, such as profiling immune cell populations, mapping T-cell and myeloid cell distributions, and analyzing immune architecture within the tumor microenvironment (TME). Following image acquisition, single-cell expression data and cell phenotypes can be extracted and analyzed, offering a deeper understanding of the TME and helping guide the development of innovative cancer therapies

[114]. Benefiting from its signal amplification, TSA-based mIF provides a stronger signal compared to conventional indirect immunofluorescence methods [111, 115]. TSA-based mIF is now commercially available as TSA-based mIF staining kits, such as the Opal™ kits from Perkin Elmer, which offer up to seven-color detection for immune cell profiling. These kits allow the evaluation of complex phenotypes within the TME, including markers like CD3, CD4, CD8, CD20, CD25, CD68, CD69, Ki-67, FOXP3, Tim-3 and PD-1 [112].

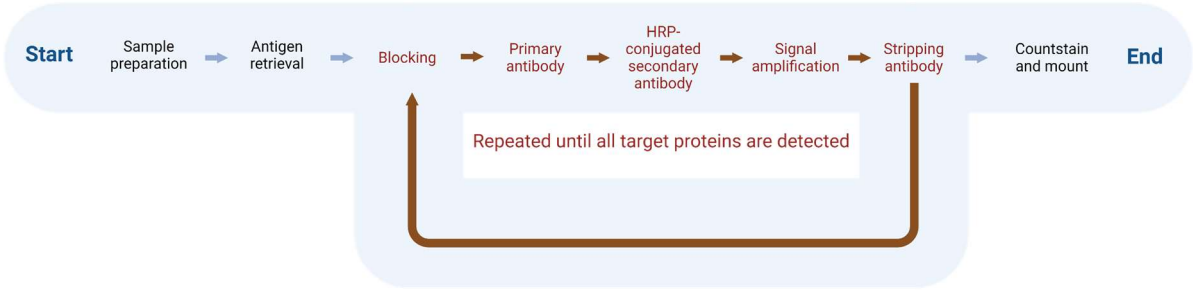

Figure 1.7 The schematic workflow of tyramide signal amplification for multiplex staining. Created in https://BioRender.com.

2. Aims and obejctives

This study aims to develop and evaluate recombinant nanobody-based substitutes for conventional secondary antibodies as a scalable, reproducible and animal-reduced alternative for indirect immunofluorescence assays (IFA). The approach focuses on overcoming common limitations of traditional secondary antibodies, including batch-to-batch variability, large molecular size, ethical concerns related to animal use and costly production process.

To achieve this, the study applies SNAP-tag technology to enable site-specific fluorescent labeling of previously established anti-mouse and anti-rabbit nanobodies for IFA. Additionally, nanobody-HRP fusion proteins are generated and characterized as recombinant alternatives to conventional HRP-conjugated secondary antibodies in WB and TSA-based mIF applications. All recombinant proteins are expressed in the HEK293T mammalian expression system to ensure high-yield, laboratory-scale production. Finally, the study assesses the performance, specificity and applicability of these nanobody-based reagents in comparison to traditional anti-mouse IgG and anti-rabbit IgG secondary antibodies.

3. Materials and methods

3.1 Materials

3.1.1 Buffers or solutions

Table 3.1 List of buffers or solutions

Buffers/solutions	Composition
10 × TBS (pH 7.6)	200 mM Tris-base 1200 mM NaCl
10 × PBS (pH 7.4)	1.54 M NaCl 76.8 mM Na_2HPO_4 23 mM NaH_2PO_4
TAE buffer (pH 8.0)	40 mM Tris-base 20 mM acetic acid 1 mM EDTA
10 × SDS-PAGE Running buffer	250 mM Tris-base 1.92 M Glycine 1% (w/v) SDS
4 × Ni-NTA Binding buffer (pH 8.0)	200 mM NaH_2PO_4 1200 mM NaCl 40 mM Imidazole
1 × Ni-NTA Binding buffer (pH 8.0)	50 mM NaH_2PO_4 300 mM NaCl 10 mM Imidazole
Ni-NTA Washing buffer (pH 8.0)	50 mM NaH_2PO_4 300 mM NaCl 40 mM Imidazole
Ni-NTA Elution buffer	50 mM NaH_2PO_4

(pH 8.0)	300 mM NaCl 250 mM Imidazole
Stripping buffer (pH 7.4)	20 mM NaH_2PO_4 500 mM NaCl 50 mM EDTA
Regeneration buffer	100mM $NiCl_2$
Sodium citrate buffer (pH 6.0)	10 mM Sodium citrate 0.05% (v/v) Tween 20
5 × Protein loading buffer	250 mM Tris-HCl 10% (w/v) SDS 30% (v/v) Glycerol 0.02% (v/v) Bromophenol blue 40.8% (v/v) Milli-Q water
LB medium (pH 7.0)	25 g LB-Medium (Luria/Miller) 1000 ml Milli-Q water
LB medium supplemented with ampicillin	LB medium 0.27 mM Ampicillin
LB medium agar supplemented with ampicillin	LB medium 0.27 mM Ampicillin 0.015% (w/v) Agar agar
TBST (pH 7.6)	20 mM Tris-base 120 mM NaCl 0.1% (v/v) Tween 20
PBST (pH 7.4)	154 mM NaCl 7.68 mM Na_2HPO_4 2.3 mM NaH_2PO_4 0.1% (v/v) Tween 20

3.1.2 Kits

Table 3.2 List of kits

Kit	Supplier
SuperSignal™ West Pico PLUS Chemiluminescent Substrate	Thermo Scientific
Vector NovaRED® Substrate Kit, Peroxidase (HRP), SK-4800	Vector Laboratories
NucleoSpin® Gel and PCR clean-up	Macherey-Nagel
NucleoSpin® Plasmid	Macherey-Nagel
Halt™ Protease Inhibitor Single-Use Cocktail (100×)	Thermo Scientific
Trans-Blot Turbo Transfer 5× Buffer	Bio-Rad
ROTI®Stock 10 × TBS	Carl Roth

3.1.3 Antibodies

Table 3.3 List of primary antibodies

Antigens	Host/Isotype	Catalog	Supplier
Epidermal growth factor receptor (EGFR, H11)	Monoclonal mouse/IgG1, kappa	MA5-13070	Thermo Fisher Scientific
EGFR (30H45L48)	Recombinant monoclonal rabbit/IgG	700308	Thermo Fisher Scientific
CD20 (L26)	Monoclonal mouse/IgG2a, kappa	14-0202-82	Thermo Fisher Scientific
EGFR (199.12)	Monoclonal mouse / IgG2a	MA5-13319	Thermo Fisher Scientific
EGFR	Polyclonal rabbit/IgG	HPA018530	Sigma-Aldrich
Human epidermal growth factor receptor 2 (HER-2, 3B5)	Monoclonal mouse/IgG1	MA5-13675	Thermo Fisher Scientific
Progesterone receptor (PR,	Monoclonal	MA5-14842	Thermo Fisher

R.809.9)	rabbit/IgG		Scientific	
Estrogen receptor alpha (ERα,1D5)	Monoclonal mouse/IgG1, kappa	MA5-13191	Thermo Scientific	Fisher
Glyceraldehyde-3-phosphate dehydrogenase (GAPDH, ZG003)	Monoclonal mouse/IgG1, kappa	39-8600	Thermo Scientific	Fisher
Nerve/glial-antigen 2 (NG2, D120.43/D4.11/N143.8/N109.6)	Monoclonal mouse/ IgG1, kappa	37-2700	Thermo Scientific	Fisher
Folate receptor alpha (FOLR1, 548908)	Monoclonal mouse/ IgG1	MA5-23917	Thermo Scientific	Fisher
Epithelial cell adhesion molecule (EpCAM, 1B7)	Monoclonal mouse/ IgG1, kappa	14-9326-82	Thermo Scientific	Fisher
beta Catenin 1 (CTNNB1)	Polyclonal Rabbit/ IgG	HPA029159	Sigma-Aldrich	
Ankyrin 3 (ANK3)	Polyclonal Rabbit/ IgG	HPA038455	Sigma-Aldrich	
CD31 (2F7B2)	Monoclonal Mouse/ IgG1	MA5-15336	Thermo Scientific	Fisher
α Smooth Muscle Actin (αSMA, ACTA2)	Monoclonal Mouse/ IgG2a	A2547	Sigma-Aldrich	

Table 3.4 List of secondary antibodies

Name	Host/Isotype	Catalog	Supplier	
Alexa Fluor™ Plus 647 conjugated with goat anti-mouse IgG (H+L)	Polyclonal Goat/ IgG	A32728	Thermo Scientific	Fisher
Alexa Fluor™ 647 conjugated anti-rabbit IgG (H+L)	Polyclonal Goat/ IgG	A21245	Thermo Scientific	Fisher
HRP-conjugated anti-mouse IgG (H+L)	Polyclonal Goat/ IgG	G21040	Thermo Scientific	Fisher
HRP-conjugated anti-rabbit IgG	Polyclonal	7074S	Cell	Signaling

	Goat/ IgG	Technology

3.1.4 Consumable materials

Table 3.5 List of consumable materials

Consumable material	Purpose	Supplier
Zeba™ Spin Desalting Columns, 7K MWCO	Size exclusion	Thermo Fisher Scientific
Ni-NTA superflow cartridge	Protein purification	Qiagen
HiTrap Desalting column	Buffer exchange	Cytiva

3.1.5 Laboratory equipment

Table 3.6 List of laboratory equipment

Equipment	Supplier
NanoDrop™ One^{C} MicrovolumeUV-Vis Spectrophotometer	Thermo Fisher Scientific
Gel Doc™ XR+ System	Bio-Rad
peqSTAR Thermocycler	VMR
Fisherbrand™ Multi-Platform Shaker	Fisher Scientific
Trans-Blot® Turbo™ Transfer System	Bio Rad
Mini-PROTEAN® Tetra Vertical Electrophoresis Cell for Mini Precast Gels	Bio Rad
CytoFLEX Flow Cytometers	Beckman Coulter
pH-Meter CG840	Schott
PowerPac™ Basic Power Supply	Bio Rad
Microwave R242INW	Sharp
Centrifuge 5427 R	Eppendorf
ThermoMixer F2.0	Eppendorf
Analytical balance ABJ 120-4NM	Kern

Precision balance 600-2NM	Kern
PCR UV cabinet, UVC/T-M-AR	Grant bio
Incubator IN75	Memmert
ÄKTA start system	GE Healthcare Bio-Sciences AB
Inverted microscope, ECLIPSE Ts2-FL	Nikon
Megafuge 16R centrifuge	Thermo Scientific
Axio Scan.Z1 slide scanner	Zeiss
DMi8 S Live-cell microscope	Leica Microsystems
Incubator Modek CB 170	BINDER
Odyssey DLx Imager	LI-COR Biosciences
Water bath WB 7	Memmert
Vortex RS-VA 10	Phoenix Instrument
Intas ECL chemostar	Intas Science Imaging
Infinite® Mplex microplate reader	Tecan

Table 3.7 Software

Program name	Supplier	Application
Image J	National Institutes of Health	Image analysis
GraphPad Prism 9.0.0	GraphPad Software	Data analysis
Adobe Photoshop 2020	Adobe	Image processing
Adobe Illustrator	Adobe	Image processing
Flow Jo 10.7.1	Becton, Dickinson & Company	Flow cytometry analysis
Qupath 0.5.1	GitHub	Image analysis
Image Lab software	Bio-Rad	Image analysis
Image Studio Lite Ver 5.2	LI-COR Biosciences	Image processing

3.1.6 Cell lines and culture medium

Breast cancer cell lines MDA-MB-468 (ACC 738), MDA-MB-231 (ACC 732), MDA-MB-453 (ACC 65), Hs578T (ACC 781) and MCF-7 (ACC 115) were purchased from the Leibniz Institute DSMZ-

German Collection of Microorganisms and Cell Cultures and maintained in DMEM (Thermo Fisher Scientific) supplemented with 10% heat-inactivated fetal calf serum (FBS) (Thermo Fisher Scientific) and 1% penicillin-streptomycin (Thermo Fisher Scientifc). The endometrioid cell lines 12Z, 49Z, THESC and Ishikawa were kindly provided by Lutz Konrad (Department of Obstetrics and Gynecology, Justus Liebig University Giessen). The cell lines 49Z and 12Z were cultured in complete DMEM. T-HESC cells were cultured in DMEM/F12 (Thermo Fisher Scientific) supplemented with 10% FBS, 1% penicillin-streptomycin and 1% insulin-transferrin-selenium-ethanolamine (ITS-X, 100 ×, Thermo Fisher Scientific). Ishikawa cells were cultured in MEM (Biowest), supplemented with 5% FBS and 1% non-essential amino acids (NEAA, Thermo Fisher Scientific). The HEK293T (American Type Culture Collection) cells was cultured in RPMI 1640 (Thermo Fisher Scientific) containing 10% FBS and 1% penicillin-streptomycin. All cells were maintained in a humidified atmosphere of 5% CO_2 at 37 °C.

3.1.7 Enzymes

All restricted enzymes were purchased from New England Biolabs. Taq polymerase and Ultra DNA polymerase were purchased from Jena Bioscience. Phusion High-Fidelity DNA Polymerase was purchased from Thermo Scientific. In-Fusion® Snap Assembly Master Mix was purchased from TaKaRa.

3.2 Methods

3.2.1 Molecular biology techniques

3.2.1.1 Preparation of chemically competent *E. coli*

DH5α *E. coli* (2 µl) was incubated in 2 ml LB medium overnight at 37 ℃ with shaking at 250 rpm. Next day, 1 ml of *E. coli* growth culture was added into 100 ml LB medium, incubating at 37 ℃ with 250 rpm shaking until the OD600 reached 0.25-0.3. The culture was then chilled on ice for 15 min. After centrifugation, the supernatant was discarded, and the *E. coli* pellet was resuspended in 35 ml ice-cold 0.1 M $CaCl_2$. The suspension was kept on ice for 30 min. Following another centrifugation step, the *E. coli* pellet was resuspended in 6 ml ice-cold 0.1 M $CaCl_2$/15% (v/v) glycerol and aliquoted

into 0.1 ml pre-cooled sterile tubes, then immediately snap-frozen in liquid nitrogen. The aliquots were stored at -80 ℃.

3.2.1.2 Transformation and inoculation of chemically competent *E. coli*

DH5α cells (100 µl) were taken from the -80℃ freezer and thawed on ice. Either 0.5 µl plasmid or 5-10 µl ligation products (10 pg-100 ng DNA) were added to the cells and incubated on ice for 30 min. The mixture was heated-shocked at 42 ℃ for 45 s and immediately chilled on ice for 5 min. Subsequently, 800 µl antibiotic-free LB medium was added to the cells and incubated for 1 h at 37 ℃ with shaking at 250 rpm. The culture was centrifuged at 5000 rpm for 2 min, and 800 µl supernatant was discarded. The cell pellet was resuspended in the remaining medium and plated on LB agar plates containing 100 µg/ml ampicillin and incubated overnight at 37 ℃. The next day, single colony was picked and inoculated into 2 ml LB medium containing 100 µg/ml ampicillin. The culture medium was incubated overnight at 37 ℃ with shaking at 250 rpm.

3.2.1.3 Extraction of plasmid DNA from *E. coli* and bacterial storage

Plasmid DNA was extracted from 1.5 ml of *E. coli* LB culture after overnight incubation using NuleoSpin® Plasmid kit according to manufacturer's instructions. The rest 0.5 ml of bacterial culture was mixed with 0.5 ml of 50% (v/v) glycerol and stored at -80 ℃.

3.2.1.4 PCR

PCR was used for amplifying the DNA of fragments and vectors. Taq polymerase, Ultra DNA polymerase and Phusion High-Fidelity DNA polymerase were applied as PCR kits in this project.
For Taq polymerase reaction system (**Table 3.8**), including the initial denaturation step for 5 min at 94 °C, 30 cycles of annealing step (30 s denaturation at 94 °C, 30 s primer annealing at 58-60 °C and 1kb/min elongation at 72 °C), then 10 min final elongation step at 72 °C.

Table 3.8 Taq polymerase reaction

Component	Volume

10 × Taq reaction buffer	5 µl
10 mM dNTP*	1-3 µl
Forward primer (10 µM)	1 µl
Reverse primer (10 µM)	1 µl
Taq polymerase	0.5 µl
DNA template	1 µl (1 ng)
PCR-grade water	Fill up to 50 µl

*1 µl of dNTP was used for fragment amplification, and 3 µl was used for vector amplification.

For Ultra DNA polymerase (**Table 3.9**), the initial denaturation step for 30 s at 98 °C, 35 cycles of annealing step (10 s denaturation at 98 °C, 30 s primer annealing at 58-60 °C, and 1kb/min elongation at 68 °C), then 10 min final elongation step at 68 °C.

Table 3.9 Ultra DNA polymerase

Component	Volume
5× Ultra DNA buffer	10 µl
10 mM dNTP*	1-3 µl
Forward primer (10 µM)	1 µl
Reverse primer (10 µM)	1 µl
Ultra DNA polymerase	0.5 µl
DNA template	1 µl (1 ng)
PCR-grade water	Fill up to 50 µl

*1 µl of dNTP was used for fragment amplification, and 3 µl was used for vector amplification.

For Phusion™ High-Fidelity DNA polymerase (**Table 3.10**), the initial denaturation step for 30 s at 98 °C, 35 cycles of annealing step (10 s denaturation at 98 °C, 30 s primer annealing at 60-64 °C and 1kb/30 s elongation at 72 °C), then 10 min final elongation step at 72 °C.

Table 3.10 Phusion™ High-Fidelity DNA polymerase reaction

Component	Volume
5 × Phusion™ HF buffer	10 µl
10 mM dNTP*	1-3 µl

Primer forward (10 μM)	2.5 μl
Primer reverse (10 μM)	2.5 μl
Phusion™ High–Fidelity DNA polymerase	0.5 μl
DNA template	1 μl (1 ng)
PCR-grade water	Fill up to 50 μl

*1 μl of dNTP was used for fragment amplification, and 3 μl was used for vector amplification.

3.2.1.5 Restriction enzyme digestion

Restriction enzyme digestion of PCR products and DNA plasmids was performed for further recombinant plasmids generation. Typically, the digestion was incubated for 1 h at the recommended temperature from manufacturer. For two-site digestions with different temperature, the reaction was incubated at 37 ℃ for 1 h followed by at 50 °C for 1 h. The preparation of restriction enzyme reaction, and reaction temperature were listed in **Tables 3.11** and **3.12**.

Table 3.11 Restriction reaction prepared in this project

Component	Volume （μl）	Final concentration
DNA	variable	1 μg
Restriction enzyme	variable	5 U
10 × rCutSmart™ Buffer	2.5	1 ×
Ultrapure water	Fill up to 25 μl	-

Table 3.12 List of restriction enzymes

Restriction enzyme	Optimal temperature
XbaI	37 °C
SfiI	50 °C
BlpI	37 °C
NdeI	37 °C

3.2.1.6 Agarose gel electrophoresis and DNA purification

Agarose gel electrophoresis was used to separate DNA fragments from PCR-amplified and restricted-

digested samples based on their size. DNA samples were mixed with 6 × purple gel loading dye (New England Biolabs) and loaded into 1% (w/v) agarose gels containing 1 × SYBR Safe DNA Gel Stain (Invitrogen) at 100 V for 30 min. The 2-Log DNA ladder (New England Biolabs) was used as DNA marker. Gel was visualized under UV light using ChemiDoc XRS+ System.

3.2.1.7 Extraction of plasmid DNA from agarose gel

For DNA extraction from agarose gel, required DNA bands were cut from the gel under UV light. NucleoSpin® Gel and PCR clean-up kit was used according to the manufacturer's instructions for DNA extraction.

3.2.1.8 Ligation

Ligation was performed by Quick Ligation™ kit (New England Biolabs) or In-Fusion® Snap Assembly Master Mix (Takara Bio Inc.), depending on the method used for amplifying the DNA insert and vector, according to the manufacturer's instructions. Ligation reactions were prepared as in **Tables 3.13** and **3.14**

Table 3.13 Ligation reaction of Quick Ligation™ kit

Component	Volume （μl）	Final concentration
Ligase	1	1 μg
2 × Reaction buffer	10	1 ×
Insert DNA*	variable	variable
Vector DNA	variable	50 ng
Nuclease-free water	Fill up to 20 μl	-

***** The molar ratio of insert DNA fragments to vector backbone was 3:1

Table 3.14 Ligation reaction of In-Fusion® Snap Assembly Master Mix

Component	Volume （μl）	Final concentration
5 × In-Fusion Snap Assembly Master Mix	2	1 ×
Vector DNA	variable	50 ng

Insert DNA*	variable	variable
Nuclease-free water	Fill up to 10 µl	-

* The molar ratio of insert DNA fragments to vector backbone was 2:1

3.2.1.9 DNA sequencing

To check the accuracy of insertions, sequencing of all generated plasmids was performed by Eurofins Genomics (Ebersberg, Germany). Here 500 ng of Plasmid and 25 pmol primer in 10 µl total volume was prepared. The primers used for sequencing was IgK-For (ACACACTCCTGCTATGGG).

3.2.1.10 Establishment of expression constructs

3.2.1.10.1 Nbs anti-IgG-SNAP plasmids

The Nbs anti-IgG-SNAP plasmids were generated using the eukaryotic expression vector pMS, which is derived from pSecTag2 vector [116]. The pMS-scFv-425-SNAP construct, previously described [107], served as a vector backbone in this project and contained SfiI and XbaI restriction sites. For cloning insert fragments, nanobody plasmids pTP943，pTP1112，pTP1005，pTP1174 and pTP1183 were gifts from Dirk Görlich (AddGene plasmid # 104157, # 104158, # 104160, # 104162, # 104163 respectively) [117]. The insert fragments were obtained from the nanobody plasmids and equipped with SfiI and XbaI restriction sites through PCR amplification using Taq polymerase. The pMS-SNAP vector and anti-IgG nanobody PCR products were digested with SfiI and XbaI restriction and subsequently ligated to generate the following constructs: pMS-Nb anti-mouse IgG1 Fab-SNAP, pMS-Nb anti-mouse IgG1 Fc-SNAP, pMS-Nb anti-mouse IgG2a Fc-SNAP, pMS-Nb anti-mouse kappa chain-SNAP and pMS-Nb anti-rabbit IgG Fc-SNAP.

Table 3.15 Anti-IgG nanobody plasmids used in this project

Plasmid name	Catalog	Features
pTP943	104157	Anti-mouse IgG1 Fab specific nanobody TP886
pTP1112	104158	Anti-mouse IgG1 Fc specific nanobody TP1107
pTP1005	104160	Anti-mouse IgG2a Fc specific nanobody TP1129

pTP1174	104162	Anti-mouse kappa chain specific nanobody TP1170
pTP1183	104163	Anti-rabbit IgG Fc specific nanobody TP897

Table 3.16 Primers used for Nbs anti-IgG-SNAP expression constructs in this project

Primer	Sequence (5'-3')	Purpose
Nano-For	CGCCGGGGCCCAGCCGG CCCAGGTGCAATTGGTAG	Amplify anti-mouse IgG1 Fab, anti-mouse IgG2a Fc, anti-mouse kappa chain, anti-rabbit IgG Fc
Nano-Rev	TTAAGATCTAGAACATG ATGAGACTGTGACC	Amplify anti-mouse IgG1 Fab, anti-mouse IgG1 Fc
pTP1112-For	CGCCGGGGCCCAGCCGG CCCAGGTGCAATTGGTGG	Amplify anti-mouse IgG1 Fc
pTP1112-Rev	AGCTAATCTAGAACATCC ACCGGAGGAG	Amplify anti-mouse IgG1 Fc, anti-mouse kappa chain, anti-rabbit IgG Fc

3.2.1.10.2 Nbs anti-IgG-HRP plasmids

To generate pMS-Nbs anti-IgG-HRP plasmids, pUC19-HRP-C (a gift from Paul Ortiz de Montellano, Addgene plasmid # 40163) was used as an insert fragment. The vectors and inserts were amplified with specific primers (**Table 3.17**) using Phusion™ High-Fidelity DNA polymerase or Ultra DNA polymerase. The amplified products were ligated with In-Fusion® Snap Assembly Master Mix to construct pMS-Nbs anti-IgG-HRP recombinant plasmids. To clone the constructs into the pHR expression vector [118], BlpI and NdeI restriction enzymes were used to digest pHR-Herceptin-HC-SNAPf (previously generated in our lab) and pMS-Nbs anti-IgG-HRP. The digested produces were ligated to generate pHR-Nbs anti-IgG-HRP recombinant plasmids.

Table 3.17 Primers used for Nbs anti-IgG-HRP expression constructs in this project

Primer	Sequence (5'-3')	Purpose
Frag nanoHRP-For	TTCGTGCTCAGCGCCAG AGTTGCTGTTGACCACTCTG	Amplifying HRP fragment
Frag	TCATCATGTTCTAGAATG	Amplifying HRP fragment for Nbs anti-

g1fabHRP-Rev	CAGTTAACCCCTACATTCTACG	mouse IgG1 Fab- and IgG2a-HRP
Vector nanoHRP-For	GGCGCTGAGCACGAATTT	Amplify vector Nbs pMS-anti-IgG
Vector g1fabHRP-Rev	TCTAGAACATGATGAGACT GTGACCT	Amplifying vector pMS-anti-mouse IgG1 Fab
Frag g1fc-Rev	GGTGGATGTTCTAGAATGCA GTTAACCCCTACATTCTACG	Amplifying HRP fragment for anti-mouse kappa chain-, IgG1 Fc- and anti-rabbit IgG Fc-HRP
Vector nanoHRP-Rev	TCTAGAACATCCACCGGAGGAG	Amplifying vector Nbs pMS-anti-mouse kappa chain, pMS-anti-mouse IgG1 Fc and pMS-anti-rabbit IgG Fc
Vector g2aHRP-Rev	TCTAGAACATGATGAGAC TGTGACCC	Amplifying vector pMS-anti-mouse IgG2a

3.2.2 Protein expression

3.2.2.1 Cell culture

The cell lines and their culture media used in this project were described in **Section 3.1.6**. Generally, every 3-4 days, when the confluence of the cell-culture flask reached 70-80%, cells were passaged. All cell lines were grown at 37 °C in a 5% CO_2 humidified incubator.

3.2.2.2 Transfection of HEK293T cells with recombinant DNA

3.2.2.2.1 Liposome-mediated transfection of HEK293T cells with Nbs anti-IgG-SNAP DNA

HEK293T cells were transfected with Nbs anti-IgG-SNAP DNA using ROTI®-Fect following the

manufacturer's instructions. A total of 400,000/well cells were seeded in a 6-well plate and incubated overnight at 37 °C in a 5% CO_2 incubator. Recombinant DNA (2 µg) was diluted in serum-free RPMI-1640 medium without antibiotics to a final 100 µl volume. Separately, 10 µl of ROTI®-Fect transfection reagent was mixed with 90 µl of serum-free RPMI-1640 without antibiotics. The two solutions were mixed and incubated at room temperature for 20 min. After replacing the cell medium with fresh antibiotic-free RPMI-1640 containing serum, 200 µl of the nucleic acid-lipid complex was added dropwise to the cells. The cells were incubated at 37 °C in a 5% CO_2 incubator overnight. After 24 h, the culture medium was replaced with complete RPMI-1640 medium supplemented with 0.1% (v/v) zeocin to select successful transfected cells.

3.2.2.2.2 Lentiviral production in HEK293T cells for Nbs anti-IgG-HRP DNA

HEK293T cells (2.5×10^6) were seeded in a 10-cm^2 culture Petri dish and cultured overnight to achieve 70%-80% confluency. For transfection, a plasmid mixture containing pHR-Nbs anti-IgG-HRP, psPAX2 and pMD2.G was prepared in a 4:3:1 ratio (6 µg total DNA). The plasmid mixture was diluted in 1 ml Opti-MEM™ Reduced Serum Medium (Thermo Fisher Scientific), followed by addition of 27 µl of TransIT293 Transfection Reagent. The mixture was gently pipetted and incubated at room temperature for 20 min. The transfection mixture was added dropwise to the plate containing HEK293T cells and 10 ml of fresh antibiotic-free RPMI-1640 containing serum. This transfection was performed in the laboratory of Molecular Cytology and Functional Genomics, Pathology Department, Justus Liebig University Giessen. The cells were incubated at 37 °C in a 5% CO_2 incubator overnight. After 24 h, the culture medium was replaced with complete RPMI-1640 medium. After 48 h, the culture supernatant was collected and spun down at 800xg for 10 min at room temperature followed by filtering through a sterile 0.22 µm syringe filter. Then 1 volume of concentrator (80 g PEG-8000, 14.0 g NaCl, 20 ml 10 × PBS (pH7.4) and 80 ml MilliQ water) pH 7.2 was added to 3 volumes of supernatant. The mixture was shaken for 60 s, then incubated with constant rocking at ~ 60 rpm for at 4 hours at 4 °C. The mixture then centrifuged at 1600 ×g for 60 min at 4 °C and the pellet was resuspended in 500 µl of PBS.

3.2.2.2.3 The lentiviral transduction into HEK293T cells for producing Nbs anti-IgG-HRP DNA

HEK293T cells (3×10^5) were seeded in 6 well plate (3×10^5 cells in 2 ml culture medium) and incubated overnight at 37 °C in a 5% CO_2 incubator. The collected lentivirus (5 µl) was added to the cells and incubated for further 24 h at 37 °C in a 5% CO_2 incubator. After that the media were replaced with fresh medium and incubated for a further 48 h. The success of the transduction was confirmed by detecting the GFP signal using fluorescence microscopy. After six passages, the absence of viral particles was confirmed by laboratory personnel in accordance with institutional biosafety protocols. Based on this confirmation, the stably transfected cells were downgraded to Biosafety Level 1. This work was performed in the laboratory of Molecular Cytology and Functional Genomics, Pathology Department, Justus Liebig University Giessen.

3.2.2.3 Recombinant expression of proteins

During the protein expression, the Nbs anti-IgG-SNAP transfected HEK293T cells were kept and selected in complete RPMI-1640 medium supplemented with 0.1% (v/v) zeocin, while Nbs anti-IgG-HRP transfected cells were cultured without zeocin selection. Direct ELISA was used to confirm that Nbs anti-IgG-HRP were expressed and secreted into the medium. Here, 100 µl of supernatant was applied as the coating antigen followed by TMB substrate (IBL International, Germany) incubation for 30 min at room temperature. After the color reaction was stopped, the optical density of the mixed solution was measured using Infinite® Mplex microplate reader at 450 nm. For high-yield production, cells were kept in a triple-layer flask containing 150-200 ml medium and replaced with fresh medium every 5-7 days. Finally, 500-600 ml supernatant was collected and stored at 4°C up to 2 weeks.

3.2.2.4 Protein enrichment

All recombinant proteins were enriched using their C-terminal 6 × His-tag. The culture supernatant was collected and centrifuged, followed by filtration through a 0.45-µm Corning® Vacuum Filter. The culture supernatant was diluted to 1 × binding buffer concentration using 4 × binding buffer. An Ni-NTA superflow cartridge was equilibrated with 1 × binding buffer before loading filtered supernatant.

Immobilized proteins were isolated sequential use of binding buffer, washing buffer and elution buffer, with recombinant proteins enriched in elution buffer. After purification, the cartridge was washed with 0.5 M NaOH to remove residual proteins, followed by using stripping buffer to remove nickel ions. The cartridge was recharged with 100 mM $NiCl_2$ for reuse for the next purification. All collected fractions were collected during the purification. To assess the activity of SNAP-tag, the SNAP-fractions were incubated with SNAP-Surface® Alexa Fluor® 488 for 20 min at room temperature in the dark. The fractions were then analyzed by 10% SDS-PAGE. For the presence of proteins, SDS gels were stained with Coomassie Brilliant Blue.

3.2.2.5 Buffer exchange of purified proteins

HiTrap™ Desalting column was used to exchange the elution buffer into PBS according to the manufacturer's protocol. After washing the column with 5-column volumes of PBS, purified proteins were applied to the desalting column. The buffer-exchanged fraction was collected when the UV absorbance started to increase until back to baseline. Proteins were stored at -20 °C.

3.2.2.6 SDS-PAGE

To separate proteins based on their molecular weight, we used SDS-PAGE. The samples were mixed with 5 × protein loading dye without boiling, then loaded and ran in 10% SDS-PAGE. The SDS-PAGE was prepared as follows:

Table 3.18 10% SDS-PAGE gel recipe used in this project

Component	10% Separation gel	4% Stacking gel
Milli-Q water	4.1 ml	6.1 ml
Acrylamide/bis (30% 37.5:1)	3.3 ml	1.3 ml
Tris-HCl (1.5 M, pH 8.8)	2.5 ml	-
Tris-HCl (0.5 M, pH 6.8)	-	2.5 ml
10% SDS	100 µl	100 µl
10% APS	32 µl	100 µl

TEMED	10 µl	10 µl

3.2.2.7 SDS-PAGE of proteins

The proteins were separated by SDS-PAGE according to their molecular weight. A 10% SDS gel was prepared, and electrophoresis was conducted at 160 V for 60 min. A blue prestained protein standard broad range (New England Biolabs) was used as a molecular weight marker. Following electrophoresis, the gel was imaged using the ChemiDoc XRS+ System under UV light or the Odyssey DLx Imager. Subsequently, the gel was incubated with Coomassie Brilliant Blue staining solution and the gel destained overnight in water to visualize the protein bands.

3.2.2.8 Protein concentration quantification

To measure the concentration of the purified proteins, a bovine serum albumin (BSA) standard was used. Different concentrations of BSA (0.2, 0.1, 0.05, 0.025 µg/µl) (New England Biolabs, 20 mg/ml) were prepared in 10 µl of 1 × PBS. The BSA standards and protein samples were applied in 10% SDS gel. The protein concentration and standard curve were determined by Image Lab™ software.

3.2.3 Labeling Nbs anti-IgG-SNAP with BG-modified fluorescent dyes

Nbs anti-IgG-SNAP were labeled with SNAP-Surface® Alexa Fluor® 488, SNAP-Surface® Alexa Fluor® 546, SNAP-Surface® Alexa Fluor® 594 or SNAP-Surface® Alexa Fluor® 647 (New England Biolabs) by incubating protein to fluorescence dye at 1:2 molar ratio at room temperature for 2 h in the dark. The residual dyes were removed by 7K MWCO Zeba ™ Spin Desalting Columns according to the manufacturer's instructions.

3.2.4 Adherent cells lysis

A 10 cm cell culture dish was placed on ice, and the culture medium was removed. The cells were washed twice with ice-cold PBS. Subsequently, PBS was completely aspirated, and 200 µl of RIPA lysis and extraction buffer (Thermo Fisher Scientific) was added to the cells. The cells were scratched

off and the suspension was transferred into a microcentrifuge tube. The tube was placed on ice for 30 min with agitation every 5 min. Subsequently, the suspension was centrifuged at 14000 rpm for 20 min under 4 ℃, and the lysis supernatant was transferred into a new tube on ice. Protein concentration in the lysate was measured using NanoDrop™ One^{C} spectrophotometer, ensuring equal amounts of proteins were loaded into the SDS-PAGE.

3.2.5 Fluorescence Western blot

A total of 125 ng of primary antibody was loaded onto a 10% SDS-PAGE. These proteins were then transferred onto ethanol-preactivated polyvinylidene difluoride (PVDF) membranes using the Trans-Blot® Turbo™ transfer system. The membranes were blocked with Western blot blocking buffer (1% BSA in TBST) for 1 h at room temperature, followed by incubation with Nb anti-IgG-SNAP-Surface® Alexa Fluor® 647 (1µg/ml), Alexa Fluor™ Plus 647 conjugated with goat anti-mouse IgG (H+L) (Thermo Fisher Scientific, A32728, 1:8000) and Alexa Fluor™ 647 conjugated anti-rabbit IgG (H+L) (Thermo Fisher Scientific, A21245, 1:8000) for another 1 h individually. After incubation, the membranes were washed three times in TBST, followed by a final wash in TBS. The membranes were imaged using the Odyssey DLx Imager (LI-COR Biosciences).

3.2.6 Western blot

The proteins were separated by SDS-PAGE and transferred onto a PVDF membrane using the Trans-Blot® Turbo™ transfer system (25V, 1.3A) for 15 min. The membrane was blocked with Western blot blocking buffer for 1 h at room temperature, followed by overnight incubation at 4 ℃ with primary antibodies (diluted in blocking buffer) with rotation. After three washing steps with TBST, the membrane was incubated for 1 h at room temperature with HRP-conjugated secondary antibodies (diluted in blocking buffer). Following another three washing steps with TBST and one final wash with TBS, the membrane was dried and incubated with SuperSignal™ west pico plus chemiluminescent substrate for 5 min. Chemiluminescent signals were visualized using an Intas ECL chemostar imaging system.

3.2.7 Flow Cytometry

In this project, flow cytometry was used to confirm the specific binding of Alexa Fluor® 647 conjugated Nbs anti-IgG-SNAP. To assess background fluorescence, cells incubated with Nbs anti-IgG-SNAP-647 or Alexa Fluor 647-conjugated commercial secondary antibodies in the absence of a primary antibody. These samples were served as negative controls to define non-specific binding of the labeled secondary reagents. All data were analyzed in FlowJo (v10.7.1).

3.2.7.1 Surface Staining

To detect surface markers, cells were suspended in PBS at a concentration of 4×10^5 cells/ml and blocked by surface blocking buffer (1% BSA in PBS). Subsequently, the diluted primary antibodies were added to the cells in 200 µl PBS and incubated for 30 min on ice. After washing twice with PBS, cells were incubated with commercial secondary antibodies or 1 µg Nbs anti-IgG-SNAP-647 for 30 min on ice in the dark. Cells were then washed twice with PBS, resuspended in 200 µl PBS, and analyzed using CytoFLEX Flow Cytometers.

3.2.7.2 Intracellular staining

To detect intracellular antigens, cells were fixed in 4% formaldehyde in PBS for 10 min at room temperature and permeabilized with 0.1% Triton X-100 in PBS for 5 min at room temperature. After washing twice with PBS, cells were blocked in permeabilization blocking buffer containing 10% FBS and 1% BSA. Primary antibodies, Nbs anti-IgG-SNAP-647 or commercial secondary antibodies were diluted in permeabilization blocking buffer and added sequentially. For each step the cells were incubated for 30 min on ice. The cells were washed twice with PBS, resuspended in 200 µl PBS and analyzed using CytoFLEX Flow Cytometers.

3.2.8 Fluorescence microscopy

To observe the specific binding of Alexa Fluor® 647 conjugated Nbs anti-IgG-SNAP to primary antibodies, fluorescence microscopy was used in this project.

3.2.8.1 Surface Staining

Cells were collected and seeded in 96-well microplates (4×10^4 cells in 100 µl culture medium) and incubated overnight at 37 °C in a 5% CO_2 incubator. The next day, cells were fixed with 4% formaldehyde in PBS for 10 min at room temperature, washed twice with PBS, and neutralized with 50 mM NH_4Cl in PBS for 5 min. After blocking with surface blocking buffer, cells were incubated with primary antibodies (as used in flow cytometry **Section 3.2.7.1**) on ice for 30 min. Following two PBS washes, commercial secondary antibodies or 1 µg Nbs anti-IgG-SNAP-647 were added, and the cells were incubated on ice for another 30 min. After additional two PBS washes, nuclear staining was performed with Hoechst 33342 (Thermo Fisher Scientific). Specific binding was visualized using a DMi8 S Live-cell microscope with a 100 × oil objective.

3.2.8.2 Intracellular staining

For intracellular antigens, cells were fixed, neutralized, and permeabilized with 0.3 (v/v) Triton X-100 in PBS for 5 min. After two PBS washes, cells were blocked in permeabilization blocking buffer for 30 min on ice. Subsequent steps, including incubation with primary antibodies, commercial secondary antibodies or Nbs anti-IgG-SNAP-647 were performed as described in the surface staining protocol **Section 3.2.8.1**. Nuclear staining and imaging were carried out similarly.

3.2.9 Cell block

Approximately 1×10^7 of endometrial cells (49Z, 12Z, Ishikawa and T-HESC) were collected separately and washed with PBS, then fixed in 1 ml of 4% formaldehyde overnight at room temperature. After PBS washing, cells were resuspended in 200 µl of 30 mg/ml Agarose Low Melt (Roth) in PBS at 42 °C. The cell-agarose mixture was kept until solidification at 4 °C. Following dehydration in a graded series of ethanol (70%, 80%, 90%, 95%, 100%), the solidified cell-agarose was kept in xylene overnight. The next day, xylene was removed by liquid paraffin at 60 °C, and the cell-agarose was embedded in melted paraffin.

3.2.10 IHC

The slides were placed in a 60 °C oven for 30 min, then deparaffinization was performed using xylene (two changes, 10 min each), and rehydrated through graded ethanol solutions (100%, 90%, 80% and

70%). Following washing with distilled water, antigen retrieval was performed by heating the slides in citrate buffer for 20 min in a microwave, followed by cooling to room temperature. The slides were washed twice with PBS and incubated with 3 % hydrogen peroxide in PBS for 15 min to block endogenous peroxidase activity. After washing with PBST, the slides were incubated with blocking buffer (10% normal goat serum in PBS) for 1 h at room temperature. Primary antibodies were applied and incubated for 1 h at room temperature or overnight at 4 °C. After three washes steps with PBST, the slides were incubated with HRP-conjugated anti-mouse IgG (1:100) or HRP-conjugated anti-rabbit IgG (1:500) for 1 h at room temperature, followed by two PBST washing steps then washed once with PBS. For chromogen immunohistochemistry, slides were treated with Vector NovaRED Substrate Kit (Vector Laboratories) for 5-15 min. The slides were washed twice with distilled water, counterstained with hemoxylin, and mounted using VectaMount® Express Mounting Medium (H-5700). Images were acquired by 40 × magnification using Axio Scan.Z1 Slide Scanner (Zeiss). Semi-quantitative analysis was performed with ImageJ IHC profiler.

3.2.11 Multicolor staining on cell block

After de-waxing, rehydration, antigen retrieval, and blocking as described in **Section 3.2.10**, sections were incubated with primary antibodies overnight at 4 ℃ or 1 h at room temperature. After three washing steps with PBST, the sections were incubated with 2µg SNAP-Surface® Alexa Fluor® 488, SNAP-Surface® Alexa Fluor® 546, SNAP-Surface® Alexa Fluor® 594 or SNAP-Surface® Alexa Fluor® 647 (New Englands Biolabs) labeled Nb anti-IgG-SNAP for 1 h at room temperature, the staining strategy is shown in **Table 3.19**. After three wash steps with PBST and additional washing step with PBS, the sections were mounted with Vectashield antifade mounting medium (H-1200, Vector Laboratories) with 4',6-diamidino-2-phenylindole (DAPI). Finally, the sections were imaged using a DMi8 S Live-cell microscope (Leica Microsystems) using a 100 × oil objective with Instant Computational Clearing method.

Table 3. 19 The strategy of multicolor staining

A#	Anti-EGFR (mouse)	Nb anti-mouse IgG2a Fc-SNAP-488	Nb anti-mouse IgG2a Fc-SNAP-647	Anti-FOLR1	Nb anti - mouse IgG1 Fab-SNAP-546	Nb anti - mouse IgG1 Fab-SNAP-647	Anti-NG2	Nb anti - mouse IgG1 Fc-SNAP-594	Nb anti - mouse IgG1Fc-SNAP-647
A1	+	+	+	+	+	+	+	+	+
A2	-	+	+	+	+	+	+	+	+
A3	+	+	+	-	+	+	+	+	+
A4	+	+	+	+	+	+	-	+	+

A (control)	-	+	+	-	+	+	-	+	+
B#	Anti-EGFR (rabbit)	Nb anti - rabbit IgG Fc-SNAP-488	Nb anti - rabbit IgG Fc-SNAP-647	Anti-HER2	Nb anti - mouse IgG1 Fab-SNAP-546	Nb anti - mouse IgG1 Fab-SNAP-647	Anti-EpCAM	Nb anti - mouse kappa chain-SNAP-594	Nb anti - mouse kappa chain-SNAP-647
B1	+	+	+	+	+	+	+	+	+
B2	-	+	+	+	+	+	+	+	+
B3	+	+	+	-	+	+	+	+	+
B4	+	+	+	+	+	+	-	+	+
B (control)	-	+	+	-	+	+	-	+	+

"+" presents positive staining; "-" presents negative staining.

3.2.12 TSA-based multiplex immunofluorescence staining

Single endometriosis FFPE and tissue microarray (TMA) were from patients in the department of Gynecology and Obstetrics and prepared by the Pathology department (University Hospital Giessen and Marburg). Slides were deparaffinized and rehydrated, and treated with antigen retrieval, endogenous quenched, and blocked as described in the IHC protocol (**Section 3.2.10**). Each primary antibody was paired with a tyramide-conjugated fluorophore (**Table 3.20**). Primary and secondary antibodies were diluted in IHC blocking buffer. Slides were incubated with primary antibodies either overnight at 4 ℃ or for 1 h at room temperature, followed by HRP-conjugated goat anti-mouse IgG (H+L) (1:100, G21040), HRP-conjugated with goat anti-rabbit IgG 1:500, 7074S） or Nbs anti-IgG-HRP (2 μg) secondary antibodies for 1 h at room temperature. After three washes with PBST, the slides were incubated with tyramide-conjugated fluorophore for 10 min at room temperature in the dark. Heat-induced epitope retrieval (HIER) with citrate buffer in a microwave for 15 min was performed between staining rounds to remove antibody cross-activity. Following cooling down and washing, slides were prepared for the next staining round. After finishing the last staining round, slides were mounted with Vectashield antifade mounting medium containing DAPI (H-1200, Vector Laboratories). Images were acquired using Axio Scan.Z1 Slide Scanner (Zeiss) at 20 × magnification, and quantitative digital analysis was performed with Qupath-v0.5.1 software.

Table 3.20 Antibody-tyramide fluorophores pairing strategy

Staining	Target	Dilution	Secondary	Fluorophore	Fluorophore

round			antibody	(catalog #)	dilution
1	ERα	1:300	Nb anti-mouse IgG1 Fab-HRP	iFluor® 430 Styramide (45096)	1:200
2	αSMA	1:500	Nb anti-mouse IgG2a Fc-HRP	Alexa Fluor™ 488 (B40952)	1:100
3	PR	1:800	Nb anti-rabbit IgG Fc-HRP	Alexa Fluor™ 546 (B40954)	1:100
4	CD20	1:500	Nb anti-mouse kappa chain-HRP	Alexa Fluor™ 647 (B40958)	1:100
5	CD31	1:400	Nb anti-mouse IgG1 Fc-HRP	iFluor® 750 Styramide (45065)	1:100

4. Results

4.1 The application of Nb anti-IgG-SNAP in indirect immunofluorescence assays as secondary antibodies

4.1.1 Design and construction of Nb anti-IgG-SNAP fusion proteins

To generate recombinant plasmids encoding Nbs anti-IgG-SNAP, the plasmid pMS-SNAP (a derivative of the pSecTag2 vector) was prepared by removing scFv-425 from the previously established pMS-scFv-425-SNAP construct using SfiI and XbaI-restriction enzymes [107]. This vector contained an internal ribosome entry site (IRES) element [116] to enable bicistronic expression of transfected cells to express enhanced green fluorescent protein (EGFP) independently of the recombinant protein. The expression of the fusion proteins was driven by the cytomegalovirus (CMV) enhancer and promoter, while an immunoglobulin κ leader sequence facilitated secretion into the culture medium. A C-terminal 6 × His-tag downstream of the SNAP-tag allowed for protein enrichment. Five previously established Nbs anti-IgG plasmids [117] were amplified via PCR to generate DNA fragments flanked by SfiI and XbaI-restriction sites. These fragments were inserted into the prepared pMS-SNAP vector between the immunoglobulin κ leader and the SNAP-tag using the same enzymes. The constructions of Nb anti-mouse IgG1 Fab-SNAP, Nb anti-mouse IgG1 Fc-SNAP, Nb anti-mouse IgG2a Fc-SNAP, Nb anti-mouse kappa chain-SNAP and Nb anti-rabbit IgG Fc-SNAP fusion proteins were ultimately achieved (**Figure 4.1**). Successful insertion was confirmed by Sanger Sequencing (Eurofins Genomics, Germany).

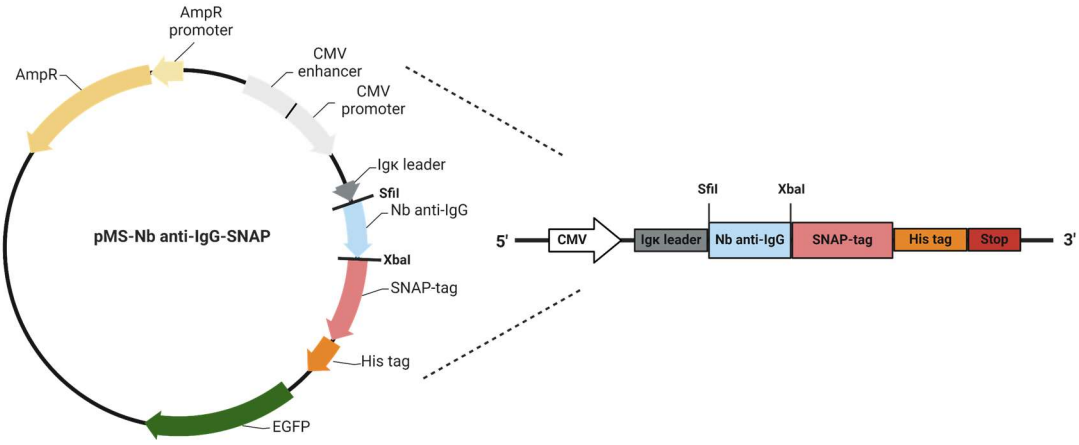

Figure 4.1. Schematic of Nb anti-IgG-SNAP construct design. AmpR: ampicillin resistance; CMV: cytomegalovirus; Igκ leader: immunoglobulin κ leader; His: histidine; EGFP: enhanced green fluorescent protein; Stop: TGA stop codon. Created in https://BioRender.com.

4.1.2 Expression and enrichment of Nb anti-IgG-SNAP fusion proteins

The Nb anti-IgG-SNAP fusion proteins were produced in transfected HEK293T cells. Successful transfection and expression were initially confirmed by monitoring EGFP signals (data not shown). As the constructs were designed for secretion, cell culture supernatants were collected from a triple-layer flask every 5-7 days. The recombinant proteins, which carry a C-terminal 6 × His-tag, were enriched from the supernatant using an Ni-NTA superflow cartridge through IMAC. To evaluate the enrichment efficiency, the SNAP-tag enzymatic activity was tested by conjugating the fusion proteins to SNAP-Surface® Alexa Fluor® 488. After conjugation, samples were analyzed via SDS gel electrophoresis, and the 488-fluorescence signal was detected using ChemiDoc XRS+ System, confirming the presence of the fusion proteins and the activity of the SNAP-tag. Gels were subsequently stained with Coomassie brilliant blue to visualize the proteins. As shown in **Figure 4.2**, the purification of Nb anti-mouse IgG1 Fc-SNAP is provided as a representative example. During the IMAC process, a stepwise imidazole elution was performed using 10 mM (E1), 40 mM (E2) and 250 mM (E3, E4) imidazole concentration. All fractions, including the filtered supernatant, flowthrough, and elution fractions, were conjugated with SNAP-Surface® Alexa Fluor® 488 prior to SDS-PAGE analysis. The filtered supernatant showed a weak fluorescence signal, whereas no signal was observed in the flowthrough, indicating complete binding of the fusion proteins to the Ni-NTA column.

Elution fraction E1 resembled the flowthrough with negligible protein presence, while E2 showed minimal fluorescence signal. In contrast, E3 fraction exhibited a strong fluorescence signal, despite loading only 3 µl compared to 10 µl for other fractions. This indicates that the target protein was

efficiently eluted in E3. Fraction E4, also eluted with 250 mM imidazole, showed no detectable signal, confirming that the bulk of the proteins had been obtained in E3 (**Figure 4.2a**). Coomassie brilliant blue staining (**Figure 4.2b**) corroborated the fluorescence results, showing the Nb anti-mouse IgG1 Fc-SNAP fusion protein was mostly in E3. The same purification and validation workflow was successfully applied to other Nbs anti-IgG-SNAP fusion proteins, including Nb anti-mouse IgG1 Fab-SNAP, Nb anti-mouse IgG2a Fc-SNAP, Nb anti-mouse kappa chain-SNAP and Nb anti-rabbit IgG Fc-SNAP. These results are shown in **Supplementary Figure 1**.

Following the purification, the elution buffer was exchanged to PBS using Zeba™ Spin Desalting columns. The HEK293T-based mammalian expression system enabled rapid protein production, yielding up to 5 mg/L from the cell culture medium.

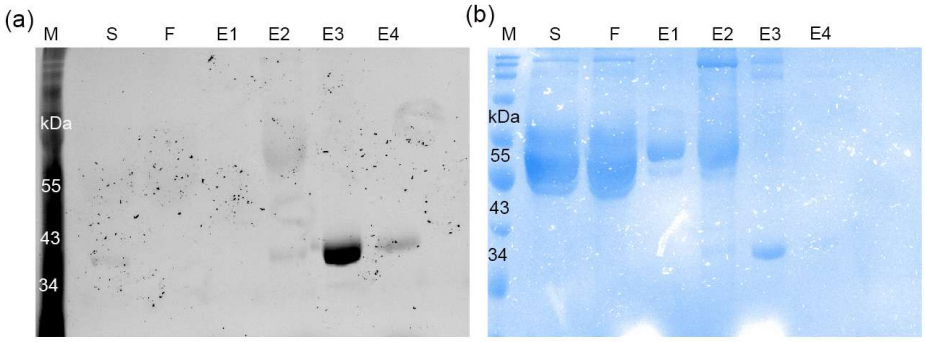

Figure 4.2. Enrichment of Nb anti-IgG1 Fc-SNAP. All fractions were collected during enrichment, then conjugated to SNAP-Surface® Alexa Fluor® 488 followed SDS-PAGE protein separation. (a) Fluorescence visualization of 488 labelled fusion protein. (b) Visualization of the corresponding SDS-PAGE in Coomassie brilliant blue staining. SDS gel was imaged by ChemiDoc XRS+ System. M: Blue prestained protein standard broad range (11-250 kDa); S: filtered supernatant; F: flowthrough; E1: protein eluted in 10 mM imidazole; E2: protein eluted in 40 mM imidazole; E3 and E4: protein eluted in 250 mM imidazole.

4.1.3 Conjugation of Nbs anti-IgG-SNAP fusion proteins with BG-fluorescence substrates

After the successful enrichment and validation of SNAP-tag self-labeling, all five Nbs anti-IgG-SNAP fusion proteins were conjugated with the fluorescence substrates SNAP-Surface® Alexa Fluor® 647 for use in IFA. The fusion proteins were incubated with the dye at 1:2 molar ratio at room temperature for 2 h in the dark. To confirm labeling efficiency and saturation of the SNAP-tag, the Alexa Fluor® 647-labeled nanobodies were subsequently incubated with SNAP-Surface® Alexa Fluor® 488. As shown in **Figure 4.3a,** no 488-fluorescence signal was detected on the ChemiDoc XRS+, indicating that SNAP-tags were fully occupied by Alexa Fluor® 647 and could no longer bind to Alexa Fluor® 488. This result confirms complete and efficient conjugation of the SNAP-tag with the initial fluorophore. Further validation was performed using the Odyssey DLx Imager, which revealed strong red fluorescence signals corresponding to Alexa Fluor® 647-labeled fusion proteins on the SDS-PAGE

gel (**Figure 4.3b**). To verify protein presence and integrity, the same gel was stained with Coomassie brilliant blue, confirming the presence of all five Nbs anti-IgG-SNAP-647 fusion proteins (**Figure 4.3c**).

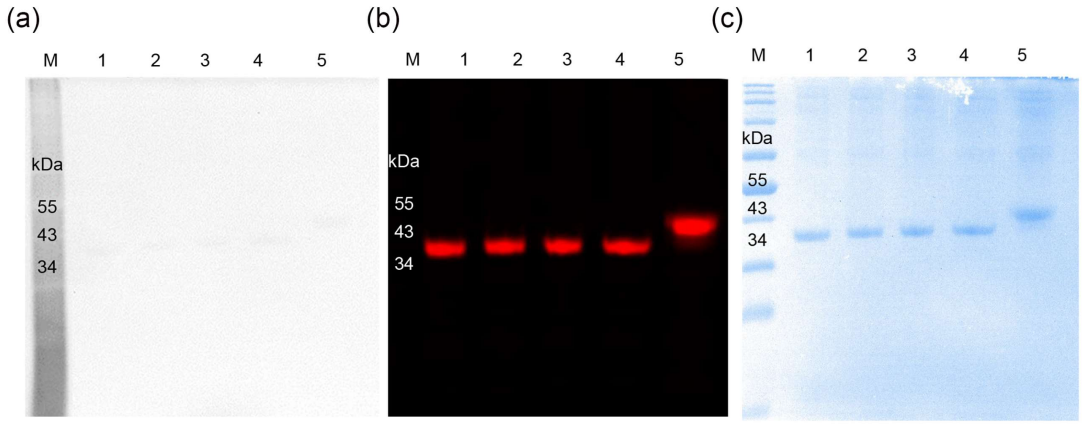

Figure 4.3. Nbs anti-IgG-SNAP labeled with SNAP-Surface® Alexa Fluor® 647. (**a**) Nbs anti-IgG-SNAP-647 were post-incubated with SNAP-Surface® Alexa Fluor® 488 and imaged by ChemiDoc XRS+ System. (**b**) Nbs anti-IgG-SNAP-647 were visualized by Odyssey DLx Imager. (**c**) The corresponding bands of Nbs anti-IgG-SNAP-647 on SDS-PAGE in Coomassie brilliant blue staining. Lane 1: Nb anti-mouse IgG1 Fab-SNAP-647; Lane 2: Nb anti-mouse IgG1 Fc-SNAP-647; Lane 3: Nb anti-mouse IgG2a Fc-SNAP-647; Lane 4: Nb anti-mouse kappa chain-SNAP-647; Lane 5: Nb anti-rabbit IgG Fc-SNAP-647.

4.1.4 The specific binding of Nb anti-IgG-SNAP fusion proteins in fluorescence Western blot

Once the Nbs anti-IgG-SNAP were conjugated to Surface® Alexa Fluor® 647, their subclass specificity toward primary antibodies was evaluated using fluorescence Western blot (**Figure 4.4**). The isotypes of primary antibodies used in this study is listed in **Table 3.3**. For comparison, commercial secondary antibodies, anti-mouse IgG (H+L) conjugated Alexa Fluor 647 and anti-rabbit IgG(H+L) conjugated Alexa Fluor 647 were included as controls. As shows in the **Table 3.3**, anti-EpCAM, anti-NG2, anti-HER2 and anti-FOLR1 antibodies belong to the mouse IgG1 subtype, while anti-EGFR is mouse IgG2a. **Figure 4.4** demonstrates that Nb anti-mouse IgG1 Fab-SNAP-647 and Nb anti-mouse IgG1 Fc-SNAP-647 bind to anti-EpCAM (IgG1, kappa), anti-NG2 (IgG1, kappa), anti-HER2 (IgG1) and anti-FOLR1 (IgG1), but do not bind to anti-EGFR (IgG2a). Conversely, Nb anti-mouse IgG2a Fc-SNAP-647 specifically detects anti-EGFR (IgG2a), and not the IgG1 antibodies.

Nb anti-mouse kappa chain-SNAP-647 shows broader specificity, recognizing all mouse-derived primary antibodies used in this study, including both IgG1 and IgG2a subclasses. This indicates that the kappa-specific nanobody targets the light chain common to all mouse antibodies tested.

Furthermore, Nb anti-rabbit IgG Fc-SNAP-647 selectively binds rabbit-derived primary antibodies, anti-ANK3, anti-CTNNB1, and anti-EGFR, demonstrating its species specificity.

Overall, these results confirm that each Nb anti-mouse or anti-rabbit IgG-SNAP-647 conjugate exhibits subclass or species-specific binding consistent with their design. Importantly, the specificity profiles of these nanobody-based secondary reagents mirror those of commercial Alexa Fluor 647-conjugated secondary antibodies, as illustrated in **Figure 4.4**.

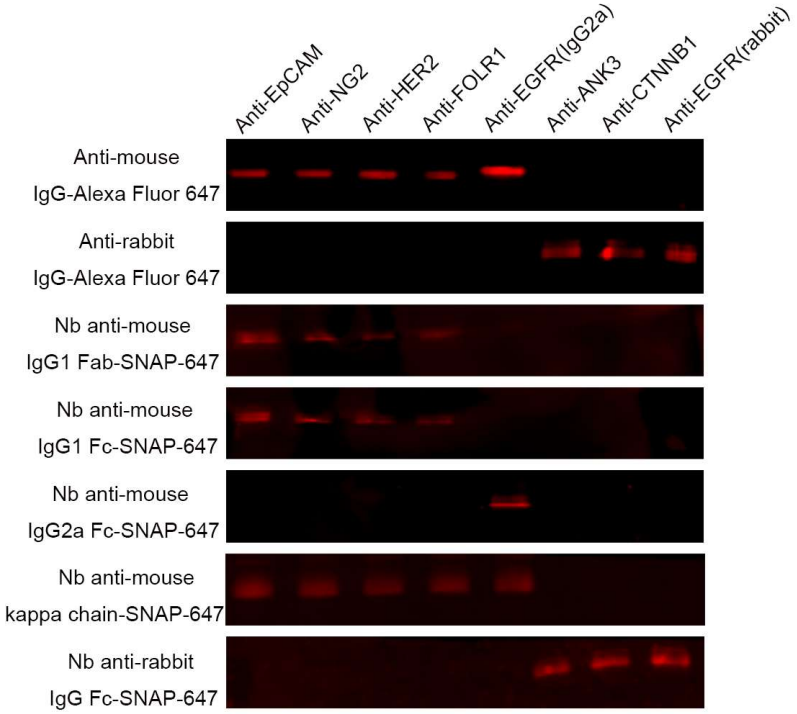

Figure 4.4. Fluorescence Western blot analysis of Nb anti-IgG-SNAP fusion proteins binding-specificity. Different subtypes mouse- and rabbit-derived primary antibodies were loaded on SDS-PAGE gel then transferred onto PVDF membranes, and probed by anti-mouse IgG-Alexa Fluor 647, anti-rabbit IgG-Alexa Fluor 647, Nb anti-mouse IgG1 Fab-SNAP-647, Nb anti-mouse IgG1 Fc-SNAP-647, Nb anti-mouse IgG2a Fc-SNAP-647, Nb anti-mouse kappa chain-SNAP-647 and Nb anti-rabbit IgG Fc-SNAP-647, separately. All membranes were imaged under Odyssey DLx Imager. Subtypes of primary antibodies: anti-EpCAM (mouse/ IgG1, kappa); anti-NG2 (mouse/ IgG1, kappa); anti-HER2 (mouse/ IgG1); anti-FOLR1 (mouse/ IgG1); anti-EGFR (mouse/ IgG2a); anti-ANK3 (rabbit / IgG); anti-CTNNB1 (rabbit / IgG); anti-EGFR (rabbit / IgG).

4.1.5 The application of Nbs anti-IgG-SNAP nanobody fusion proteins for flow cytometry as secondary antibodies.

After confirming the specific binding of Nbs anti-IgG-SNAP-647 in fluorescence Western blot analysis,

the utility of these labeled fusion proteins as secondary antibodies was further assessed in flow cytometry for IFA. Both commercial secondary antibodies and our Nbs anti-IgG-SNAP-647 were used to detect the same panel of primary antibodies tested in fluorescence Western blot, across various cell lines expressing different levels of the targeted antigens (**Table 4.1** and **4.2**). Initially, breast cancer cell lines (MDA-MB-231, MDA-MB-468, Hs578T, MCF-7, MDA-MB-453) were stained with primary antibodies targeting EpCAM, NG2, EGFR, ANK3 and CTNNB1. **Figure 4.5** displays the expression profiles of EpCAM (IgG1, kappa) and NG2 (IgG1, kappa) detected using goat anti-mouse IgG-Alexa Fluor 647, Nb anti-mouse IgG1 Fab-SNAP-647, Nb anti-mouse IgG1 Fc-SNAP-647, and Nb anti-mouse kappa chain-SNAP-647. High EpCAM expression was observed in MDA-MB-468, MDA-MB-453, and MCF-7, while MDA-MB-231 showed weak expression, and Hs578T showed minimal signal (**Figure 4.5a**). Conversely, NG2 expression was prominent only in Hs578T, with negligible staining in the remaining lines (**Figure 4.5b**).

EGFR expression (IgG2a) was analyzed using goat anti-mouse IgG-Alexa Fluor 647, Nb anti-mouse IgG2a Fc-SNAP-647, and Nb anti-mouse kappa chain-SNAP-647 (**Figure 4.6**). EGFR was highly expressed in MDA-MB-468 and MDA-MB-231, moderately expressed in Hs578T, minimally expressed in MCF-7, and nearly absent in MDA-MB-453. In **Figure 4.7**, all five breast cell lines stained positively for ANK3 and CTNNB1(rabbit-derived) using both goat anti-rabbit IgG-Alexa Fluor 647 and Nb anti-rabbit IgG Fc-SNAP-647, confirming effective detection of rabbit primary antibodies. To further evaluate specificity, endometrial cell lines (49Z, 12Z, Ishikawa, T-HESC) were examined (**Figure 4.8)**. EGFR (mouse IgG2a or rabbit IgG) was detected in all endometrial cell lines using both commercial and Nb-based secondary antibodies. Anti-FOLR1 (IgG1) and anti-EpCAM (IgG1, kappa) showed strong staining exclusively in Ishikawa cells, when detected using goat anti-mouse IgG-Alexa Fluor 647, Nb anti-mouse IgG1 Fab-SNAP-647, and Nb anti-mouse kappa chain-SNAP-647. In contrast, anti-NG2 (IgG1, kappa) expression was observed in 49Z, 12Z and T-HESC, but not in Ishikawa, when detected using goat anti-mouse IgG-Alexa Fluor 647 and Nb anti-mouse IgG1 Fc-SNAP-647. HER2 (IgG1) was expressed by all endometrial cell lines and was successfully detected using goat anti-mouse IgG-Alexa Fluor 647 and Nb anti-mouse IgG1 Fab-SNAP-647. These results collectively demonstrate that Nbs anti-IgG-SNAP exhibited antigen detection in flow cytometry assays

that is comparable to that of commercial secondary antibodies.

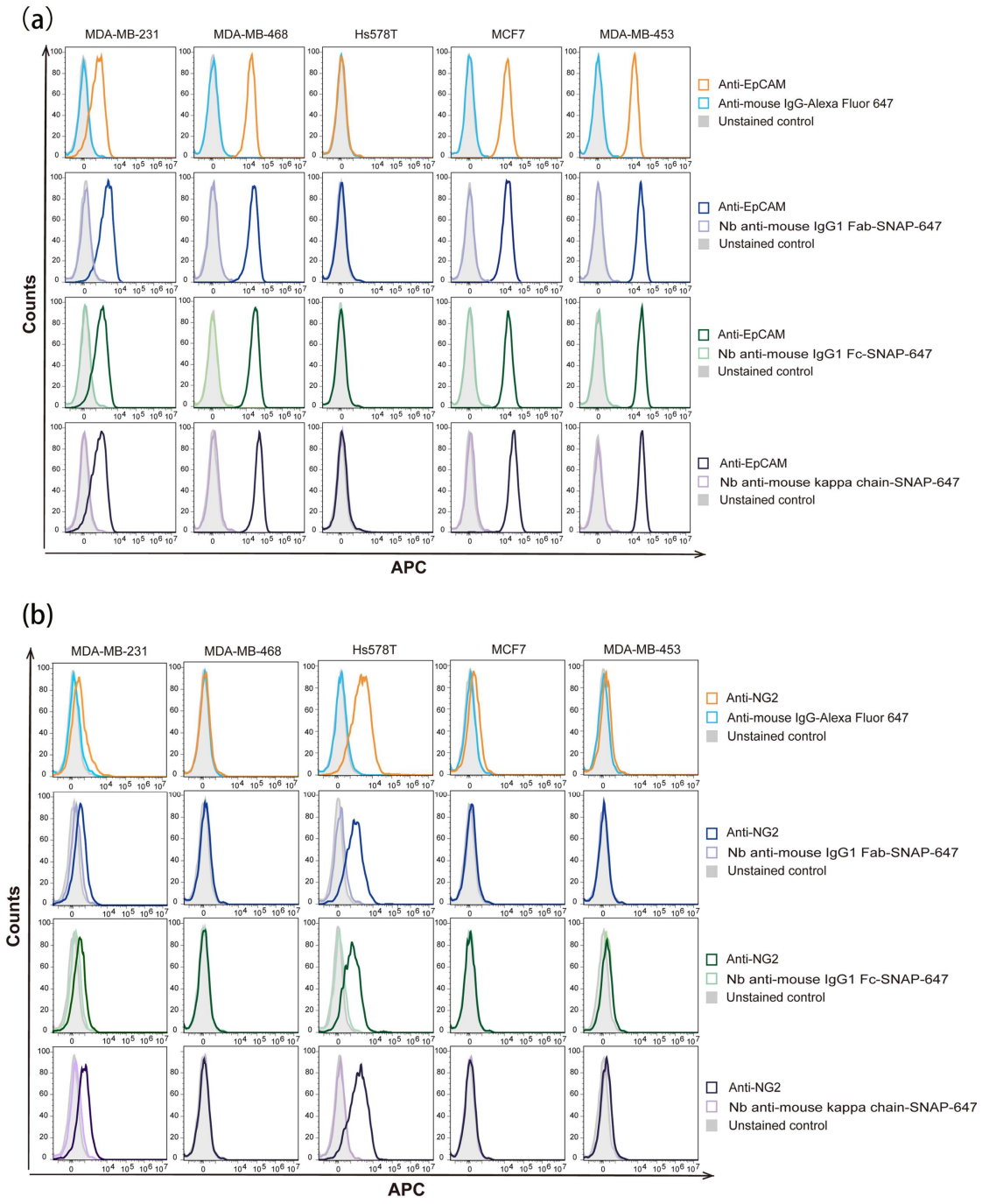

Figure 4.5. Flow cytometry analysis with Nbs anti-IgG-SNAP in breast cancer cell lines. (a) Cells were incubated with anti-EpCAM; (b) Cells were incubated with anti-NG2. Anti-EpCAM and anti-NG2 were detected with goat anti-mouse IgG-Alexa Fluor 647, Nb anti-mouse IgG1 Fab-SNAP-647, Nb anti-mouse IgG1 Fc-SNAP-647 and Nb anti-mouse kappa chain-SNAP-647.

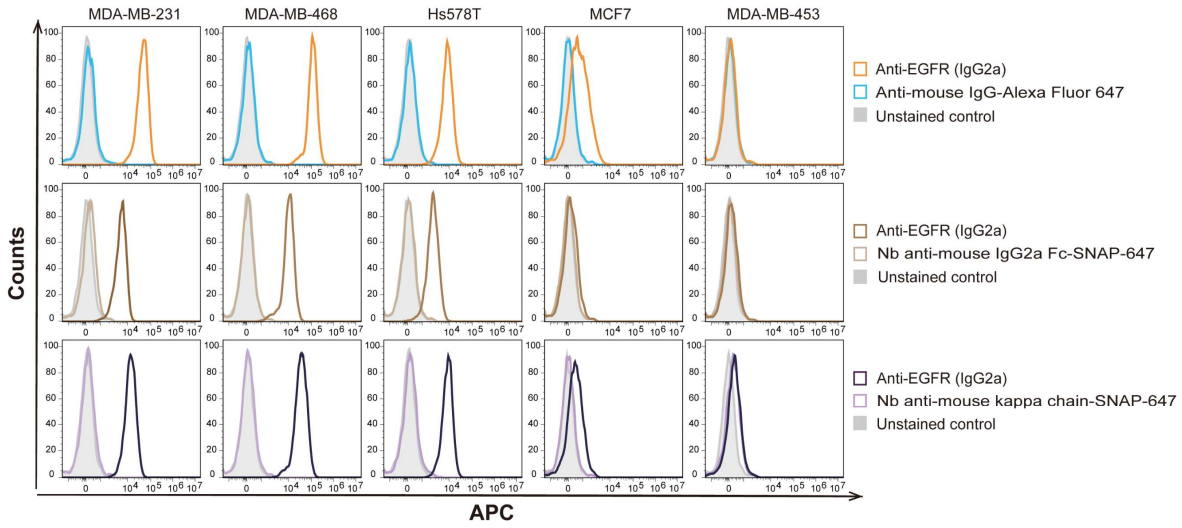

Figure 4.6. Flow cytometry analysis with Nbs anti-IgG-SNAP in breast cancer cell lines. Cells were incubated with anti-EGFR (IgG2a), then detected with goat anti-mouse IgG-Alexa Fluor 647, Nb anti-mouse IgG2a Fc-SNAP-647 and Nb anti-mouse kappa chain-SNAP-647.

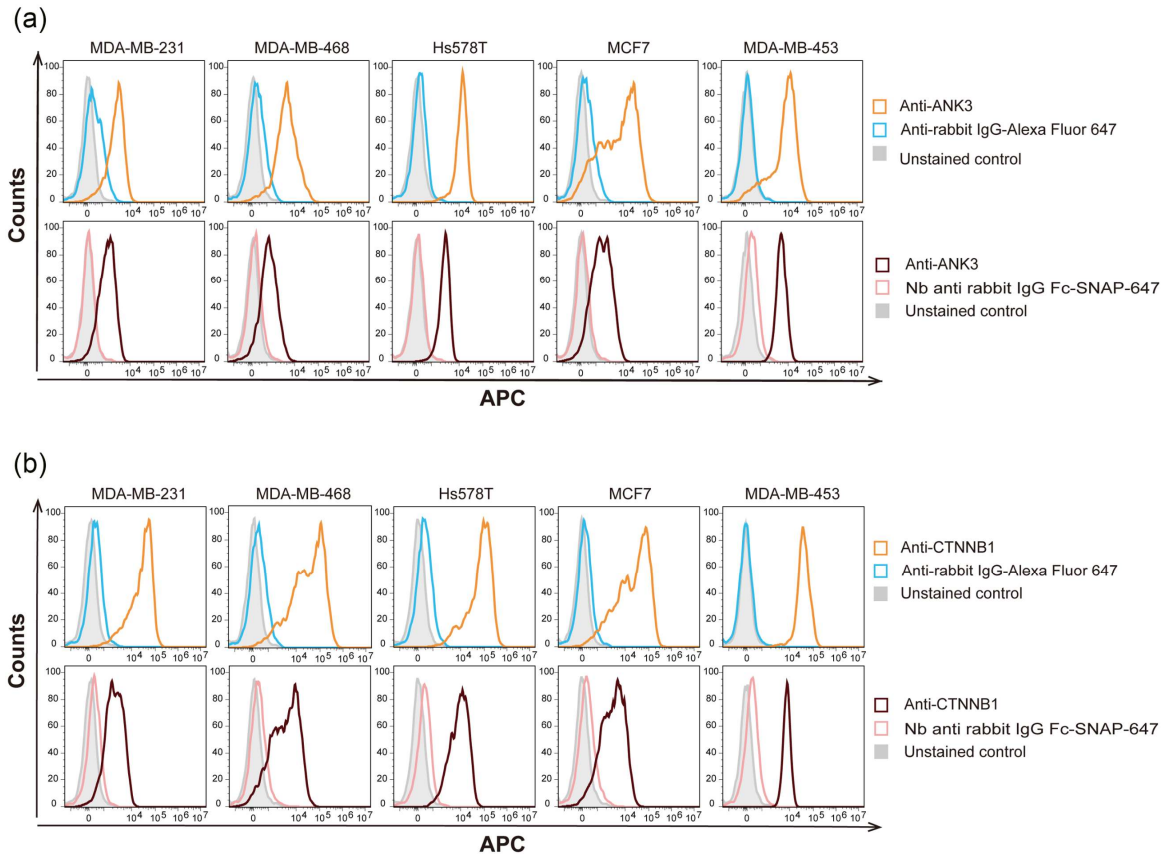

Figure 4.7. Flow cytometry analysis with Nbs anti-IgG-SNAP in breast cancer cell lines. (a) Cells were incubated with anti-ANK3; (b) Cells were incubated with anti-CTNNB1. Anti-ANK3 and anti-CTNNB1 were detected with

goat anti-mouse IgG-Alexa Fluor 647 and Nb anti-rabbit IgG Fc-SNAP-647.

Table 4.1 Different antigens expressed levels in breast cancer cell lines

	MDA-MB-231	MDA-MB-468	Hs578T	MCF-7	MDA-MB-453
EpCAM	low	medium	low	high	high
NG2	medium	low	high	low	low
EGFR	high	high	medium	low	low
ANK3	medium	medium	high	medium	high
CTNNB1	medium	medium	high	medium	high

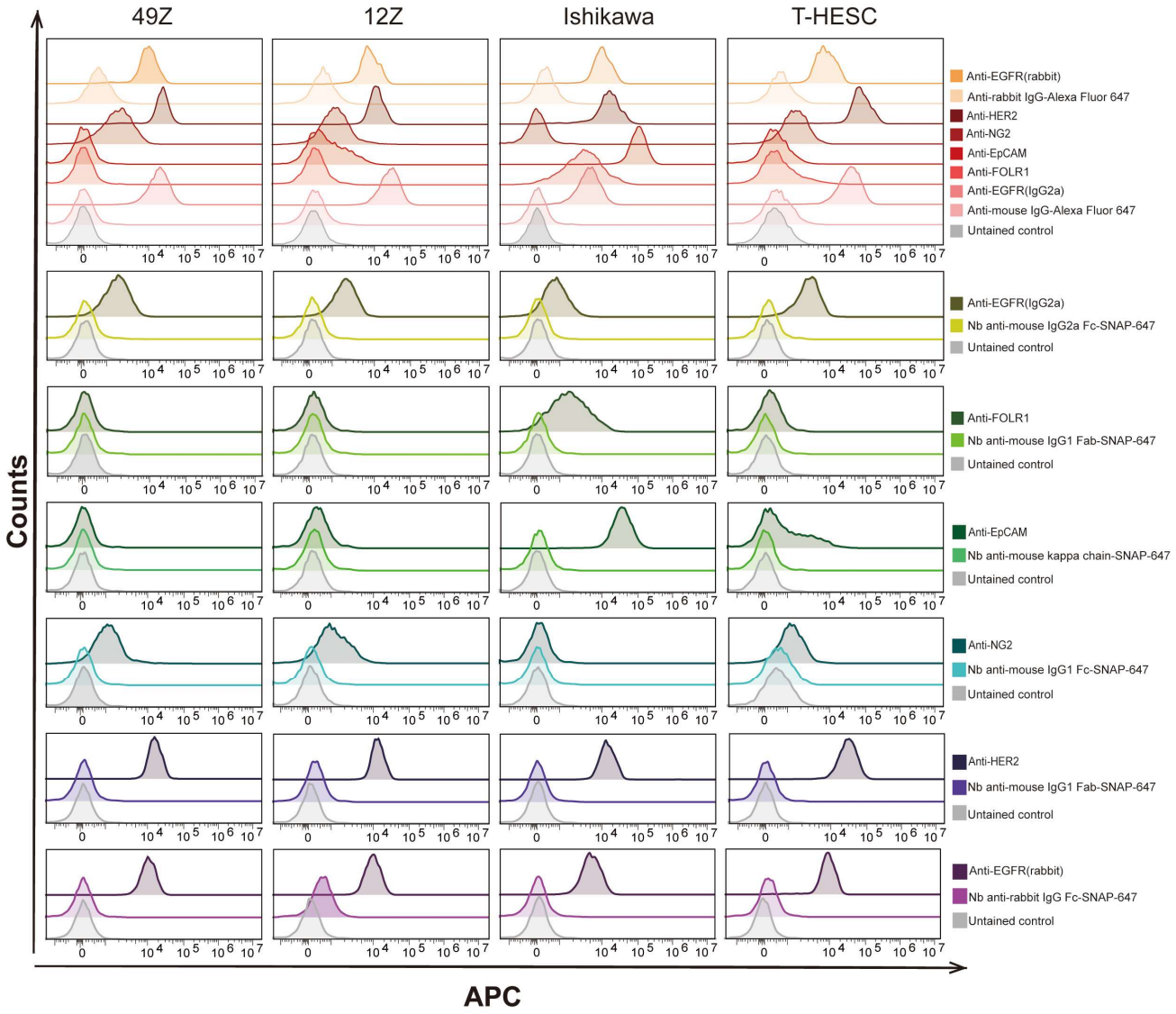

Figure 4.8. Flow cytometry analysis with Nbs anti-IgG-SNAP in endometrial cell lines. Cells were incubated

with anti-EGFR, anti-FOLR1, anti-EpCAM, anti-NG2 and anti-HER2, then detected with Surface®Alexa Fluor® 647-labeled Nbs anti-IgG-SNAP or corresponding commercial antibodies.

Table 4.2 Different antigens expressed levels in endometrial cell lines

	49Z	12Z	Ishikawa	T-HESC
EGFR	high	high	high	high
HER2	high	high	high	high
NG2	medium	medium	low	medium
EpCAM	low	low	high	low
FOLR1	low	low	high	low

4.1.6 The application of Nb anti-IgG-SNAP fusion proteins for fluorescence microscopy as secondary antibodies.

Following their successful application in flow cytometry, the Nbs anti-IgG-SNAP-647 conjugates were further evaluated for their utility in fluorescence microscopy. To validate their specific binding capacity and explore their potential as secondary antibodies in imaging applications, the same experimental conditions used in flow cytometry were applied. Here, breast cancer and endometriosis cell lines were fixed, incubated with the same panel of primary antibodies, and subsequently stained using either Alexa Fluor 647-labeled commercial secondary antibodies or the corresponding Nbs anti-IgG-SNAP, as described in **Section 4.1.5**. The stained cells were visualized using fluorescence microscopy to assess the localization and distribution of target proteins. Consistent with the flow cytometry results, the Nb-based secondary antibodies produced strong fluorescence signals with high specificity, closely matching the performance of their commercial counterparts (**Figure 4.7-4.12**). These results reinforce the ability of Nbs anti-IgG-SNAP to selectively recognize mouse and rabbit primary antibodies, and importantly, to distinguish between antibody subclasses within the same species, particularly among mouse IgG subclasses. Overall, the combined results from flow cytometry and fluorescence microscopy demonstrate the robustness and specificity of Nbs anti-IgG-SNAP-647 conjugates. These findings underscore their potential for use in multi-color immunofluorescence staining and broader

imaging applications in future research.

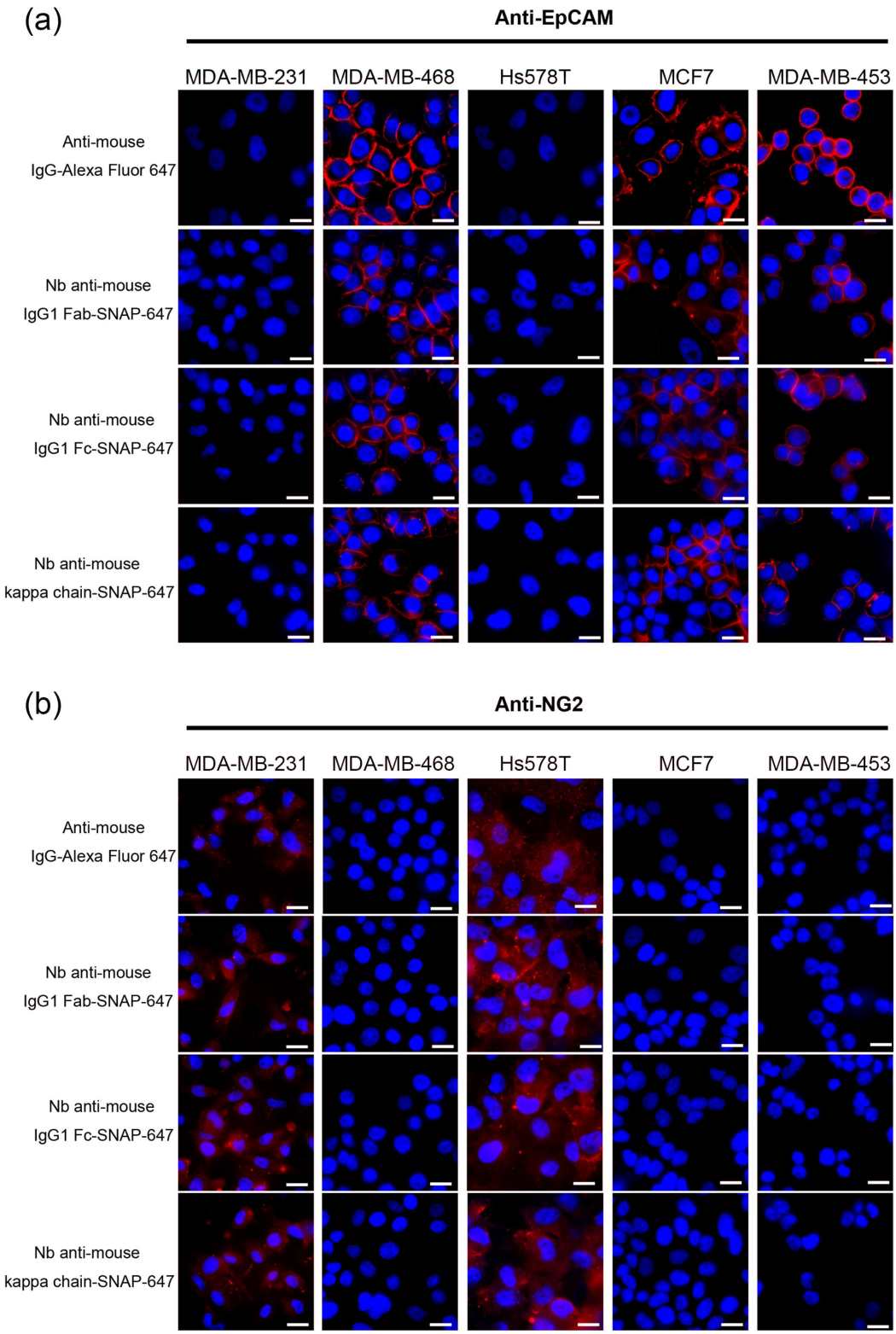

Figure 4.9. The specific binding of Nbs anti-IgG-SNAP was visualized by fluorescence microscope on breast cancer cells. (a) Cells were incubated with anti-EpCAM (IgG1, kappa); (b) Cells were incubated with anti-NG2 (IgG1, kappa). Then these primary antibodies were incubated with goat anti-mouse IgG-Alexa Fluor 647, Nb anti-

mouse IgG1 Fab-SNAP-647, Nb anti-mouse IgG1 Fc-SNAP-647 or Nb anti-mouse kappa chain-SNAP-647. The red signal represents 647 fluorescence signal; blue signal represents nuclear counterstain with Hoechst 33342. The scale bar is 20 µm.

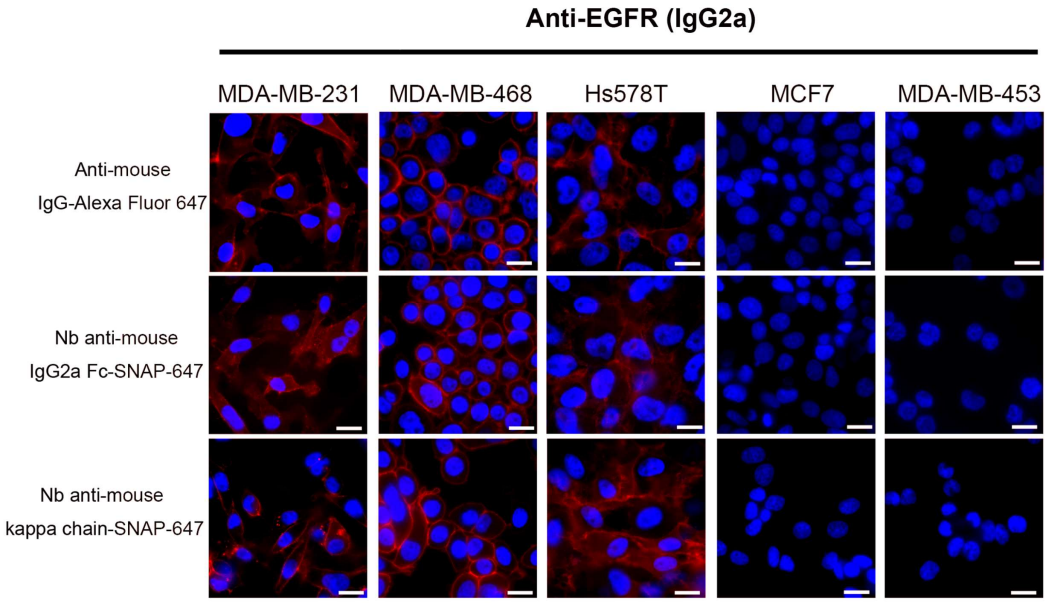

Figure 4.10. The specific binding of Nbs anti-IgG-SNAP was visualized by fluorescence microscopy. Primary antibodies targeting EGFR (IgG2a) were incubated with five different breast cancer cells followed by detecting with goat anti-mouse IgG-Alexa Fluor 647, Nb anti-mouse IgG2a Fc-SNAP-647 or Nb anti-mouse kappa chain-SNAP-647. The red signal represents 647 channel; blue signal was nuclear counterstain with Hochest 33342. The scale bar is 20 µm.

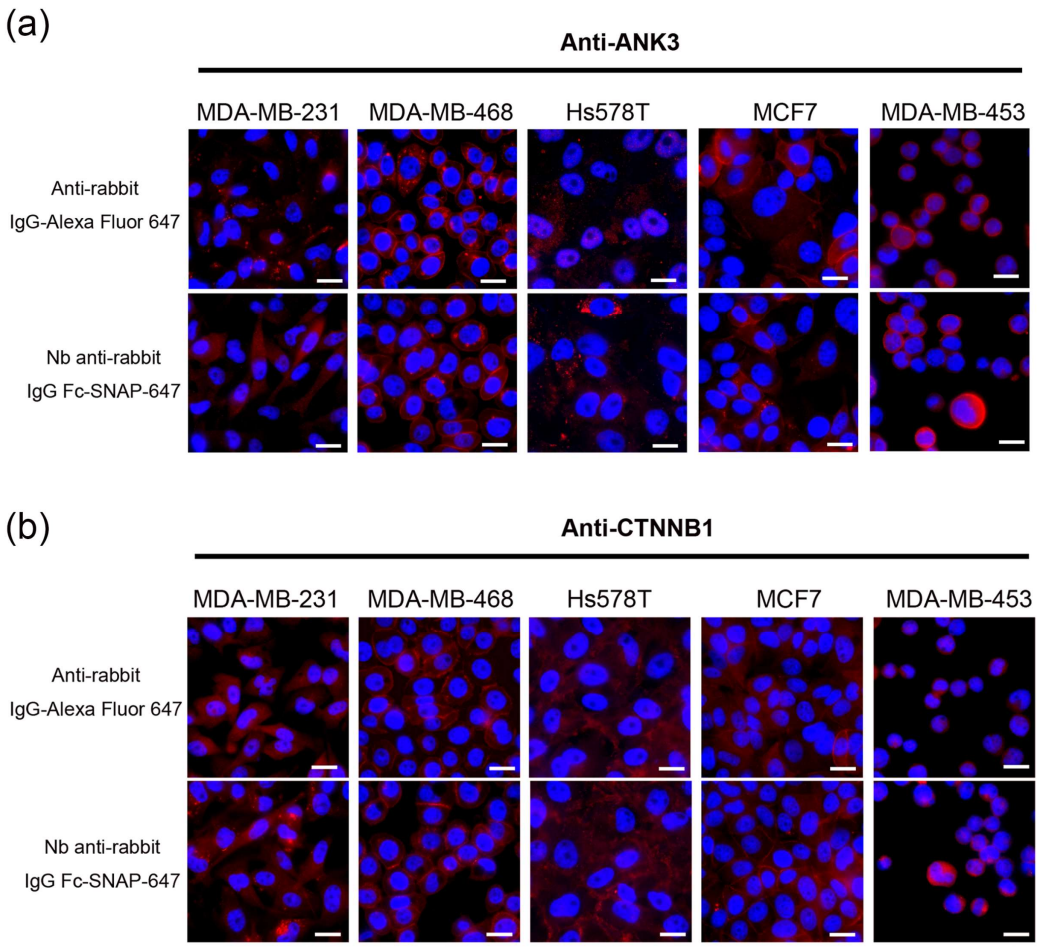

Figure 4.11. The specific binding of Nbs anti-IgG-SNAP was visualized by fluorescence microscope on breast cancer cells. (a) Cells were incubated with anti-ANK3 (rabbit, IgG); (b) Cells were incubated with anti-CTNNB1 (rabbit, IgG). Then these primary antibodies were incubated with either goat anti-rabbit IgG-Alexa Fluor 647 or Nb anti-rabbit IgG Fc-SNAP-647. The red signal represents 647 fluorescence signal; blue signal represents nuclear counterstain with Hoechst 33342. The scale bar is 20 μm.

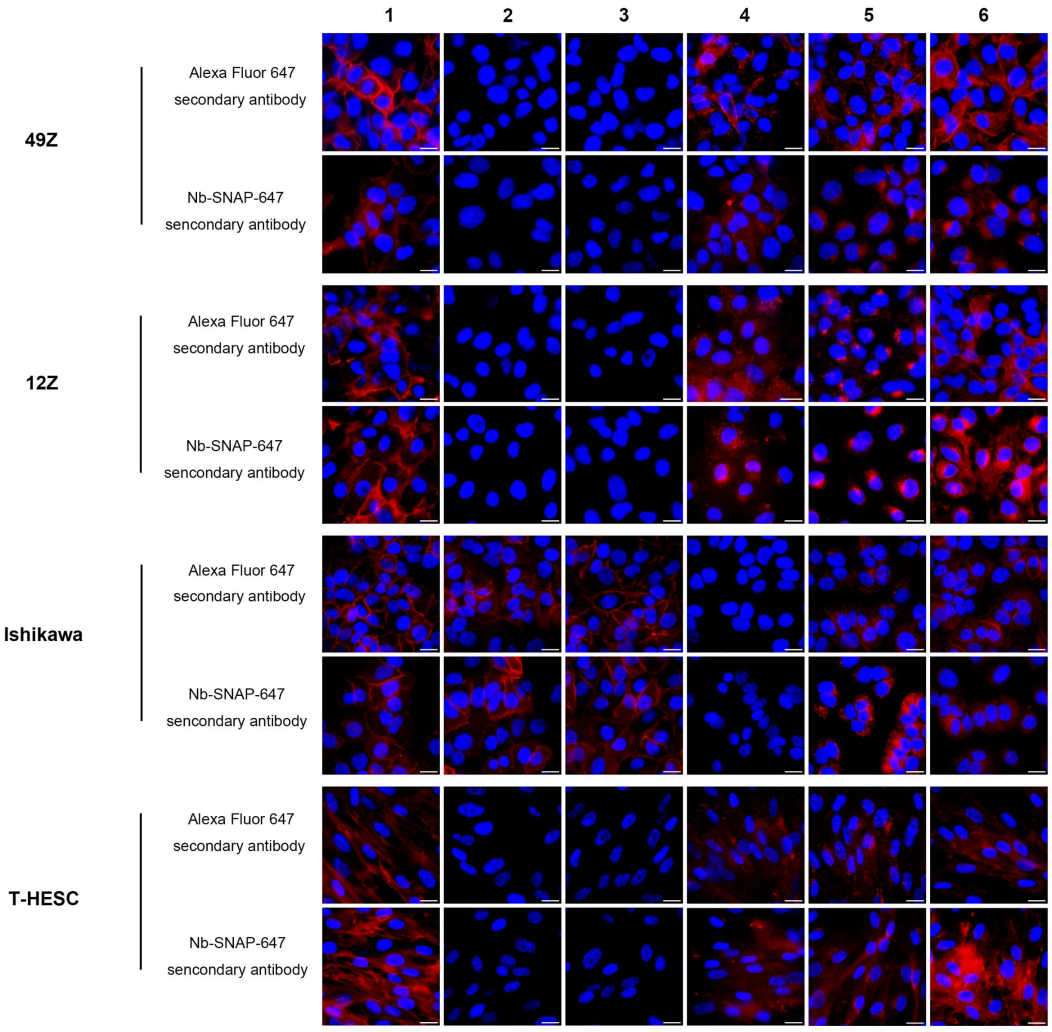

Figure 4.12. The specific binding of Nbs anti-IgG-SNAP visualized by fluorescence microscope on endometrial cells. Primary antibodies targeting EGFR, FOLR1, EpCAM, NG2 and HER2 were incubated with four different endometrial cell lines followed by detecting with either commercial secondary antibodies conjugated with Alexa Fluor 647 or Nbs anti-IgG-SNAP- Alexa Fluor® 647. The red signal represents 647 channel, blue signal is nuclear counterstain with Hoechst 33342. Lane1: anti-EGFR (IgG2a) antibody; Lane 2: anti-FOLR1 (IgG1) antibody; Lane 3: anti-EpCAM (IgG1, kappa) antibody; Lane 4: anti-NG2 (IgG1, kappa) antibody; Lane 5: anti-HER2 (IgG1) antibody; Lane 6: anti-EGFR (rabbit) antibody. The scale bar is 20 μm.

4.1.7 Multicolor immunofluorescence in cell block

Before multi-color fluorescence staining of cell block section, the expression levels of EGFR, FOLR1, EpCAM, NG2 and HER2 were evaluated using IHC and quantified semi-quantitatively via the IHC profiler plug （ImageJ） [119]. As in shown **Figure 4.13**, all endometrial cells were identified as EGFR-positive and HER2-positive. NG2 expression was detected in all three cell types except

Ishikawa. In contrast, strong staining for EpCAM and FOLR1 was observed exclusively in Ishikawa cells.

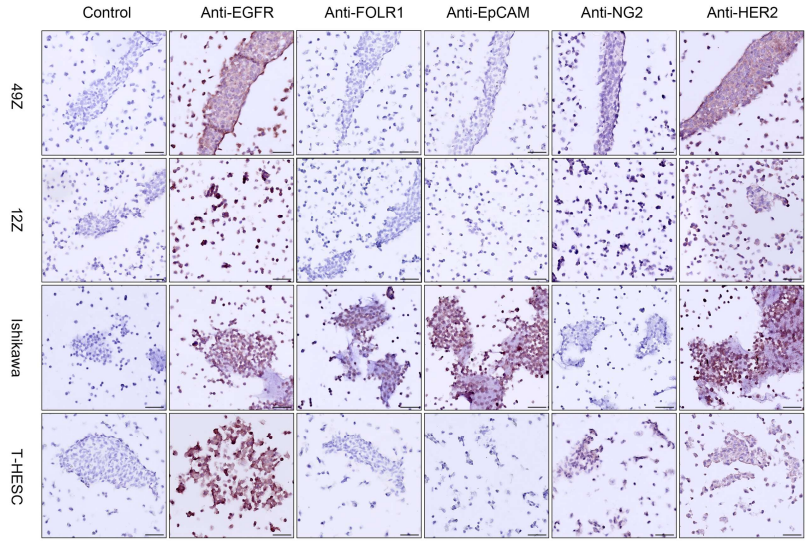

Figure 4.13. IHC images of endometrial cell block (49Z, 12Z, Ishikawa and T-HESC) stained with anti-EGFR, anti-FOLR1, anti-EpCAM, anti-NG2, and anti-HER2 separately. EGFR and HER2 were both positive (brown signal) in all cells. EpCAM and FOLR1 were only positive in Ishikawa. NG2 was positive in 49Z, 12Z. The scale bar is 50 μm.

For multi-color immunofluorescence staining, Nbs anti-IgG-SNAP were labeled with various SNAP-Surface® Alexa Fluor® dyes to serve as secondary antibodies. It was previously confirmed that Nbs anti-IgG-SNAP could be fully conjugated with Surface® Alexa Fluor® 647 at a 1:2 molar ratio. Using this approach, Nbs anti-IgG-SNAP were successfully conjugated with SNAP-Surface® Alexa Fluor® 488, SNAP-Surface® Alexa Fluor® 546, and SNAP-Surface® Alexa Fluor® 594, respectively. A staining protocol was developed using panel A and panel B, targeting EGFR, FOLR1, EpCAM, NG2 and HER2 **(Table 3.19)**. The binding activity of Alexa Fluor® 647-conjugated Nbs anti-IgG-SNAP and potential cross-reactivity were evaluated using leave-one-out control stains. Panel A served as an example for this analysis. In the first staining round, slide A1 was incubated with anti-EGFR (IgG2a) and detected using Nb anti-mouse IgG2a Fc-SNAP-488. To assess remaining binding activity, the slide was further stained with Nb anti-mouse IgG2a Fc-SNAP-647. In the second staining round, A1 was incubated with anti-FOLR1 (IgG1), detected using Nb anti-mouse IgG1 Fab-SNAP-546, and subsequently stained with Nb anti-mouse IgG1 Fab-SNAP-647 to evaluate remaining binding activity. In the third round, A1 was stained with anti-NG2 (IgG1, kappa) followed by sequential staining with

Nb anti-mouse IgG1 Fc-SNAP-594 and Nb anti-mouse IgG1 Fc-SNAP-647. The fully stained slide A1 was imaged using the DMi8 S Live-cell microscope, as illustrated in **Figure 4.14a**. Leave-one-out control staining was conducted on slides A2, A3, and A4 to assess cross-reactivity. Each slide was incubated with all primary antibodies and Alexa Fluor® dye-labeled Nbs anti-IgG-SNAP from panel A, except for one excluded primary antibody per slide. Specifically, slide A2 anti-EGFR (IgG2a) was excluded (**Figure 4.14b**); slide A3 anti-FOLR1 was excluded (**Figure 4.14c**); slide A4 anti-NG2 was excluded (**Figure 4.14d**). Additionally, a control slide (A control, **Figure 4.14e**) was incubated with Alexa Fluor dyes labeled Nbs anti-IgG-SNAP without any primary antibodies of panel A to measure the background signal.

A similar protocol was applied for panel B, using anti-EGFR (rabbit), anti-HER2 (IgG1), and anti-EpCAM (IgG1, kappa). These primary antibodies were detected using Nb anti-rabbit IgG Fc-SNAP-488, Nb anti-mouse IgG1 Fab-SNAP-546 and Nb anti-mouse kappa chain-SNAP-594, respectively. To confirm binding activity, final post-incubation with Nb anti-rabbit IgG Fc-SNAP-647, Nb anti-mouse IgG1 Fab-SNAP-647, or Nb anti-mouse kappa chain-SNAP-647 was performed. For panel B, all antibodies of panel B were used to stain slide B1; slides B2, B3 and B4 were subjected to leave-one-out stains (**Figure 4.15a-d**). A control slide (slide B) was used to measure the background signals (**Figure 4.15e**). The multi-color fluorescence staining results for both panel A and panel B were summarized in **Table 4.3**.

The mean fluorescence intensity for each channel was analyzed using ImageJ software. In panel A, **Figure 4.14f-i** illustrates the detection of anti-EGFR (IgG2a)-488 (red) and anti-NG2-594 (magenta) signals, while no signal was observed for anti-FOLR1-546 (green) or Nbs anti-IgG-SNAP-647 (yellow) in 49Z of panel A. Similarly, in panel B (**Figure 4.15f-i**), anti-EGFR (rabbit)-488 (red) and anti-HER2-546 (green) were detected, whereas anti-EpCAM-594 (magenta) and Nbs anti-IgG-SNAP-647 (yellow) showed no signal in 49Z. The fluorescence intensity profiles of leave-one-out control stains and background signals (slides A control and B control) are shown in **Figures 4.14j** and **4.15j**. These profiles confirm the absence of cross-reactivity among Alexa Fluor® dye-labeled Nbs anti-IgG-SNAP in the multi-color immunofluorescence staining process.

As we confirmed that, there was no cross-reactivity in either the leave-one-out control stains or the

Nbs anti-IgG-SNAP-647 post-incubation, fluorescence intensities of A (control), B (control), A1, and B1 were analyzed using corrected total cell fluorescence (CTCF) by ImageJ software. This analysis allows statistical comparisons between A (control) and A1, as well as B (control) and B1 (**Figure 4.16**). Specifically, in the Alexa Fluor 488 channel (red), significant differences in fluorescence intensities of anti-EGFR (IgG2a) and anti-EGFR (rabbit) were observed compared to the control. For the Alexa Fluor 546 channel (green), anti-FOLR1 from panel A exhibited a difference only in Ishikawa cells, whereas all endometrial cells displayed high fluorescence intensities of anti-HER2 in panel B. In the Alexa Fluor 594 channel (magenta), 49Z, 12Z and T-HESC exhibited a considerable difference with anti-NG2 in panel A, whereas Ishikawa cells displayed a distinguishable difference with anti-EpCAM in panel B. No obvious binding signals were observed in the Alexa Fluor 647 channel (yellow) for either panel A or panel B. The CTCF analysis confirmed findings from flow cytometry, fluorescence microscopy, and IHC, validating the specificity and reliability of the multi-color immunofluorescence staining strategy.

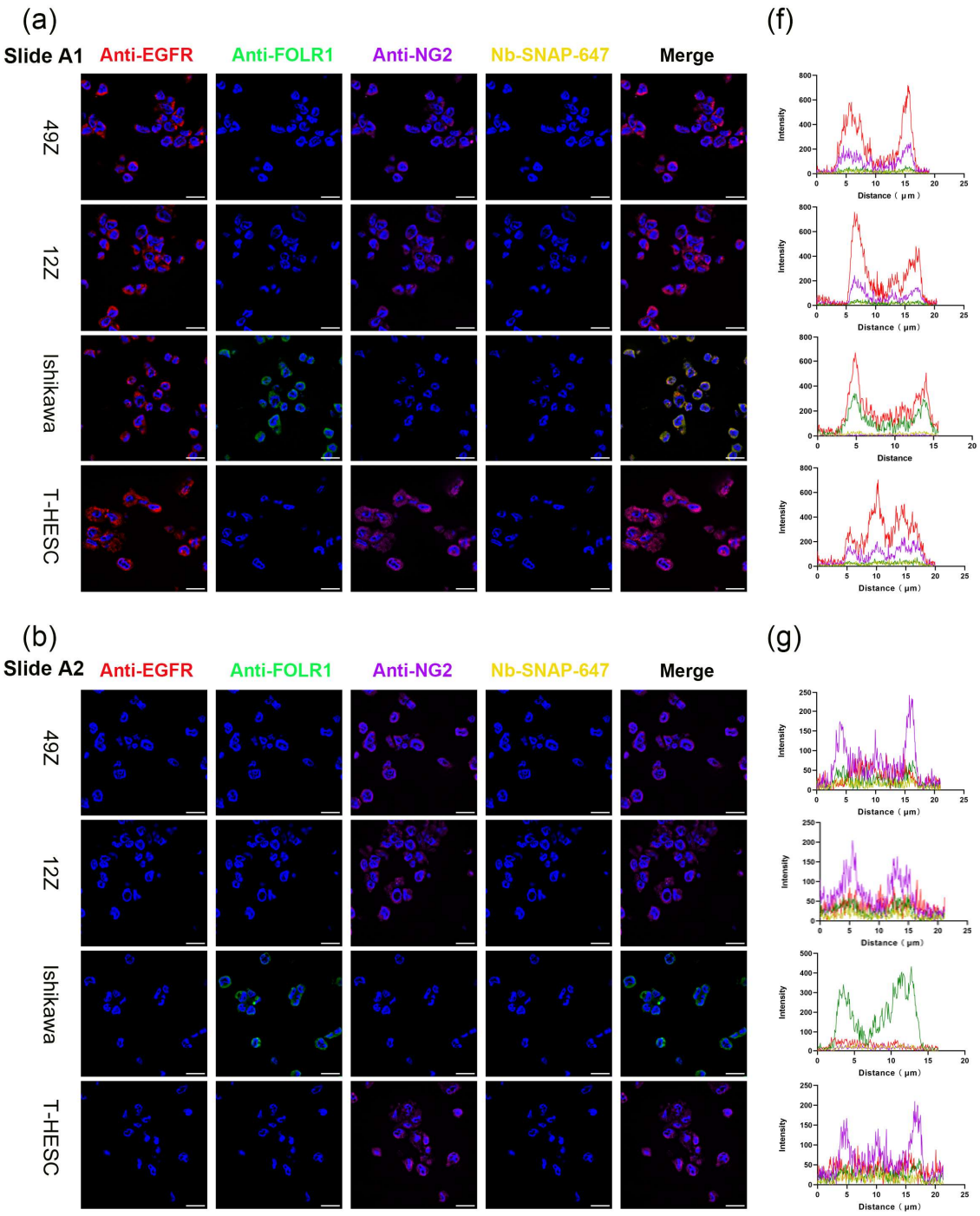
(a)
Slide A1
Anti-EGFR
Anti-FOLR1
Anti-NG2
Nb-SNAP-647
Merge
49Z
12Z
Ishikawa
T-HESC
(f)
Intensity
Distance (μm)
(b)
Slide A2
Anti-EGFR
Anti-FOLR1
Anti-NG2
Nb-SNAP-647
Merge
49Z
12Z
Ishikawa
T-HESC
(g)
Intensity
Distance (μm)

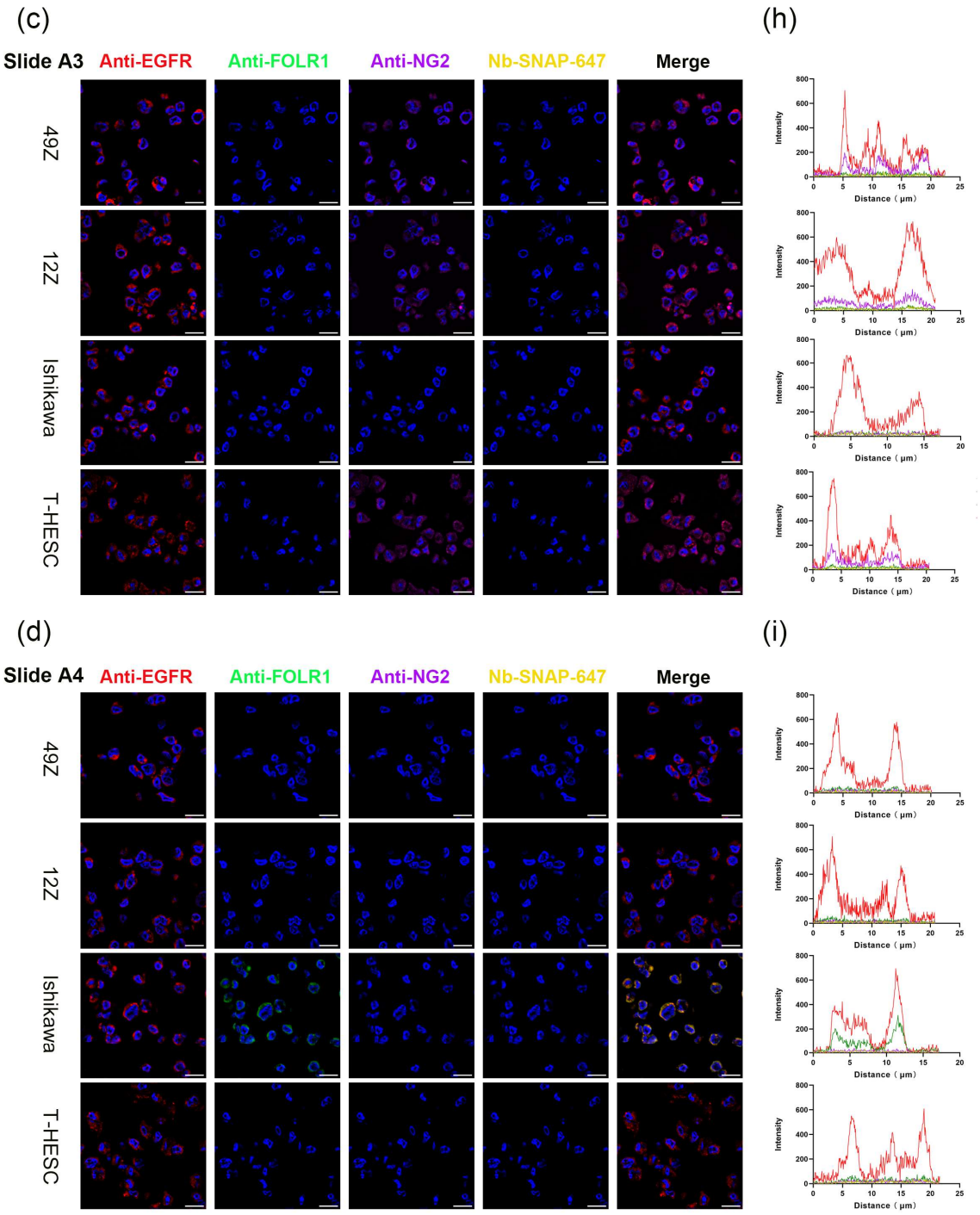
(c)
(h)
Slide A3
Anti-EGFR
Anti-FOLR1
Anti-NG2
Nb-SNAP-647
Merge
49Z
12Z
Ishikawa
T-HESC
Intensity
Distance（μm）
(d)
(i)
Slide A4
Anti-EGFR
Anti-FOLR1
Anti-NG2
Nb-SNAP-647
Merge
49Z
12Z
Ishikawa
T-HESC
Intensity
Distance（μm）

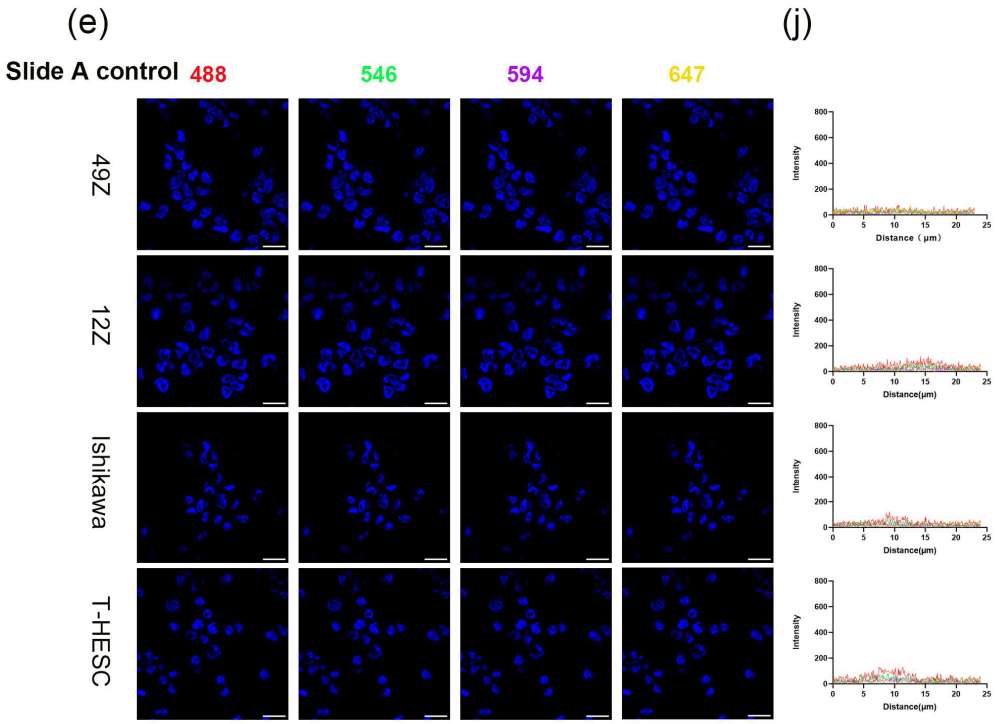

Figure 4.14. The panel A multi-color immunofluorescence staining of endometrial cell block (49Z, 12Z, Ishikawa and T-HESC). (a) Nbs anti-IgG-SNAP-488 (red), Nbs anti-IgG-SNAP-546 (green), Nbs anti-IgG-SNAP-594 (magenta) detected following primary antibodies; anti-EGFR (IgG2a), anti-FOLR1 (IgG1), and anti-NG2 (IgG1, kappa). Nbs anti-IgG-SNAP-647 (yellow) were post-incubated to confirm binding activity. (b) No anti-EGFR (IgG2a)-488 staining (red); (c) No anti-FOLR1 (IgG1)-546 staining (green); (d) No anti-NG2 (IgG1, kappa)-594 staining (magenta); (e) Slides were only stained with Nbs anti-IgG-SNAP-Alexa Fluor dyes; (f-j) Fluorescence intensity profiles of Alexa Fluor® 488 (red curve), Alexa Fluor® 546 (green curve), Alexa Fluor® 594 (magenta curve) and Alexa Fluor® 647 (yellow curve) for each slide. The scale bar is 20 μm.

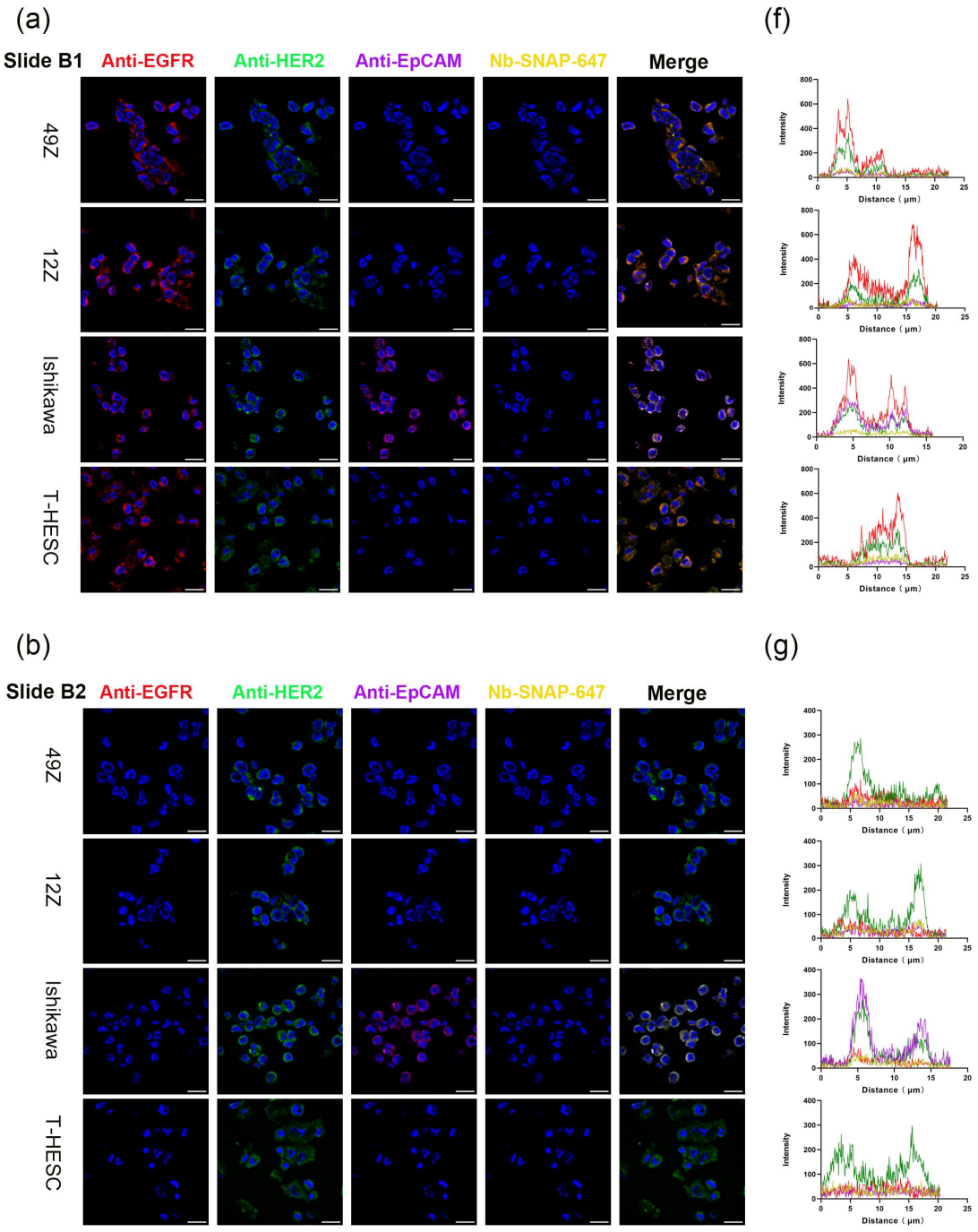
(a)
Slide B1
Anti-EGFR
Anti-HER2
Anti-EpCAM
Nb-SNAP-647
Merge
49Z
12Z
Ishikawa
T-HESC
(f)
Intensity
Distance（μm）
(b)
Slide B2
Anti-EGFR
Anti-HER2
Anti-EpCAM
Nb-SNAP-647
Merge
49Z
12Z
Ishikawa
T-HESC
(g)
Intensity
Distance（μm）

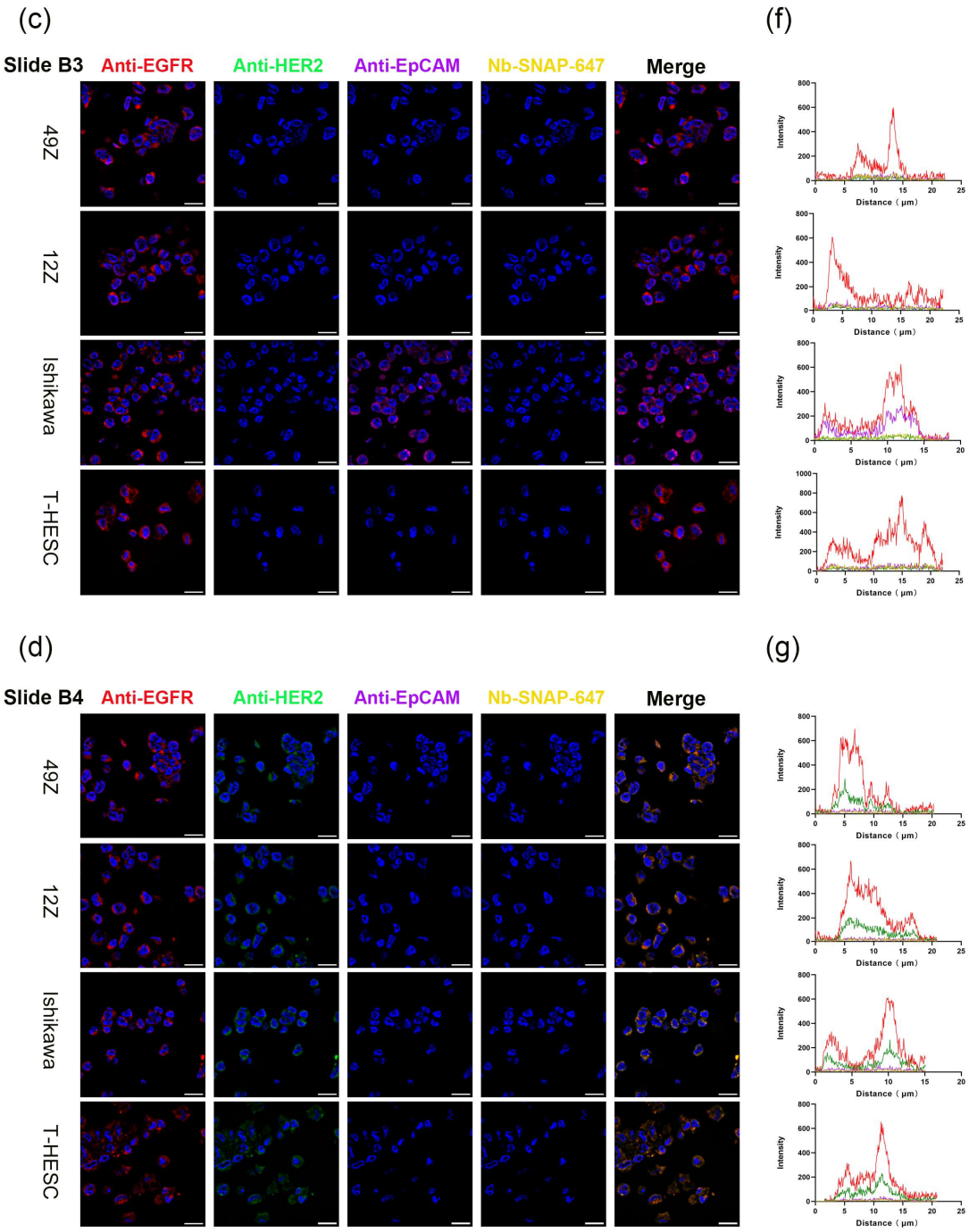
(c)
(f)
Slide B3
Anti-EGFR
Anti-HER2
Anti-EpCAM
Nb-SNAP-647
Merge
49Z
12Z
Ishikawa
T-HESC
Intensity
Distance（μm）
(d)
(g)
Slide B4
Anti-EGFR
Anti-HER2
Anti-EpCAM
Nb-SNAP-647
Merge
49Z
12Z
Ishikawa
T-HESC
Intensity
Distance（μm）

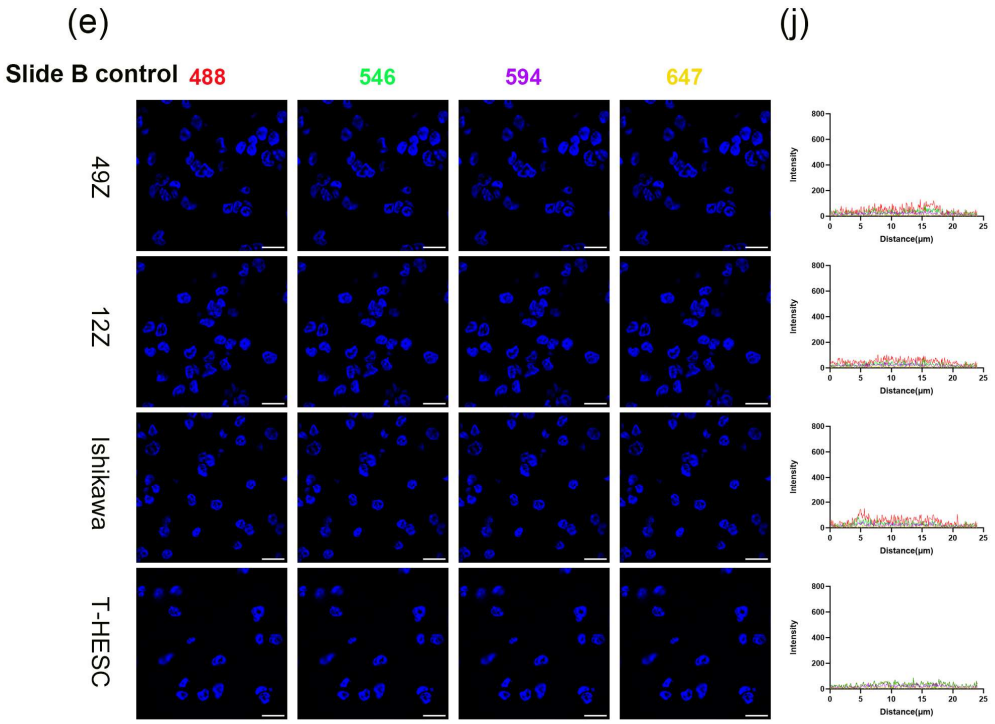

Figure 4.15. The panel B multi-color immunofluorescence staining of endometrial cell block (49Z, 12Z, Ishikawa and T-HESC). (a) Nbs anti-IgG-SNAP-488 (red), Nbs anti-IgG-SNAP-546 (green), Nbs anti-IgG-SNAP-594 (magenta) detected following primary antibodies, anti-EGFR (rabbit), anti-HER2 (IgG1) and anti-EpCAM (IgG1, kappa). Nbs anti-IgG-SNAP-647 (yellow) were post-incubated to confirm binding activity. (b) No anti-EGFR (rabbit)-488 staining (red); (c) No anti-HER2 (IgG1)-546 staining (green); (d) No anti-EpCAM (IgG1, kappa)-594 staining (magenta); (e) Slides were only stained with Nbs anti-IgG-SNAP-Alexa Fluor dyes; (f-j) Fluorescence intensity profiles of Alexa Fluor® 488 (red curve), Alexa Fluor® 546 (green curve), Alexa Fluor® 594 (magenta curve) and Alexa Fluor® 647 (yellow curve) for each slide. The scale bar 20 μm.

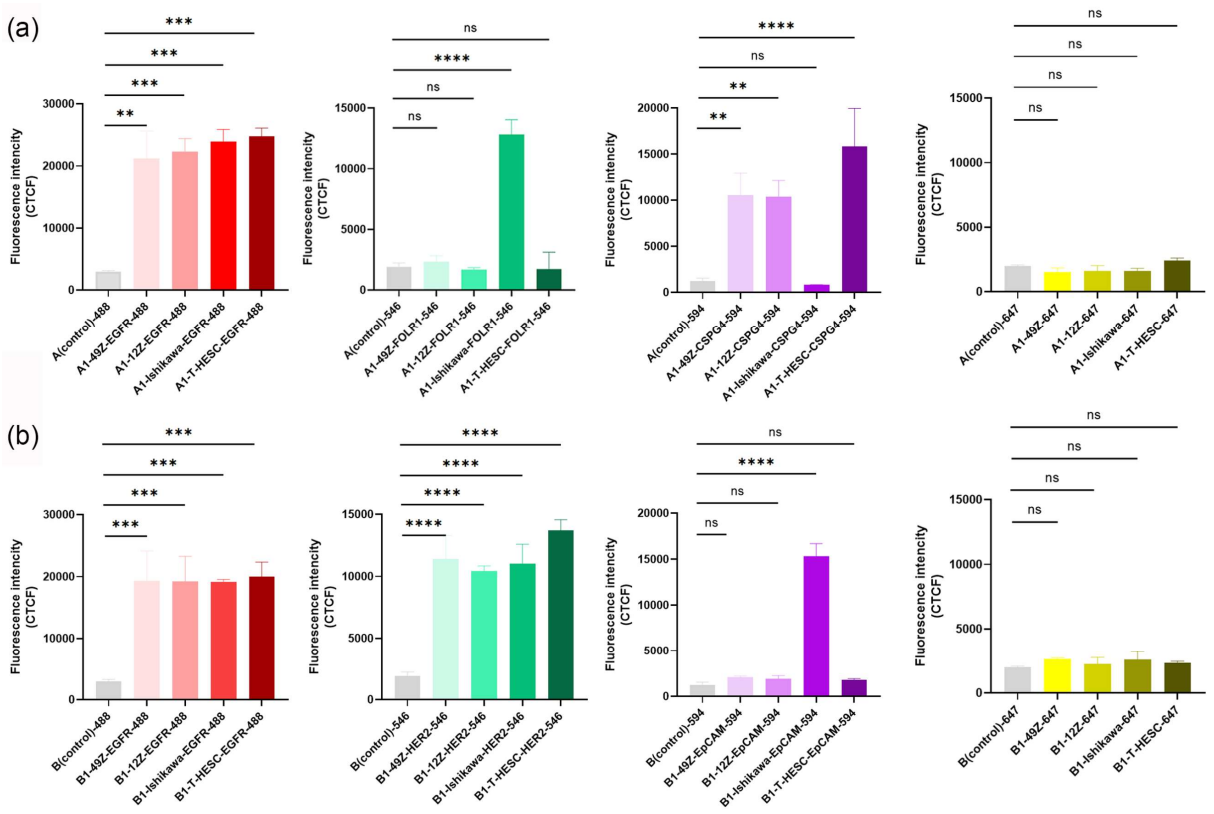

Figure 4.16. CTCF analysis of the fluorescence intensity of multi-color immunofluorescence staining on cell block (49Z, 12Z, Ishikawa and T-HESC). (a) Comparing A1 slide with the A control slide for anti-EGFR (IgG2a)-488 (red), anti-FOLR1 (IgG1)-546 (green), anti-NG2 (IgG1, kappa)-594 and Nbs anti-IgG-SNAP-647 (yellow). (b) Comparing B1 slide with the B control slide for anti-EGFR (rabbit)-488 (red), anti-HER2 (IgG1)-546 (green), anti-EpCAM (IgG1, kappa)-594 and Nbs anti-IgG-SNAP-647 (yellow). Data were analyzed by one-way analysis of variance (ANOVA) with Dunnett's multiple comparisons test using GraphPad Prism 9.0.0 (**** $p < 0.0001$).

Table 4.3. The summary of multi-color fluorescence staining results. The (+) indicates the presence and the detection of the target antigen, (-) indicates that the target antigen is absent or below detectable levels in the stained sample.

		Panel A					Panel B			
Endometrial cells	Slide	488 anti-EGFR	546 anti-FOLR1	594 anti-NG2	647 channel	Slide	488 anti-EGFR	546 anti-HER2	594 anti-EpCAM	647 channel
49Z	1	+	-	+	-	1	+	+	-	-
	2	-	-	+	-	2	-	+	-	-
	3	+	-	+	-	3	+	-	-	-
	4	+	-	-	-	4	+	+	-	-
	Control	-	-	-	-	Control	-	-	-	-
12Z	1	+	-	+	-	1	+	+	-	-

	2	-	-	+	-	2	-	+	-	-
	3	+	-	+	-	3	+	-	-	-
	4	+	-	-	-	4	+	+	-	-
	Control	-	-	-	-	Control	-	-	-	-
	1	+	+	-	-	1	+	+	+	-
	2	-	+	-	-	2	-	+	+	-
Ishikawa	3	+	-	-	-	3	+	-	+	-
	4	+	+	-	-	4	+	+	-	-
	Control	-	-	-	-	Control	-	-	-	-
	1	+	-	+	-	1	+	+	-	-
	2	-	-	+	-	2	-	+	-	-
T-HESC	3	+	-	+	-	3	+	-	-	-
	4	+	-	-	-	4	+	+	-	-
	Control	-	-	-	-	Control	-	-	-	-

4.2 The application of Nb anti-igG-HRP in Western blot and TSA-based multiplex immunofluorescence as secondary antibodies

4.2.1 Design and construction of Nb anti-IgG-HRP fusion proteins

Using the previously developed pMS-Nb anti-IgG-SNAP constructs, the HRP fragment from pUC19-HRP-C [120] was inserted instead of SNAP-tag, resulting in the generating of pMS-Nb anti-IgG-HRP constructs. The DNA cloning was successfully performed using PCR and In-Fusion Snap Assembly cloning reaction (Takara Bio). Subsequently, the Nb anti-IgG-HRP insets from the pMS vector were subcloned into the lentiviral and mammalian expression vector backbone pHR [118] using NdeI and BlpI-restriction sites (**Figure 4.17**). The pHR expression vector includes the minimum essential *cis*-acting human immunodeficiency virus (HIV) elements, such the 3' long terminal repeat (LTR) and 3' LTR (ΔU3), which facilitate the stable integration of the target gene into the host genome as proviral DNA. Other features include the central polypurine tract and central termination sequence (cPPT/CST), the Rev response element (RRE), enabling Rev-dependent mRNA export from the nucleus to the cytoplasm, and the Ψ packaging signal. Additionally, the construct retained the CMV ehancer, CMV promoter and Igκ leader, ensuring efficient expression and releasing of the recombinant proteins into culture supernatant. Following this design, other constructs were generated, including pHR-Nb anti-mouse IgG1 Fab-HRP, pHR-Nb anti-mouse IgG1 Fc-HRP, pHR-Nb anti-mouse IgG2a Fc-HRP, pHR-Nb anti-mouse kappa chain-HRP and pHR-Nb anti-rabbit IgG1 Fc-HRP constructs. The interted DNA sequences of these new constructs were confirmed by DNA sequencing (Sanger Sequencing services, Eurofins Genomics, Germany).

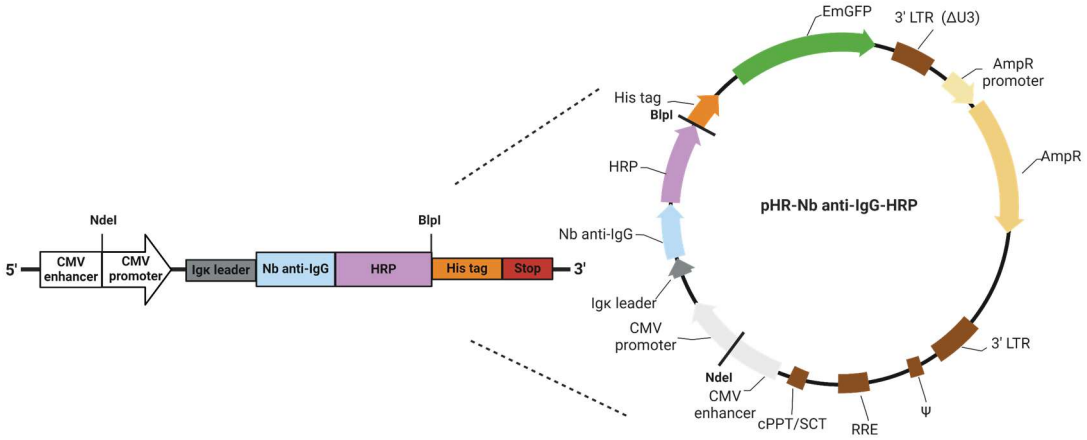

Figure 4.17. Schematic of Nb anti-IgG-HRP construct design. AmpR: ampicillin resistance; CMV: cytomegalovirus; Igκ leader: immunoglobulin κ leader; His: histidine; EmGFP: emerald green fluorescent protein; LTR: long terminal repeat; RRE: Rev response element; cPPT/CST: central polypurine tract and central termination sequence; Stop: TGA stop codon. Created in https://BioRender.com.

4.2.2 Expression and enrichment of Nb anti-IgG-HRP fusion proteins

Similar to the production of the Nb anti-IgG-SNAP fusion proteins, Nb anti-IgG-HRP fusion proteins were also produced in transfected HEK293T cells, but without requiring zeocin selection. Compared to cells transfected with the recombinant plasmids encoding Nbs anti-IgG-SNAP, those expressing Nbs anti-IgG-HRP exhibited a stronger GFP signal when the proteins were expressed (data not shown). Following GFP signal detection, culture supernatants were collected from the transfected HEK293T cells. To confirm successful expression and secretion of the Nbs anti-IgG-HRP fusion proteins, two complementary methods were used. The first method was direct ELISA, in which the supernatants were used as coating antigens to directly assess HRP enzymatic activity using TMB substrate. The presence of active Nbs anti-IgG-HRP fusion proteins in the cell culture medium was confirmed (**Figure 4.18a**). The second method was the IFA. The fusion proteins, tagged with a His-tag, were detected using Alexa Fluor 647 conjugated anti-penta-His antibody. Fluorescence microscopy was then performed after staining with anti-EGFR antibodies on breast cancer cells (MDA-MB-468, MDA-MB-453). As shown in **Figure 4.18b** Alexa Fluor 647 signal was observed in MDA-MB-468, but not in MDA-MB-453 cells, indicating specific recognition and expression.

Once sufficient supernatant was collected, the fusion proteins were purified using IMAC with a Ni-NTA superflow cartridge. Protein enrichment was confirmed by separating the collected proteins fractions on SDS-PAGE followed by Coomassie brilliant blue. As an example, Nb anti-mouse IgG1 Fc-HRP was purified using 10 mM and 40 mM imidazole for washing, and 250 mM imidazole for

elution (fractions E3 and E4). A distinct band at approximately 95 kDa was observed in fraction E3, which contained the majority of the fusion protein (**Figure 4.19a**). Although E4 also showed the protein band, it was less concentrated, as most protein had eluted in E3. Notably, the volume of E3 loaded was only one-third of that of other fractions.

Other fusion proteins, including Nb anti-mouse IgG1 Fab-HRP, Nb anti-mouse IgG2a Fc-HRP, Nb anti-mouse kappa chain-HRP and Nb anti-rabbit IgG Fc-HRP, were expressed and purified following the same protocol (**Supplementary Figure 2**). This high-yielding expression system enabled the rapid production of up to 3 mg/L of fusion protein in the culture medium.

To further validate Nbs anti-IgG-HRP fusion proteins, Western blot analysis was performed. Equal amounts of each fusion protein were applied to SDS-PAGE, transferred to PVDF membrane. and incubated with anti-Penta-His antibody as the primary antibody. Detection was carried out using HRP-conjugated goat anti-mouse IgG as the secondary antibody and visualization was achieved with INTAS ECL ChemoStar (**Figure 4.19b**).

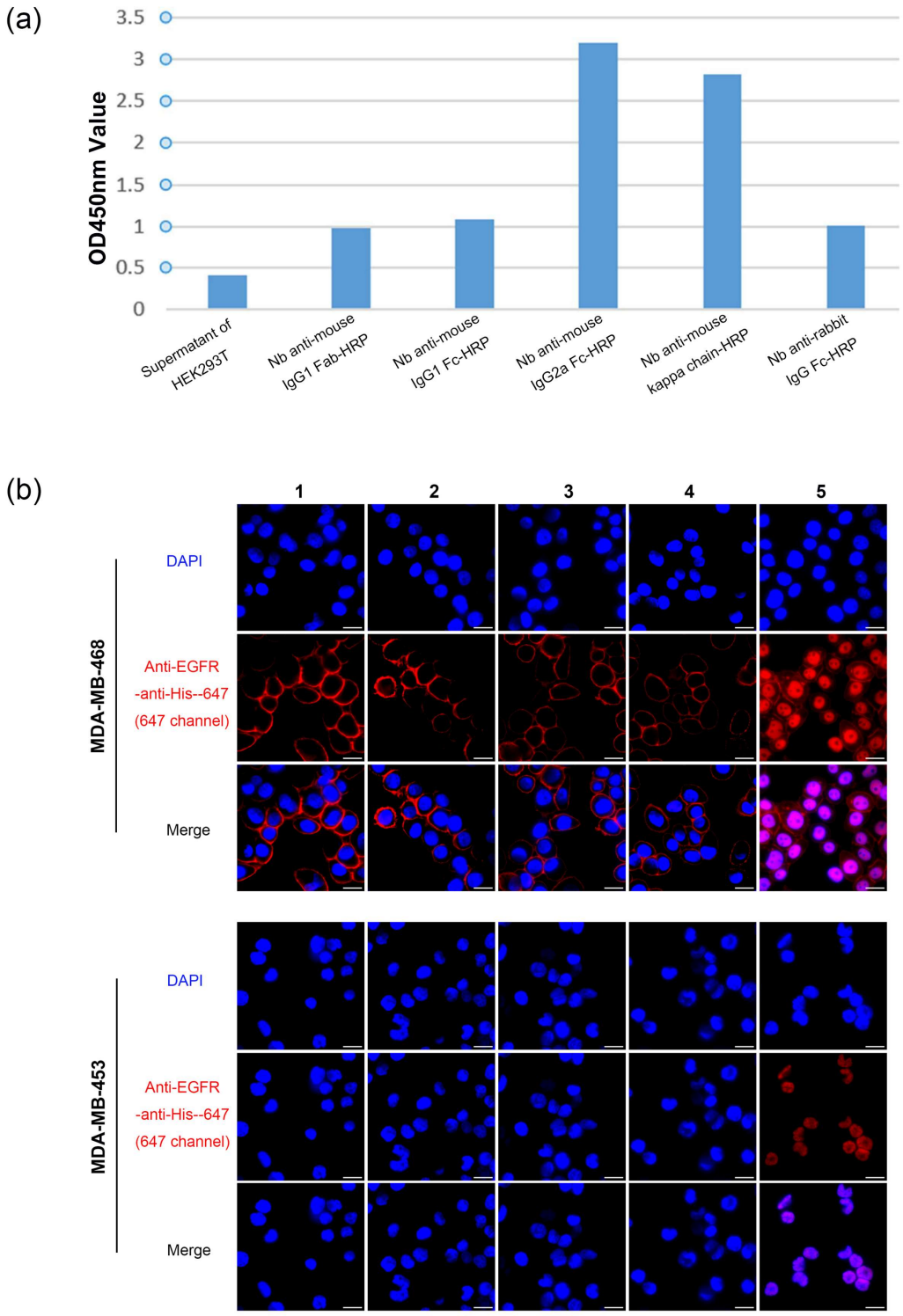

Figure 4.18. Expression of Nbs anti-IgG-HRP fusion proteins in HEK293T cells. (a) Nbs anti-IgG-HRP fusion proteins in the supernatants from HEK293T cells showed HRP activity reacting with TMB substrate. (b) Detection of Nbs anti-IgG-HRP fusion proteins expressed in HEK29T cells by IFA. Breast cancer cells MDA-MB-468 (EGFR positive) and MDA-MB-453 (EGFR negative) were incubated with anti-EGFR antibodies, followed by secondary antibodies Nbs anti-IgG-HRP fusion proteins. Alexa Fluor 647-conjugated anti-penta-His antibody was used as a tertiary antibody with His tag of Nbs anti-IgG-HRP, the treated cells were imaged by fluorescence microscopy. Lane1:

Nb anti-mouse IgG1 Fab-HRP. Lane 2: Nb anti-mouse IgG1 Fc-HRP. Lane 3: Nb anti-mouse IgG2a Fc-HRP. Lane 4: Nb anti-mouse kappa chain-HRP. Lane 5: Nb anti-rabbit IgG Fc-HRP. The scale bar is 20 µm.

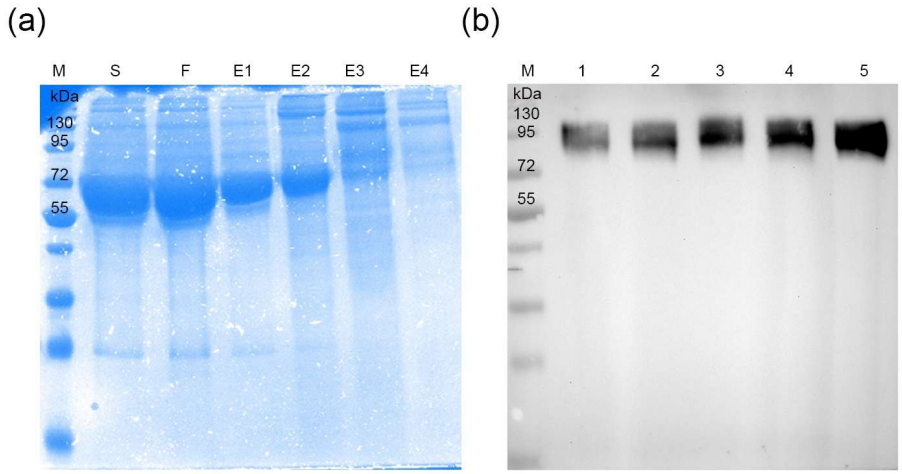

Figure 4.19. Enrichment of Nbs anti-IgG-HRP. (a) All fractions were collected during the enrichment of Nb anti-mouse IgG1 Fc-HRP, after running SDS-PAGE, the gel was stained with Coomassie brilliant blue, then imaged by ChemiDoc XRS+ System. M: Blue prestained protein standard broad range (17-250 kDa). S: filtered supernatant. F: flowthrough. E1: protein eluted in 10 mM imidazole. E2: protein eluted in 40 mM imidazole. E3 and E4: protein eluted in 250 mM imidazole. (b) Western blot showed the presence of Nb anti-mouse IgG1 Fab-HRP (lane 1), Nb anti-mouse IgG1 Fc-HRP (lane 2), Nb anti-mouse IgG2a Fc-HRP (lane 3), Nb anti-mouse kappa chain-HRP (lane 4) and Nb anti-rabbit IgG Fc-HRP (lane 5). The fusion proteins were subjected to SDS-PAGE followed by anti-Penta-His antibody, then visualized by INTAS ECL ChemoStar. M: Blue prestained protein standard broad range (17-250 kDa).

4.2.3 The specific binding of Nb anti-IgG-HRP fusion proteins in Western blot

After the enrichment process, the five Nbs anti-IgG-HRP fusion proteins were characterized for their subclass specificity and cross-reactivity with primary antibodies derived from two species (mouse and rabbit) using Western blotting (**Figure 4.20**). For comparison, commercial HRP-conjugated goat anti-mouse IgG and HRP-conjugated goat anti-rabbit IgG secondary antibodies were included as controls. Notably, the Nbs anti-IgG-HRP exhibited high specificity and a strong ability to distinguish between different antibody subclasses and species. Nb anti-mouse IgG1 Fab-HRP and Nb anti-mouse IgG1 Fc-HRP specially react with the mouse anti-EGFR antibody (IgG1, kappa), while Nb anti-mouse IgG2a-HRP detected only the mouse anti-EGFR antibody (IgG2a). Moreover, Nb anti-mouse kappa chain-

HRP was reactive with both mouse anti-EGFR antibodies, whereas the four Nbs anti-mouse IgG-HRP did not react with the rabbit anti-EGFR antibody. Conversely, Nb anti-rabbit IgG Fc-HRP specifically recognized the rabbit anti-EGFR antibody (IgG) and showed no cross-reactivity with mouse-produced antibodies.

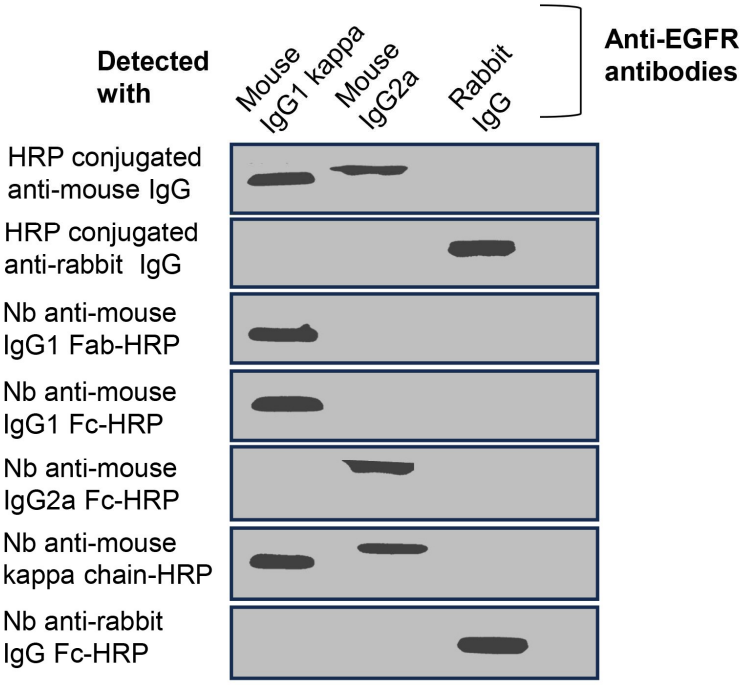

Figure 4.20. Western blot analysis of specific reactivity of Nbs anti-IgG-HRP. Anti-EGFR antibody (mouse/ IgG1, kappa), anti-EGFR (mouse/ IgG2a) and anti-EGFR (rabbit/ IgG Fc) were subjected to SDS-PAGE followed by Western blot with Nbs anti-IgG-HRP or corresponding commercial HRP-conjugated secondary antibodies incubated. The PVDF membranes were developed with ECL reagent and visualized by INTAS ECL ChemoStar.

4.2.4 The application of Nb anti-IgG-HRP fusion proteins for Western blot as secondary antibodies.

Having confirmed their specific binding to primary antibodies, the Nb anti-IgG-HRP fusion proteins were next evaluated for their performance as secondary antibodies in Western blotting, a standard application of HRP-conjugated reagents. In this study, three different anti-EGFR antibodies (described in **Section 4.2.3)** were used to assess EGFR expression levels in two breast cancer cells (MDA-MB-468, MDA-MB-453) and two endometrial cells (Ishikawa, T-HESC).

When Nb anti-mouse IgG1 Fab-HRP, Nb anti-mouse IgG1 Fc-HRP, and Nb anti-mouse kappa chain-HRP were used to detect the anti-EGFR antibody (mouse/ IgG1, kappa), the results (**Figure 4.21a**) indicate significantly higher EGFR expression in MDA-MB-468, Ishikawa, and T-HESC, with no detectable expression in MDA-MB-453. Consistent findings were observed in **Figure 4.21b and c**, where Nb anti-mouse IgG2a Fc-HRP, Nb anti-mouse kappa chain-HRP, and Nb anti-rabbit IgG Fc-HRP were used in conjunction with their respective primary antibodies (mouse/ IgG2a, rabbit/ IgG Fc). In each case, the Nbs anti-IgG-HRP reagents produced comparable signal intensities and specificity of those obtained with commercial HRP-conjugated secondary antibodies.

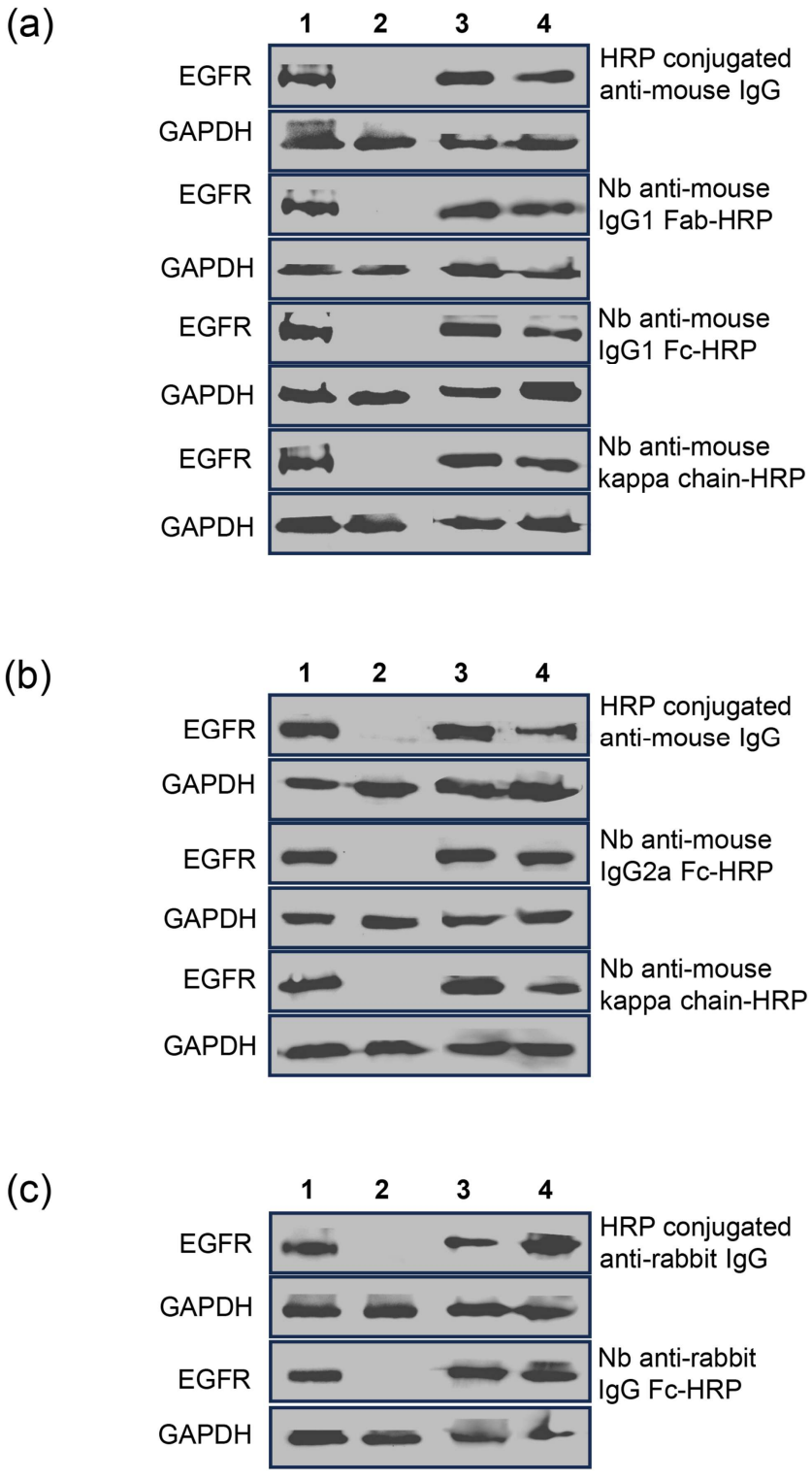

Figure 4.21. Western blot analysis of Nbs anti-IgG-HRP for EGFR expression in breast cancer cell lines and endometrial cells. Cell extracts were blotted and incubated with (a) anti-EGFR antibody (mouse/ IgG1, kappa), (b) anti-EGFR antibody (mouse/ IgG2a), (c) anti-EGFR antibody (rabbit/ IgG). All anti-EGFR antibodies were then probed with Nbs anti-IgG-HRP or corresponding commercial HRP-conjugated secondary antibodies. The housekeeping protein GAPDH was used as a control. Lane 1: MDA-MB-468. Lane 2: MDA-MB-453. Lane 3:

Ishikawa. Lane 3: T-HESC.

4.2.5 Multiplex immunofluorescence TSA of paraffin-embedded endometriosis tissues

4.2.5.1 The specific binding of Nbs anti-IgG-HRP for primary antibodies

Before applying Nbs anti-IgG-HRP fusion proteins in TSA-based mIF experiments, their specific-binding capabilities were validated via Western blot. The primary antibodies used for this validation included: anti-ERα antibody（mouse/IgG1, kappa）, anti-CD31 antibody (mouse/IgG1), anti-αSMA antibody（mouse/IgG2a）, anti-CD20 antibody (mouse/IgG2a, kappa) and anti-PR antibody (rabbit/IgG) all of which are planned for subsequent mIF applications. These primary antibodies were first separated by SDS-PAGE and transferred onto PVDF membranes. The membranes were then probed using either Nbs anti-IgG-HRP fusion proteins or corresponding commercial HRP-conjugated secondary antibodies. As shown in **Figure 4.22,** Nb anti-mouse IgG1 Fab-HRP and Nb anti-mouse IgG1 Fc-HRP specifically recognized anti-ERα and anti-CD31, while Nb anti-mouse IgG2a Fc-HRP reacted exclusively with anti-αSMA and anti-CD20. Additionally, Nb anti-mouse kappa chain-HRP bound to all tested mouse-derived antibodies, demonstrating broad kappa chain specificity. Conversely, Nb anti-rabbit IgG-HRP selectively detect anti-PR, confirming species specificity. These findings underscore the precise subclass- and species-specific binding characteristics of the Nb anti-IgG-HRP fusion proteins, distinguishing them from commercial polyclonal secondary antibodies, which often lack this level of discrimination. This subclass specificity makes Nbs anti-IgG-HRP highly suitable for mIF applications requiring minimal cross-reactivity.

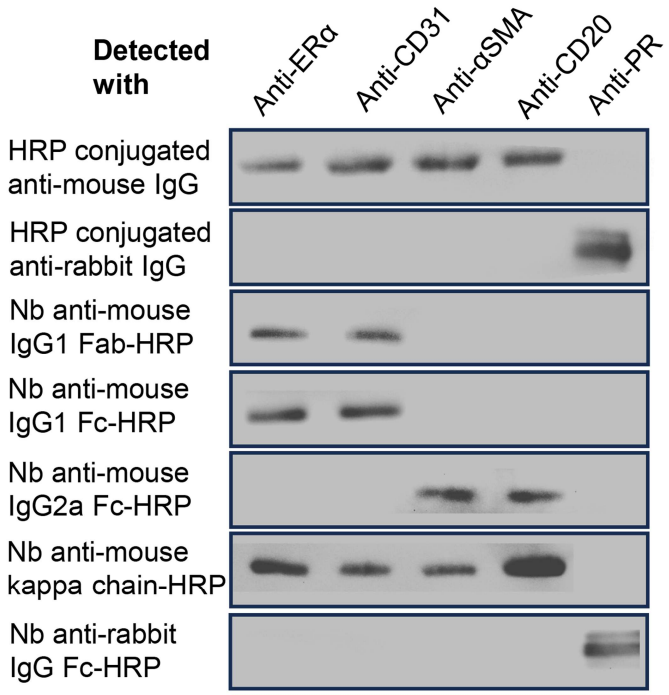

Figure 4.22. Western blot analysis of specific binding of Nbs anti-IgG-HRP for primary antibodies using in TSA-based mIF. Anti-ERα antibody (mouse/IgG1, kappa), anti-CD31 antibody (mouse/IgG1), anti-αSMA antibody (mouse/IgG2a), anti-CD20 antibody (mouse/IgG2a, kappa) and anti-PR (rabbit/IgG) were transferred to PVDF membranes, then detected by Nbs anti-IgG-HRP or corresponding commercial HRP-conjugated secondary antibodies. All membranes were visualized by INTAS ECL ChemoStar.

4.2.5.2 TSA-based multiplex immunofluorescence of Nb anti-IgG-HRP in single paraffin-embedded endometriosis tissues as secondary antibodies

To initiate staining using TSA-based mIF, the expressions of ERα, αSMA, PR, CD20 and CD31 in an endometriosis tissue sample was first confirmed using IHC (**Figure 4.23**), followed by semi-quantification analysis using ImageJ. As reported in previous study [121, 122], ERα and PR are typically expressed in the nuclei of glandular and stromal cells in endometriosis tissues. CD20 serves as a marker for B lymphocytes, CD31 marks vascular and intercellular junctions, and αSMA identifies vascular and visceral smooth muscle cells [123]. IHC analysis confirm the positive expression of αSMA, PR, CD20 and CD31 in endometriosis sections, while ERα expression was not detected. Given the potential for overlapping signals between ERα and PR, and the fact that αSMA and CD31 are both

vascular markers, a 5-color mIF staining panel plus DAPI was performed as described in the **Table 4.4**. To minimize spectral overlap in regions of co-expression, ERα and PR were labeled with iFluor® 430 and Alexa Fluor™ 546, respectively, while αSMA and CD31 were labeled with Alexa Fluor™ 546 and iFluor® 750, respectively.

Antibody dilutions were consistent with those used for IHC, and the tyramide-fluorophore dilutions are detailed in **Table 3.20**. Tissue sections from the same tissue blocks used for IHC were stained using either the Nbs anti-IgG-HRP fusion proteins or the corresponding commercial HRP-conjugated secondary antibodies. Imaging parameters, including excitation channels and exposure time were defined using the on Axio Scan.Z1 slide scanner and provided on **Supplementary Figure 3**. As shown in **Figure 4.23**, stanning patterns obtained with the Nbs anti-IgG-HRP closely matched those produced by commercial secondary antibody and were consistent with the IHC results in the bright field.
To assess cross-reactivity of the TSA-based mIF panel, leave-one-out control stains were performed (**Figure 4.24**). In this experiment, five slides from the same endometriosis tissue blocks were stained using a previously designed panel (**Table 4.4**), with each slide omitting one primary antibody. Each row in **Figure 4.24** shows the signal corresponding to a specific primary antibody paired with a tyramide-fluorophore. For instance, when anti-ERα was excluded from Slide 1, the yellow signal in the ERα-430 channel was absent, while all other four fluorophore signals channels remained detectable. Similarly, omission of anti-αSMA from Slide 2, resulted in the absence of green-αSMA-488, with retention of the remaining of the signals. Slide 3, 4, and 5, showed the absence of each target signal along with diagonal of the imaging panel confirms the lack of cross-reactivity among different Nb anti-IgG-HRP fusion proteins (from top left to bottom right). Furthermore, the consistent absence of a yellow signal in the ERα-430 channel across all mIF images was aligned with the IHC data **Figure 4.23**) showing negative ERα expression in this section, further validating the specificity of the assay.

Table 4.4. The list of primary antibodies, Nbs anti-IgG-HRP and fluorophores used for mIF

Primary antibody	Nbs anti-IgG-HRP	Position in mIF	Tyramide-fluorophore	Excitation	Emission

	secondary antibody				
Anti-ERα	Nb anti-mouse IgG1 Fab-HRP	1	iFluor® 430 Styramide	433 nm	498 nm
Anti-αSMA	Nb anti-mouse IgG2a Fc-HRP	2	Alexa Fluor™ 488	495 nm	519 nm
Anti-PR	Nb anti-rabbit IgG Fc-HRP	3	Alexa Fluor™ 546	556 nm	573 nm
Anti-CD20	Nb anti-mouse kappa chain-HRP	4	Alexa Fluor™ 647	650 nm	668 nm
Anti-CD31	Nb anti-mouse IgG1 Fc-HRP	5	iFluor® 750 Styramide	757 nm	779 nm
		6	DAPI	360 nm	460 nm

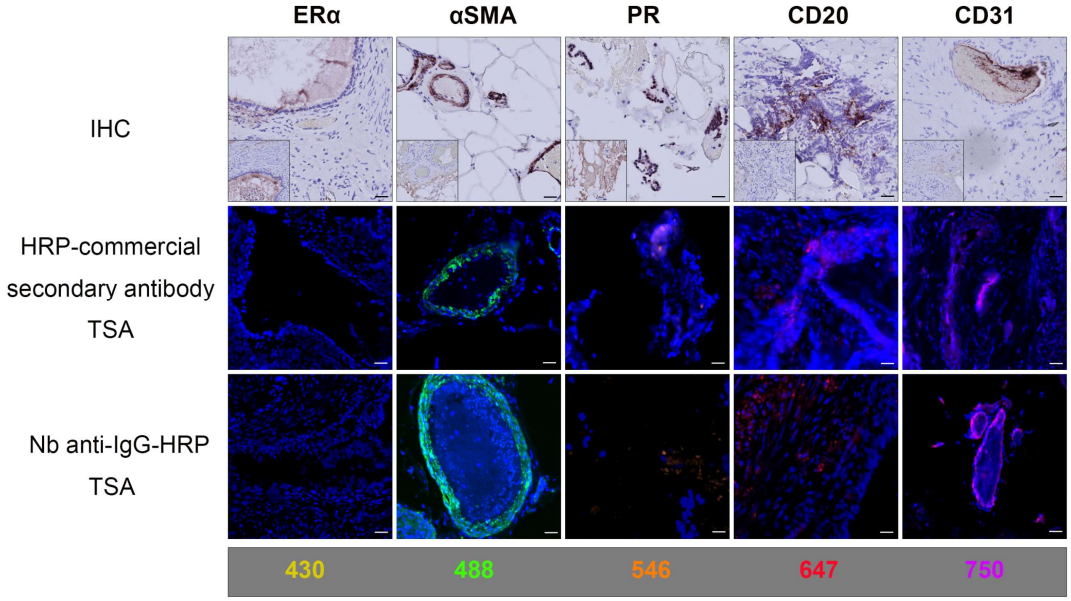

Figure 4.23. Validation of TSA-based mIF of Nb anti-IgG-HRP in single FFPE endometriosis tissues as secondary antibodies using the 5-marker plus DAPI panel. Single staining against selected marker using IHC

(top), except ERα was negative, other 4 markers were expressed on endometriosis tissues (brown signal). Staining with mIF for all 5 markers, ERα （yellow, 430 channel）, αSMA （green, 488 channel）, PR (orange, 546 channel), CD20 (red, 647 channel) and CD31 (magenta, 750 channel) were detected by corresponding commercial HRP-conjugated secondary antibodies (middle), or Nbs anti-IgG-HRP (bottom), blue signal was DAPI staining. Image inset shows only stained with secondary antibody. The scale bar is 20 μm.

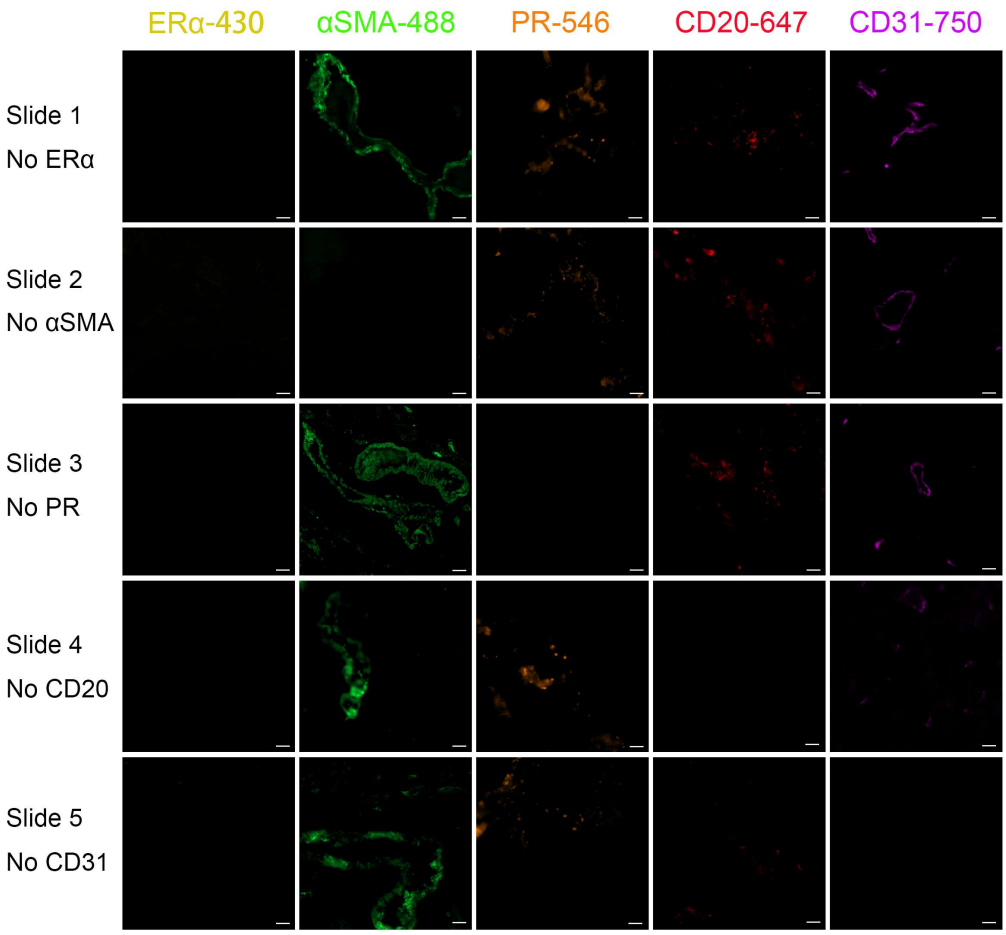

Figure 4.24. Leave-one-out control stains for confirming the cross-reactivity among Nbs anti-IgG-HRP. Five serial slides were stained following the multiplex IF panel with Nbs anti-IgG-HRP. Each row of images shows one slide in which one primary antibody was left out of the staining protocol. For example, row 1 of side 1, no ERα had anti-ERα left out. ERα（yellow, 430 channel）, αSMA（green, 488 channel, PR (orange, 546 channel), CD20 (red, 647 channel) and CD31 (magenta, 750 channel). The lack of signal along the diagonal in the images indicates there was no cross-reactivity among Nbs anti-IgG-HRP (from top left to bottom right). The scale bar 20 μm.

4.2.5.3 TSA-based mIF of Nb anti-IgG-HRP in human endometriosis tissue microarray as secondary antibodies

After antibodies were validated through chromogenic IHC, and the mIF panel was optimized using a single endometriosis section, the endometriosis tissue microarray (TMA) containing 50 cores was stained using the same mIF panel. The expressions of ERα, αSMA, PR, CD20 and CD31 was first validated using IHC. These five primary antibodies were then employed in TSA-based mIF using either Nbs anti-IgG-HRP or the corresponding HRP-conjugated commercial secondary antibodies. Each tissue core was designated as a region of interest (ROI) and imaged using whole-slide scanning with the Axio Scan.Z1 slide scanner. As illustrated in **Figure 4.25**, the first lane shows representative chromogenic IHC staining of a TMA core with individual primary antibodies. Positive cells (brown signals) are marked with black arrows. The full TSA-based mIF panel staining was applied to the TMA using both secondary detection approaches, commercial secondary antibodies or Nbs anti-IgG-HRP, following the same protocol used for the single endometriosis section. Corresponding fluorescent images are displayed in the second and third lanes of **Figure 4.25**, respectively. Each row in these lanes corresponds to one primary antibody labeled with a specific tyramide-fluorophore, matching the chromogenic IHC shown in the first lane. Comparison of bright-field and fluorescent-field images revealed consistent positive signals for ERα, αSMA, CD20, and CD31 across both methods. However, no detectable signal (brown or fluorescent) was observed for PR. Importantly, the staining patterns obtained with Nbs anti-IgG-HRP closely mirrored those achieved with commercial secondary antibodies.

The potential of Nb anti-IgG-HRP as an alternative to conventional secondary antibodies in the TSA-based mIF method was further assessed. **Figure 4.26** provides an example from the endometriosis TMA, with six-color composite images showed on the left, and individual channels for DAPI, iFluor® 430, Alexa Fluor™ 488, Alexa Fluor™ 546, Alexa Fluor™ 647 and iFluor® 750 displayed on the right. High-magnification images confirmed that both detection strategies, Nbs anti-IgG-HRP and commercial secondary antibodies, produced specific and comparable staining.

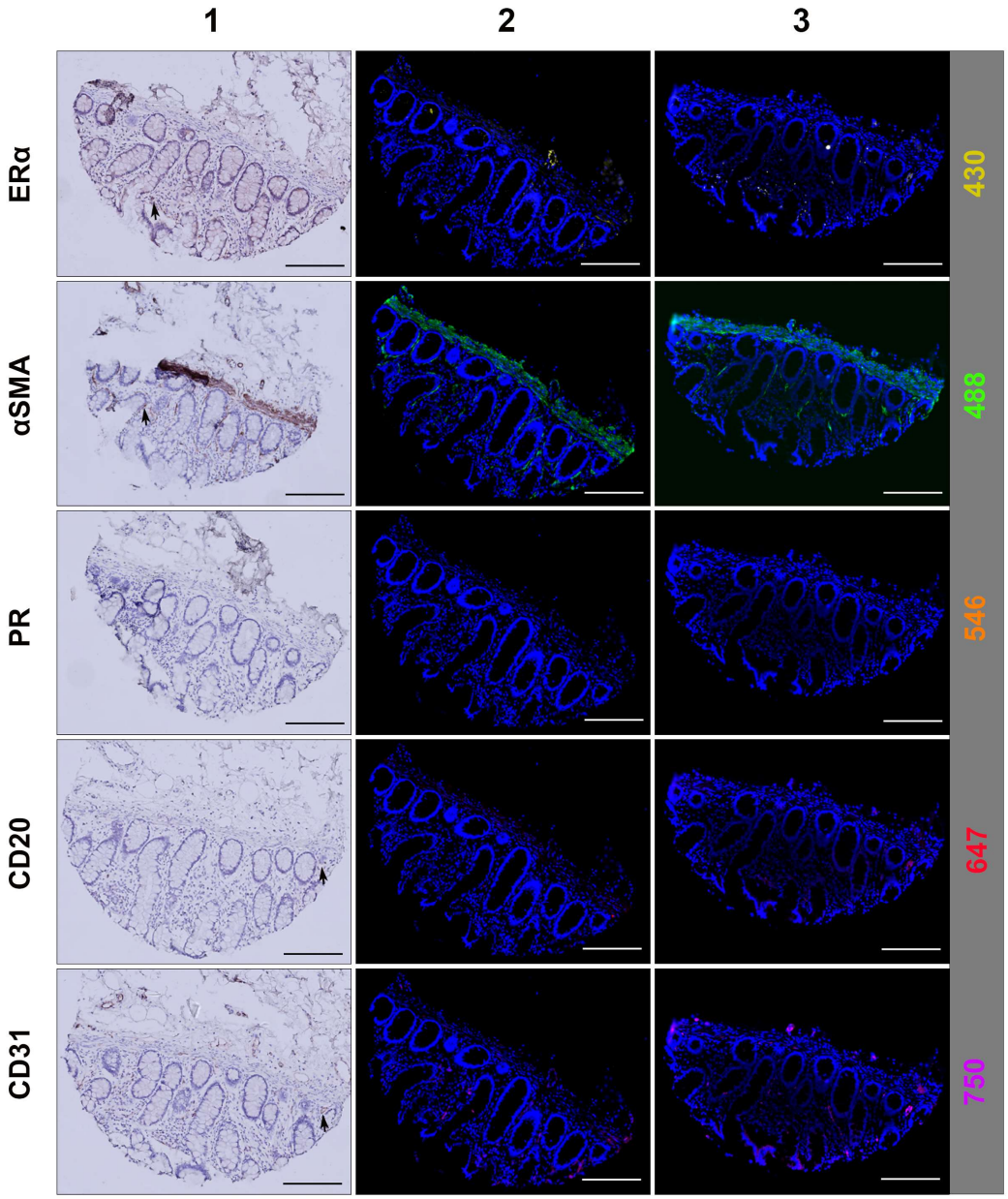

Figure 4.25. Representative validation examples from IHC, TSA-based mIF panel using Nbs anti-IgG-HRP as secondary antibodies on endometriosis TMA. All samples were incubated with primary antibodies, anti-ERα, anti-αSMA, anti-PR, anti-CD20 and anti-CD31. **Lane 1**: IHC staining, with black arrows indicated positive cell exhibiting brown signals. **Lane 2**: mIF panel with HRP-conjugated with commercial secondary antibodies. **Lane 3**: mIF panel with Nbs anti-IgG-HRP. The fluorescent signals correspond to ERα（yellow, 430 channel）, αSMA（green, 488 channel）, PR (orange, 546 channel), CD20 (red, 647 channel), and CD31 (magenta, 750 channel). The blue signal is DAPI. Scale bar: 250 μm.

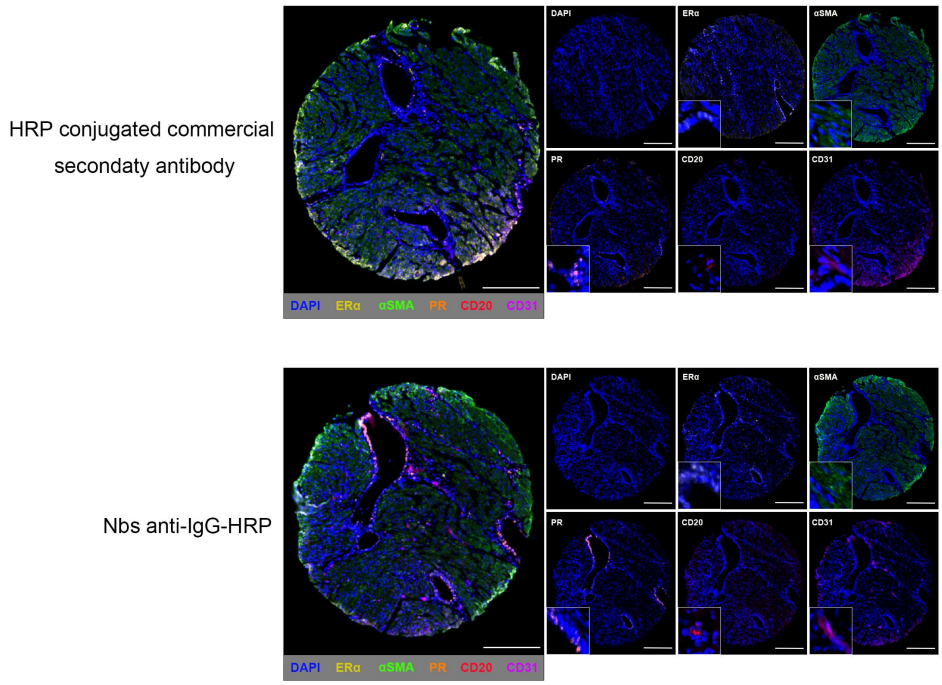

Figure 4.26. TSA-based mIF six-color detection method and multispectral images. Representative examples of endometriosis TMA were stained with five markers: ERα （yellow, 430 channel）, αSMA （green, 488 channel）, PR (orange, 546 channel), CD20 (red, 647 channel), and CD31 (magenta, 750 channel). Signals were developed using either HRP-conjugated commercial secondary antibody or Nbs anti-IgG-HRP. Nuclei were counterstained with DAPI (blue). Scale bar: 250 μm.

4.2.5.4 Image analysis of endometriosis TMA using Qupath

Following whole-slide scanning of the endometriosis TMA and generation of multispectral images using the Axio Scan.Z1 slide scanner, several imaging software platforms were considered for analyzing the multiplexed data. In this study, an open-source digital pathology image analysis (QuPath) [124], was employed to analyze the endometriosis TMA and compare the performance of Nbs anti-IgG-HRP with that of commercially available HRP-conjugated secondary antibodies.

Using Qupath, each of the 50 cores within the TMA was individually annotated. Total cell counts within each region were determined using the *Cell Detection* algorithm based on the DAPI nuclear channel. For the five marker-specific channels–ERα-430 channel, αSMA-488 channel, PR-546 channel, CD20-647 channel, and CD31-750 channel–positive cells were quantified using the *Create single measurement classifier* tool. Statistical analysis of cell counts across all five markers revealed no significant differences in detection between commercial HRP-conjugated secondary antibodies and

Nb anti-IgG-HRP, as shown in **Figure 4.27a** ($p < 0.001$).

To assess marker detection efficiency, the percentage of positive cells per core was calculated for each marker channel using the total DAPI-positive cell count as the denominator. As illustrated in **Figure 4.27b**, the percentages of positive cells for ERα, αSMA, PR, CD20, and CD31 showed no significant difference between the two secondary-antibody detection methods ($p < 0.0001$) for all comparisons. Additionally, a heatmap (**Figure 4.27c**) visualizes the expression levels of each marker across the TMA. In this heatmap, rows represent individual tissue cores (n = 50), columns to the five markers, and the color intensity within each cell reflects the percentage of marker-positive cells. The heatmap further supports the consistency in staining patterns and quantification between the two secondary-antibody approaches.

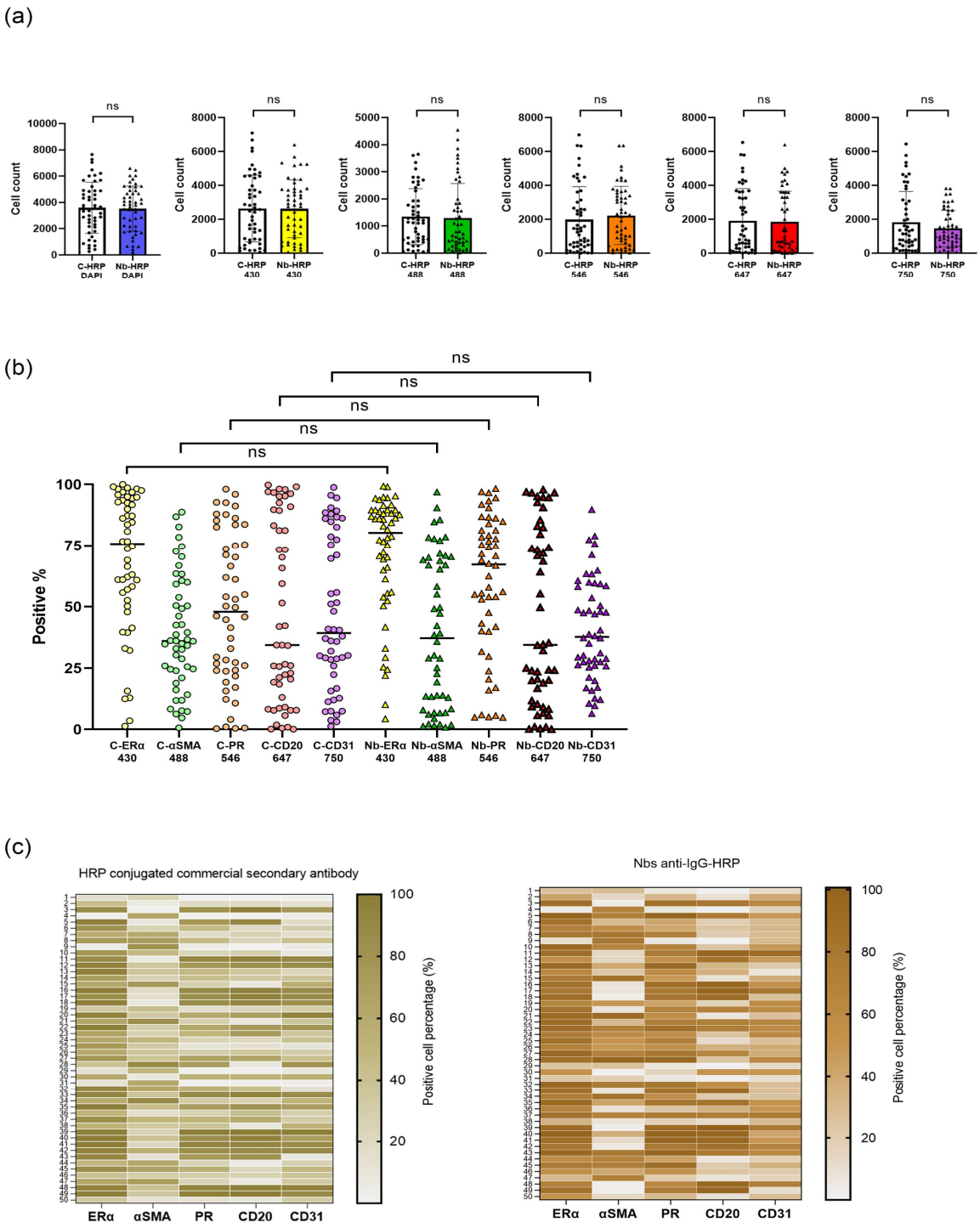

Figure 4.27. Statistical analysis of TSA-based mIF comparing HRP-conjugated commercial secondary antibodies and Nbs anti-IgG-HRP. (a) Cell counts of DAPI channel, 430 channel, 488 channel, 546 channel, 647 channel and 750 channel were analyzed using a t-test ($p < 0.001$). (b) Positive cell percentages for ERα (430 channel), αSMA (488 channel), PR (546 channel), CD20 (647 channel), and CD31 (magenta, 750 channel) were analyzed using one-way ANOVA and corrected by Sidak's multiple comparisons test ($p < 0.0001$). Data are presented as mean ± SEM. (c) Heatmap depicting the positive cell percentages for each marker across the TMA cores (n = 50). Rows represent individual cores, and columns correspond to the five markers. Each cell shows the positive cell percentage for a given marker. Dots or triangles indicate individual cores.

5. Discussion

Secondary antibodies are fundamental components in immunological research and diagnostics, playing a critical role in indirect immunoassays. By amplifying the signal from primary antibodies, they significantly enhance assay sensitivity and offer versatility across a wide range of techniques. This amplification capability renders secondary antibodies indispensable for disease diagnosis, therapeutic development, and clinical research applications [125]. Recent advancements in secondary antibody technology have emerged in response to evolving research demands. These innovations include animal-free production methods and the engineering of antibody structures to improve specificity and minimize background noise. Moreover, newly developed secondary antibodies are increasingly tailored for specialized applications, thereby expanding their utility in both basic and translational research [117, 126, 127].

This study contributes to the innovation of secondary antibody alternatives by harnessing SNAP-tag technology in conjugation with anti-mouse and anti-rabbit IgG secondary nanobodies. The goal is to develop next-generation substitutes for conventional secondary antibodies used in indirect immunofluorescence assays. Additionally, the research investigates the potential of nanobody-HRP fusion proteins as replacements for traditional HRP-conjugated secondary antibodies. These fusion proteins are evaluated for their performance in Western blotting and TSA-based mIF, demonstrating enhanced sensitivity and greater adaptability for these applications. Through these advancements, this work aims to provide more efficient, scalable and innovative tools for immunoassays, thereby broadening their impact in molecular and cellular biology research.

5.1 Issues of secondary antibody production

Traditional secondary antibodies, like their primary counterparts, can be either monoclonal or polyclonal in nature. Polyclonal antibodies are often preferred due to their stronger signals and cost-effective production, making them more commonly used. These antibodies are typically generated in animals through immunization, which stimulates an immune response to produce the desired antibodies. However, this process raises ethical concerns regarding animal welfare and the use of

animals in scientific research. These issues are addressed by the European Union's Directive 2010/63/EU, which emphasizes the 3Rs principles—Replacement, Reduction, and Refinement—to minimize the use of animals in scientific studies [128].

Another critical challenge associated with secondary antibodies is the reproducibility and consistency of their production. Immune responses can vary significantly among individual animals, leading to batch-to-batch variability and potentially unreliable research outcomes [126]. To overcome these limitations, technological advancements have led to recombinant antibody production through *in vitro* methods. These approaches offer a more consistent and reliable alternative to traditional animal-derived antibody production, ensuring greater standardization and reproducibility in research applications [129].

5.2 Mammalian cell expression in recombinant antibody production

Recombinant antibodies are monoclonal antibodies produced using recombinant DNA technology. In this method, antibody genes are inserted into an expression vector, which is then transfected into host cells for antibody expression. Both bacterial and mammalian systems can be used for this purpose. For example, *E. coli* can express antibody fragments in the periplasm [130]. Mammalian cell lines are often preferred when proper protein folding, secretion or solubility is essential, particularly for complex fusion constructs [131]. Mammalian cell expression also offers greater consistency due to the highly controlled conditions of cell culture, which help minimize variability. Moreover, genetic engineering enables the production of antibodies with precise, defined features, further enhancing reproducibility [132]. In this study, HEK293T cells were selected as the expression system to produce Nbs-based fusion proteins used in IFA. This choice was driven by the cell line’s compatibility with transient transfection, rapid growth, adaptability to various culture conditions, and ability to efficiently secrete recombinant proteins into the culture supernatant [133]. Importantly, which are derived from human embryonic kidney cells, provide an expression system that preserves human-like PTMs, eliminating the risk of introducing non-human immunogenic PTMs. This feature enhances the suitability of recombinant proteins for diagnostic applications involving human samples by reducing potential cross-reactivity or background signals [134].

FBS-supplemented media were used in this study due to their robust support for HEK293T cell growth, transfection efficiency and recombinant protein secretion. HEK293T cultures with 10% FBS are widely adopted for transient expression, and studies using HEK293 cells have shown that they maintain high viability and expression yields without requiring adaption, which make them ideal for laboratory-scale production of secreted Nbs-based recombinant proteins [135]. Although serum-free, chemically defined media are increasingly favored for large-scale recombinant protein production, they have notable drawbacks in research settings. A recent study demonstrated that adapting HEK293 cells to serum-free conditions required approximately one month before achieving stable growth [136]. Moreover, the high cost of serum-free media can be a significant barrier for normal laboratory-scale research. Given the aim of producing Nbs-based fusion proteins for diagnostic applications, FBS-supplemented adherent culture systems provided a practical, reproducible and cost-effective method. While suspension HEK293 cells can achieve higher yield [136, 137], our lab's established adherent protocols offered consistent performance well-suited to the demands of research-scale protein production [107, 138].

5.3 Mammalian cell expression vectors

Mammalian cell expression vectors are essential tools for producing recombinant proteins in mammalian systems. These vectors are carefully designed to ensure efficient target gene expression, facilitate proper protein folding, and support PTMs, which are critical for the full biological function of recombinant proteins [139]. In this study, the pMS vector [116] was used to express Nbs anti-IgG SNAP, that our lab has used this vector to generate pMS-scFv-EpCAM-SNAP and expressed fusion proteins in HEK293T cells successfully [138]. The pMS vector utilizes the CMV immediate-early enhancer and promoter, widely used for transgene expression in mammalian cell culture. It also contains the AmpR to facilitate the selection of correct recombinant plasmid in *E. coli*. For selecting the transfected mammalian cells, the zeocin resistance gene (ZeoR) enables the selection of successfully transfected HEK293T cells. A critical feature of this vector is the Igκ leader sequence, which directs the secretion of fusion proteins into cell culture medium, allowing protein collection from the supernatant. Additionally, the His-Tag epitope located at 3' end enables efficient protein

purification using IMAC (**Figure 4.1**).

However, when the pMS vector was used to express Nbs anti-IgG-HRP fusion proteins, the transfection efficiency was insufficient to produce adequate amounts of fusion proteins. To overcome this limitation, pHR vector was considered as another mammalian cell expression vector here [118] (**Figure 4.17**), a lentiviral-based expression system suitable for large-scale recombinant protein production in HEK293 cell lines. This approach resulted in a 3-to 10-fold increase in protein production compared to conventional transfection methods. The pHR vector offers several advantages over traditional vectors such like pMS. Notably, it enables long-term and stable expression by integrating the target genes into the host cell genome. This eliminates the need for a Zeocin selection process, which is required for pMS, and addresses the transient nature of expression observed with pMS, where protein production diminishes over time. Moreover, pHR exhibits high transduction efficiency across a wide range of mammalian cell types, effectively delivering target genes into host cells. In contrast, pMS vector relies on transfection methods, which can be less efficient and show variability depending on the cell types. Additional advantages of the pHR vector include its ability to transduce non-dividing cells, enhanced safety features, and versatility to design, making it a superior choice for application requiring sustained and efficient expression across diverse cell types [140].

5.4 Nanobodies in recombinant antibody production

Nanobodies possess unique properties, such as small size, high stability, and strong antigen-binding capacity, which make them ideal candidates for various applications in recombinant antibody research. Numerous studies have demonstrated the effectiveness of nanobodies in generating recombinant antibodies for imaging, therapy and biosensing. Their small size (~15 kDa) facilitates ease of genetic engineering, enhances tissue penetration, and rapid clearance from non-target sites, further underscoring their versatility and potential in these fields [141, 142]. The sizes of Nb anti-mouse IgG1 Fab, Nb anti-mouse IgG1 Fc, Nb anti-mouse IgG2a Fc, Nb anti-mouse kappa chain, and Nb anti-rabbit IgG Fc ranged from 12.8 kDa to 13.7 kDa, which are significantly smaller than traditional antibodies (~150 kDa). This smaller size enables deeper and more uniform tissue penetration, enhancing the detection of target antigens in complex tissue environments. Additionally, nanobodies consist of a

single antigen-binding domain (**Figure 1.2**), allowing for precise targeting of epitopes targeting while minimizing non-specific binding and background signals [143].

In this study, nanobodies were engineered specific to various IgG domains by fusing them with the SNAP-tag and the reporter enzyme HRP. This recombinant strategy allowed to generate versatile secondary antibody constructs capable of direct, one-step detection of primary antibodies. Compared to other immunoassay designs that required multiple detection steps, including nanobodies as primary detection reagents, followed by secondary anti-nanobody antibodies and additional fluorophore-conjugated tertiary antibodies [144, 145], our design simplified assay workflows and minimized background noise. Additionally, recombinant production of nanobody-based antibodies ensures high purity and batch-to-batch consistency, thereby improving the reliability of diagnostic assays [143].

5.5 SNAP-tag for fluorescence labeling

When selecting a fluorescence labeling strategy, it is important to balance specificity, efficiency and experiment flexibility. The SNAP-tag system offers a combination of these properties. As previously described, SNAP-tag reacts specially and rapidly with BG derivatives, enabling irreversible covalent labeling of the SNAP-tag with a synthetic probe under physiological conditions. This approach allows BG-modified fluorophores to covalently conjugate with the protein of interest. The reaction accepts standard aqueous buffers and does not need catalysts, and can be applied to both purified proteins and live cells. In comparison, NHS-ester chemistry, as one of the most widely used labeling methods [89, 90, 146], it target primary amines, including ε-amino group of lysine residue and α-amino group at N-terminus. While the reaction is straightforward and benefits from the abundance of target sites, it cannot distinguish between individual lysine or protein often resulting in heterogeneous labeling. By exploiting the pKa difference between the N-terminal α-amino group and lysine ε-amino group, the reaction can be driven toward the N-terminus at neutral/low-neutral pH where lysines are few reactive [147]. However, this efficient approach is heavily dependent on pH environment. In addition, standard NHS-ester labeling is typically performed at high-pH conditions and is not bioorthogonal, making it unsuitable for live-cell research [89]. The second labeling strategy, cysteine-specific labeling method utilizes the thiol group, the second most common functional group in chemical cross-linking reactions

[90]. This method often employs the maleimide-modified fluorophores for site-specific labeling under mildly acidic conditions [91], thus minimizing non-specific reactions with amine groups at higher pH. However, many proteins contain few or no surface-exposed cysteines, and disrupting disulfide bridges or introducing additional cysteine residues to conjugate the target protein with maleimide-fluorophores may impact protein stability and functionality [148]. Another labeling strategy, sortase-mediated fluorescence labeling is a technique that utilizes the enzyme sortase A to recognize a specific peptide motif, "Lys-Pro-X-Thr-Gly/Ala" (LPXTG/A), where "X" represents any amino acid, enabling the covalent binding of fluorophores to the C- or N- terminus of proteins [98, 149]. However, this method suffers from relatively low enzymatic efficiency and reversibility, often requiring excess nucleophilic labeling reagent to drive the reaction forward [150]. Additionally, the requirement for specific peptide sequences and the limited availability of fluorescent sortase substrates constrain its general applicability.

In this study, a simple and efficient protocol for conjugating BG-modified fluorophores to Nbs anti-IgG-SNAP was developed, as described in **Section 3.2.3**. Using SNAP-Surface® Alexa Fluor® 647, we achieved complete labeling by incubating the dye with the protein at a 2:1 molar ratio in PBS at room temperature for 2 h in the dark. The result of this labeling is shown in **Figure 4.3b**. The absence of signal from subsequent labeling with SNAP-Surface® Alexa Fluor® 488 (**Figure 4.3a**) confirmed that all SNAP-tag binding sites were occupied under this protocol. This efficient, stoichiometrically controlled labeling, conjugated with numerous commercial availabilities of BG-conjugated dyes, demonstrates the suitability of SNAP-tag for producing highly defined and reproducible labeling reagents. Compared with NHS-ester, cysteine-specific and sortase-mediated methods, SNAP-tag labeling combines the advantages of site specificity, gentle reaction conditions and adaptability, making it especially well-suited for applications that require low background and precise fluorophore stoichiometry.

5.6 Expression and enrichment of Nb anti-IgG-SNAP and -HRP fusion proteins

In this study, the pMS vector was employed for the expression of Nbs anti-IgG-SNAP fusion proteins. This vector contains a bicistronic mRNA enables the simultaneous expression of the target fusion

proteins and EGFP, without incorporating EGFP into the proteins. This feature allowed the monitoring of transfected HEK293T cells under an inverted microscope via GFP fluorescence channel. GFP-positive cells were typically detected within 2-3 days. Subsequent conjugation of the supernatant with SNAP-Surface® Alexa Fluor® 488 and SDS-PAGE analysis confirmed the presence of Nbs anti-IgG-SNAP fusion proteins, as visualized using ChemiDoc XRS+ System (**Supplementary Figure 4**), validating their successful expression. For Nbs anti-IgG-HRP fusion proteins, the pHR vector was used [118]. This lentiviral expression system also employs a bicistronic design via an IRES, allowing EmGFP ($\lambda_{EX}/\lambda_{EM}$= 487/509 nm) co-expressed with the target proteins [151]. As with pMS, the fluorescent protein was not part of the fusion construct but served as a transfection and expression marker. Due to the advantages of the lentiviral system, including the high transfection efficiency and robust protein expression [118], GFP fluorescence in pHR-transfected cells was notable stronger than that observed in pMS-transfected HEK293T cells. Expression of Nbs anti-IgG-HRP in the supernatant was validated not by SNAP-tag labeling but by direct ELISA and IFA (**Figure 4.18**), both of which showed significant positive results compared to the supernatant from non-transfected HEK293T cells. In the IFA, Alexa Fluor 647 conjugated anti-penta-His antibody was used as tertiary antibody to detect the His-tagged Nbs anti-IgG-HRP. Interestingly, fluorescence in the Alexa Fluor 647 channel was observed both on the cell membranes and within the cell nucleus when rabbit-produced anti-EGFR was used as the primary antibody. This nuclear signal was likely due to the permeabilization conditions applied during IFA, which permit antibody into the nucleus, and the use of cell culture supernatant as the secondary antibody, potentially increasing nonspecific interaction.

All fusion proteins were engineered with a His-tag at the C-terminus, composed of six histidine residues, allowing their straightforward isolation by IMAC [152]. In this method, imidazole competes with the histidine residues for binding to the immobilized Ni^{2+} ions on the resin. Stepwise elution with increasing imidazole concentrations (10, 40 and 250 mM) revealed that specific binding occurred at a high concentration, with efficient protein recovery at 250mM imidazole (E3 and E4; **Figure 4.2, Figure 4.19a**). This approach yielded approximately 5 mg/L for Nbs anti-IgG-SNAP and 3 mg/L for Nbs anti-IgG-HRP. Moreover, the mild nature of imidazole elution preserved protein integrity and activity, supporting its suitability for recombinant nanobody purification. The workflows for achieving

high purity and yield in Nbs recombinant protein enrichment was described in **Section 3.2.2.4**.

Following enrichment, Nbs anti-IgG-SNAP fusion proteins were rapidly visualized using SNAP-Surface® Alexa Fluor® 488 labeling (**Figure 4.2a**, **Supplementary Figure 1)**. The calculated molecular weight, incorporating the nanobody (12.8-13.7 kDa), SNAP-tag (20 kDa), Igκ leader and His-tag, was approximately 39 kDa, consistent with the SDS-PAGE. For the Nbs anti-IgG-HRP fusion proteins displayed molecular weight of ~95 kDa (**Figure 4.19b**), which was larger than our expected 55 kDa. This size discrepancy is likely due to PTMs, particularly glycosylation, which is common for HRP expressed in mammalian cells such as HEK293T cells [133]. HRP contains consensus N-glycosylation motifs (Asn-X-Ser/Thr) recognized by the mammalian glycosylation machinery [153], leading to the addition of carbohydrate chains to HRP [154]. Additionally, native plant-derived HRP is also heavily glycosylated, which contributes to its enzymatic stability and activity [155]. Therefore, it is probable that the HEK293T-expressed Nbs anti-IgG-HRP retained similar glycosylation patterns, accounting for its higher molecular weight.

Overall, these results confirm that both pMS and pHR expression systems can successfully produce functional Nbs anti-IgG fusion proteins, with lentiviral delivery providing higher expression efficiency [118]. The combination of fluorescent co-reporters for monitoring, IMAC for enrichment and functional assays for validation ensured high-confidence and recovery of the target proteins. The observed PTMs modification in Nbs anti-IgG-HRP highlight the important of considering host-cell glycosylation in the design and interpretation of recombinant fusion proteins containing glycoprotein components [133] [153] [154] [155].

5.7 The specificity of Nbs anti-IgG-SNAP and Nbs anti-IgG-HRP as secondary antibodies

The global demand for primary antibodies in both research and clinical diagnostics has significantly increased, with mouse- and rabbit-derived antibodies dominating the market. According to Labome antibody data, as of 2021, there were 414,178 rabbit-derived polyclonal antibodies targeting 52,288 genes across 157 species, including 18,749 human genes [156]. By 2022, there were 254,742 mouse-derived monoclonal antibodies identifying 11,079 genes products for 156 species [157]. While monoclonal antibodies are predominantly produced in mice, polyclonal antibodies are mainly derived

from rabbits, making these two species as the main targets for secondary antibody development.

In this study, we adapted a panel of nanobodies originally described by Pleiner et al. [117], comprising four anti-mouse nanobodies—Nb anti-mouse IgG1 Fab (TP886), Nb anti-mouse IgG1 Fc (TP1107), Nb anti-mouse IgG2a Fc (TP1129), Nb anti-mouse kappa chain (TP1170)—and one anti-rabbit nanobody, Nb anti-rabbit IgG Fc (TP897). These nanobodies were fused to SNAP-tag or HRP, creating recombinant secondary antibodies tailored for both species and subclass discrimination. When conjugated with SNAP-Surface® Alexa Fluor® 647 via the SNAP-tag, the resulting Nbs anti-IgG-SNAP-Alexa Fluor® 647 reagents demonstrated species specificity comparable to commercial Alexa Fluor 647 labeled secondary antibodies (**Figure 4.4**). The four Nbs anti-mouse IgG-SNAP-647 bound exclusively to mouse-derived primary antibodies, while the Nb anti-rabbit IgG Fc-SNAP-647 only recognized rabbit-derived antibodies. Subclass testing further confirmed the precision of these reagents: mouse IgG1 antibodies (anti-EpCAM, anti-NG2, anti-HER2, and anti-FOLR1) were detected by both Nb anti-mouse IgG1 Fab-SNAP-647 and Nb anti-mouse IgG1 Fc-SNAP-647, but not by Nb anti-mouse IgG2a Fc-SNAP-647. Conversely, the mouse IgG2a antibody anti-EGFR was detected only by Nb anti-mouse IgG2a Fc-SNAP-647. The kappa light chain, specific nanobody bound all mouse-derived antibodies tested. This observation is consistent with the fact that approximately 95% of mouse-derived antibodies possess kappa chains, while only ~5% contain lambda chains [158]. This predominant increases the likelihood of the kappa-specific nanobody broadly reactive across mouse IgG subclasses. The results underline the specificity and versatility of the Nbs anti-IgG-SNAP-647 for different species and subclasses detection in indirect immunoassays. Nbs anti-IgG-HRP fusions were evaluated for specificity using both Western blot and TSA-based mIF. In Western blot assays (**Figure 4.20**), Nb anti-mouse IgG1 Fab-HRP and Nb anti-mouse IgG1 Fc-HRP bound exclusively to IgG1 antibody, Nb anti-mouse IgG2a Fc-HRP bound only IgG2a antibody, and Nb anti-mouse kappa chain-HRP detected both subclasses, again reflecting light chain distribution. For species specificity, the nanobody-HRP fusions performed comparable to commercial HRP-conjugated secondary antibodies. In TSA-based mIF experiments (**Figure 4.22**), these HRP-fusions maintained subclass discrimination when detecting mouse IgG1 (anti-ERα, anti-CD31), mouse IgG2a (anti-αSMA, anti-CD20) and rabbit IgG (anti-PR). The strong agreement with commercial secondary antibodies and with precious reports

reinforces that Nbs-based secondaries can combine high specificity with the advantages of recombinant production [117], including batch-to-batch consistency and the potential for customizable labeling.

Overall, both SNAP- and HRP- fused Nbs secondaries demonstrated exceptional species and subclass specificity, matching the performance of conventional secondary antibodies while offering additional flexibility for Western blot and TSA-based mIF applications.

5.8 The application of Nbs anti-IgG-SNAP in indirect immunofluorescence assays as secondary antibodies

5.8.1 Nbs anti-IgG-SNAP in flow cytometry and fluorescence microscopy

In this study, various breast cancer cell lines (MDA-MB-231, MDA-MB-468, Hs578T, MCF-7, MDA-MB-453) and endometrial cells (49Z, 12Z, Ishikawa, T-HESC) were used to investigate the expression levels of target molecules and to demonstrate the broad applicability of Nbs anti-IgG-SNAP across diverse cell types. Flow cytometry plays a pivotal role in immunofluorescence assays, as its capacity for rapid and quantitative of extracellularly and intracellularly antigens [159], revealed expression profile consistent with previous studies for multiple markers. Using either Nbs anti-IgG-SNAP-Alexa Fluor® 647 or Alexa Fluor 647 conjugated commercial secondary antibodies, the expression of EGFR, EpCAM, NG2, ANK3 and CTNNB1 was analyzed in breast cancer cell lines (**Figure 4.5**-**4.7**). As shown in **Figure 4.5**, and consistent with previous studies, Nb anti-mouse IgG1 Fab-SNAP-647, Nb anti-mouse IgG1 Fc-SNAP-647 and Nb anti-mouse kappa chain-SNAP-647 detected high EpCAM expression in MDA-MB-468, MCF-7 and MDA-MB-453 cell lines [138]. In contrast, Hs578T and MDA-MB-231 exhibited minimal EpCAM expression [160]. NG2 was abundant in Hs578T and moderate in MDA-MB-231 [161], In contrast, other three cell lines showed minimal NG2 expression, while few studies have reported on these cell lines. EGFR expression, measured by Nb anti-mouse IgG2a Fc-SNAP-647 and Nb anti-mouse kappa chain-SNAP-647 (**Figure 4.6**), was highest in MDA-MB-468 and MDA-MB-231, moderate in Hs578T, and minimal in MDA-MB-453 and MCF-7 [138, 162, 163]. **Figure 4.7** showed the detection of anti-ANK3 and anti-CTNNB1 using Nb anti-rabbit IgG

Fc-SNAP-647 in all breast cancer cell. ANK3 plays a role in maintaining cellular structure and function, with data from The Cancer Genome Atlas (TCGA) indicating its expression in breast cancer tissues [164]. This suggests its potential as a prognostic marker [165]. CTNNB1 is implicated in cancer progression, with previous studies reporting its expression in MDA-MB-468, MDA-MB-231 and MCF-7 [166-168]. Subsequently, the expression of EGFR, HER2, EpCAM and FORL1 in endometrial cells was analyzed using the Nbs anti-IgG-SNAP-Alexa Fluor® 647 (**Figure 4.8**). EGFR was consistently expressed [169-171], and HER2, though less studied its expression in endometrial cells, was also detected in all cells. Using Nb anti-mouse IgG1 Fab-SNAP-647 and Nb anti-mouse kappa chain-SNAP-647, both FOLR1 and EpCAM were presented in Ishikawa cells, supporting their association with endometrial cancer progression [172, 173]. The positive signals for anti-NG2 were observed in 49Z, 12Z and T-HESC cell lines, which represent endometrial epithelial cells or stromal cells. This observation aligned with reports highlighting the role of NG2 in the normal regenerative process of the endometrium [174].

Comparisons of fluorescence intensities (**Figure 4.6-4.8**) revealed that signals from Nb anti-mouse IgG2a Fc-SNAP-647 and Nb anti-rabbit IgG Fc-SNAP-647 yielded relatively weaker than those for commercial Alexa Fluor 647-conjugated secondary antibodies. This is likely due to the fluorophore stoichiometry: the Alexa Fluor 647 conjugated commercial secondary antibodies (Thermo Fisher Scientific) typically carry 2-8 fluorophores per IgG molecule, producing sustainable amplification for low-abundance targets, whereas Nbs anti-IgG-SNAP bind a single BG-modified fluorophore (e.g. SNAP-Surface® Alexa Fluor® 647) in a strict 1:1 ratio [102, 175]. Nb anti-mouse kappa chain-SNAP-647 generated stronger signals than Nb anti-mouse IgG2a Fc-SNAP-647 **(Figure 4.6)**, consistent with its ability to bind four sites per primary, while Nb anti-mouse IgG2a Fc-SNAP-647 provides two binding sites per primary antibody (**Figure 1.1**).

Fluorescence microscopy complemented these findings by visualizing the localization and distribution of fluorescently labeled molecules within individual cells. In this study, the same cells, primary antibodies and their corresponding Nbs anti-IgG-SNAP-Alexa Fluor® 647 or Alexa Fluor 647 conjugated commercial secondary antibodies, used for flow cytometry, were also applied to fluorescence microscopy (**Figure 4.9-4.12)**. EGFR was expressed on the cell membrane and in the

cytoplasm, HER2 localized predominantly in the cytoplasm, while EpCAM, FOLR1 and NG2 were membrane associated expression, and ANK3 and CTNNB1 were cytoplasmatic antigens. These findings were in agreement with both our flow cytometry data and previous studies [176-182]. In **Figure 4.9a**, MDA-MB-231 cells showed no detectable EpCAM expression by fluorescence microscopy, which has a discrepancy in the minimal expression observed in **Figure 4.5a** using flow cytometry. This difference reflects the higher sensitivity of flow cytometry compared to fluorescence microscopy, as it is more adept at detecting lower levels of expression [183].

In summary, these results demonstrate that Nbs anti-IgG-SNAP-Alexa Fluor® 647 secondaries provide accurate species- and subclass-specific detection in both quantitative (flow cytometry) and spatial (fluorescence microscopy) assays. The defined labeling stoichiometry of the SNAP-tag ensures reproducibility, while the ability to maintain performance across diverse cell types underscores its potential for standardized IFA workflows.

5.8.2 Nbs anti-IgG-SNAP for multicolor immunofluorescence

After evaluating the performance of Nbs anti-IgG-SNAP in flow cytometry and fluorescence microscopy, their potential for multicolor immunofluorescence in paraffin-embedded cell blocks was explored. SNAP-tag technology has been shown to effectively covalently conjugate various BG-modified fluorophores, enabling multicolor imaging in live-cell [109]. Since cell block is a paraffin-embedded technique, it is valuable for both IHC and long-term storage, and it plays a crucial role in diagnostic cytology, bridging a gap between cytology and histology [184].Given its importance, cell block technology is an ideal platform for IHC and multicolor immunofluorescence in this study. This approach enabled the exploitation of the versatility of Nbs anti-IgG-SNAP for high-quality, multi-color imaging, while preserving the diagnostic relevance of the cell block format. In **Figure 4.13**, the endometrial cell block (49Z, 12Z, Ishikawa, T-HESC) analyzed with IHC yield consistent results with previous results in flow cytometry and fluorescence microscopy. All cells were positive for EGFR and HER2, while Ishikawa cells were FOLR1- and EpCAM-positive but NG2-negative. Subsequently, Nbs anti-IgG-SNAP were labeled with SNAP-Surface® Alexa Fluor® 488, 546 or 594, following the protocol described in **Section 3.2.3**. The multicolor staining strategy was outlined in **Table 3.19**. The

staining patterns in panel A and B are shown in **Figure 4.14a, f** and **4.15a, f**. These results revealed target-specific fluorescence without cross-interference, as confirmed by leave-one-out controls or post-incubation with Nbs anti-IgG-SNAP-647 (**Figure 4.14**, **Figure 4.15**), validating the multi-color staining approach and the specificity of the Nbs anti-IgG-SNAP conjugates for simultaneous detection of multiple antigens in a single cell block.

Compare to live-cell multicolor staining using some BG-modified fluorophores [109], the multicolor strategy of Nbs anti-IgG-SNAP conjugates here yielded clean, specific signals. While previous dual-color SNAP-tag methods have relied on CLIP-tag or Halo-tag [185-187], these direct detection methods labeled proteins with individual fluorophores to detect two target molecules, our Nbs anti-IgG-SNAP enables the indirect detection for multiple targets. This offers greater flexibility for labeling endogenous targets without genetic modification and expands the number of detectable markers by combining Nbs anti-IgG-SNAP fusions with primary antibodies of defined species and subclass specificity.

The performance of Nbs anti-IgG-SNAP in multi-color immunofluorescence was consistent with earlier assay. In flow cytometry, Nbs anti-IgG-SNAP-Alexa Fluor® 647 exhibited fluorescence intensities and quantitative reliability comparable to those of Alexa Fluor 647 conjugated commercial secondary antibodies, accurately distinguishing low- and high-expression targets. In fluorescence microscopy, the Nbs anti-IgG-SNAP-Alexa Fluor® 647 produced high-resolution fluorescence signals, comparable to those generated by commercial secondary antibodies. Additionally, the smaller sizes of the Nbs (≈ 39 kDa) provide enhanced accuracy for protein localization, offering an advantage over larger commercial antibodies (~150 kDa) [127]. These capabilities enable precise visualization of protein localization in fixed cells. Unlike pre-conjugated commercial secondary antibodies, which are restricted to fixed fluorophores and may increase costs, complexity and potential spectral overlap in multi-color imaging, the generated Nbs anti-IgG-SNAP permits customized fluorophore conjugation. This flexibility minimizes spectral interference, facilitates optimal channel selection and reduced costs associated with maintaining multiple dye-conjugated secondary reagents. In addition, the unique feature of SNAP-tag conjugates with a defined 1:1 stoichiometry to fluorophores is essential for quantitative flow cytometry, improving the reliability of data in protein expression or interaction

analyses [188].

Taken together, these findings demonstrate that Nbs anti-IgG-SNAP combined high specificity, low back ground and flexible fluorophore selection, making them as a competitive alternative to traditional secondary antibodies in both researches and diagnostics.

5.9 The application of Nbs anti-IgG-HRP in Western blot

To date, most studies focused on developing nanobodies conjugated with HRP as detection reagents for ELISA applications, demonstrating excellent sensitivity for pathogen detection, antibody quantification and biomarker analysis [189-191]. While ELISA remains a powerful and high-throughput format for protein quantification, Western blotting provides complementary advantages, particularly in the ability to separate proteins by molecular weight via SDS-PAGE. This character enables not only the identification of target proteins and the verification of their sizes but also the detection of PTMs such as phosphorylation, glycosylation, and ubiquitination, which are important for understanding the function and regulation of target proteins [192, 193]. Additionally, the gel separation step reduces the risk of false positives caused by non-specific binding in complex biological samples. In this study, Nb anti-mouse IgG1 Fab-HRP, Nb anti-mouse IgG1 Fc-HRP, Nb anti-mouse IgG2a Fc-HRP, Nb anti-mouse kappa chain-HRP and Nb anti-rabbit IgG Fc-HRP were generated to be used as secondary antibodies for Western blot. Their species and subclass specificities were first validated (**Figure 4.20**), confirming that each Nbs anti-IgG-HRP recognized only its intended target without cross-reactivity. We then applied these reagents to detect three anti-EGFR antibodies in two breast cancer cell lines (MDA-MB-468, MDA-MB-453) and two endometrial cell lines (Ishikawa, T-HESC) (**Figure 4.21**). Using anti-GAPDH as an internal control, EGFR was detected in MDA-MB-468, Ishikawa and T-HESC cells but was absent in MDA-MB-453 cells. Subcalss-specific recognition was clearly maintained: **Figure 4.21a** shows that Nb anti-mouse IgG1 Fab-HRP, Nb anti-mouse IgG1 Fc-HRP, and Nb anti-mouse kappa chain-HRP detected anti-EGFR (mouse/IgG1); **Figure 4.21b** shows Nb anti-mouse IgG2a Fc-HRP and Nb anti-mouse kappa chain-HRP detected anti-EGFR (mouse/IgG2a). **Figure 4.21c** shows Nb anti-rabbit IgG Fc-HRP detected anti-EGFR (rabbit/IgG).

These results demonstrate that our Nbs anti-IgG-HRP fusion proteins mirrored the performance of

commercial HRP-conjugated secondary antibodies and aligned with earlier studies confirming the high specificity and low background of Nbs anti-IgG-HRP constructs [117, 194]. Importantly, no inaccurate binding was observed, reinforcing the value of Nbs anti-IgG-HRP fusions as highly selective reagents. By extending the application of HRP-conjugated nanobodies beyond ELISA into Western blotting, this study demonstrates that such reagents can provide the same species and subclass specificity, reduced background and batch-to-batch reproducibility, while retaining the additional molecular weight that Western blotting uniquely offers. Given this small size, recombinant origin and engineering flexibility, Nbs anti-IgG-HRP represent a competitive and versatile alternative to traditional HRP-conjugated secondary antibodies for both research and diagnostic protein analysis.

5.10 The application of Nbs anti-IgG-HRP in TSA-based mIF

TSA-based mIF enables simultaneous detection of multiple antigens within a single tissue section by amplifying fluorescence signals. This method utilizes the catalytic activity of HRP to deposit tyramide-conjugated fluorophores near the target proteins, leading to enhance signal intensity and facilitating visualization of low-abundance target proteins. Moreover, TSA-base mIF enables to use multiple primary antibodies from the same species without significant cross-reactivity, and is particularly effective for FFPE tissues, which are commonly used in clinical diagnosis. These advantages make TSA-base mIF to be a powerful tool for investigating tumor immune microenvironment (TIME) and cancer immunotherapy [112, 195, 196].

Opal methodology is commonly used in TSA-base mIF, providing a standardized reagents and workflows [197-199], but its high cost and dependence on specialized imaging systems can limit adoption in standard laboratory settings [200]. To address these challenges, this study evaluated Nbs anti-IgG-HRP in a cost-effective, fully manual TSA-based mIF protocol using commercially available tyramide fluorophores and a conventional multispectral slide scanner.

Five biologically and clinically relevant antigens (ERα, PR, αSMA, CD31 and CD20) were selected. ERα and PR are key factors in the pathogenesis and progression of endometriotic lesions, and reflect its hormone-dependent nature [201, 202], αSMA and CD31 can evaluate vascularization in deep endometriosis [203], while CD20 indicates proinflammatory microenvironment in endometriosis [204].

Specificity of each Nb anti-IgG-HRP was confirmed by IHC in both single endometriosis tissue sample and TMA (**Figure 4.23**-**4.25**). Expression analysis revealed that ERα and PR were not consistently expressed in the endometriosis tissues, aligning with previous studies that highlight the complex hormone disturbances associated with endometriosis [202, 205]. Based on the IHC results, ERα and PR staining were observed in the nuclei of glandular or stromal cells, consistent with previous studies [121, 122] and spatial proximity between proximity CD31- and αSMA-positive cells were observed. This frequent challenge in mIF has been previously reported, emphasizing the need to carefully design panels with antigens exhibiting similar expression patterns while ensuring they are paired with tyramide-fluorophores featuring sufficiently distinct excitation and emission spectra [197, 206, 207]. To minimize spectral overlap, a five-plex mIF panel was designed carefully (**Table 4.4**) using alternative tyramide fluorophores: iFluor® 430 Styramide for Opal 480, Alexa Fluor™ 488 for Opal 520, Alexa Fluor™ 546 for Opal 570, Alexa Fluor™ 647 for Opal 690 and iFluor® 750 Styramide for Opal 780.

The manual mIF protocol was optimized by adjusting several parameters, including: dilutions of primary antibodies and tyramide-fluorophores, antigen retrieval buffer, antigen retrieval time, tyramide-fluorophores, fluorescence incubation time and heat-induced epitope retrieval (HIER) time for stripping the bound primary-secondary antibodies complex away, was described in **Section 3.2.12**. Chromogenic IHC confirmed that Nbs anti-IgG-HRP and HRP-conjugated commercial secondary antibodies yielded identical staining patterns (**Figure 4.23**). The optimized mIF protocol achieved consistent, high-quality signals with minimal cross-reactivity over five sequential staining cycles (**Figure 4.24**). Leave-on-out controls verified that the observed fluorescence signals originated solely from the intended primary antibody, ruling out residual antibody complexes from previous cycle. This result validated the reliability of the manual mIF protocol for FFPE tissues. Furthermore, Nbs anti-IgG-HRP demonstrated high precision in targeting specific antigen epitopes, significantly enhancing the efficiency of TSA-based mIF. Their monoclonal nature minimized cross-reactivity and background noise, generating distinct and well-defined fluorescent signals. In contrast, commercial polyclonal antibodies, which bind multiple epitopes, increased the likelihood of non-specific interactions and higher background signals [208], while their small molecular size improves tissue penetration, which

is especially advantageous in TSA-based mIF, where uniform staining and precise antigen detection are critical [209].

To assess broader applicability of this protocol, endometriosis TMAs were analyzed, with imaging parameters for Axio Scan.Z1 slide scanner detailed in **Supplementary Figure 3**. As shown in **Figure 4.25**, mIF performed with Nbs anti-IgG-HRP and commercial HRP-conjugated secondary antibodies produced similar positive cells patterns as chromogenic IHC. The mIF method exhibited greater sensitivity and stronger fluorescence signal, owing to the enhanced amplification capabilities of the TSA technique [210]. Quantification of full six-color staining in TMA (**Figure 4.26)** was performed using the advanced image analysis tool Qupath [124, 211, 212]. No statistical differences were observed in positive cell numbers or positive cell percentage between Nbs and commercial antibodies (**Figure 4.27a, b**). A heatmap (**Figure 4.27c**) further corroborated their comparable performance.

In conclusion, Nbs anti-IgG-HRP demonstrated equivalent performance to commercial HRP-conjugated secondary antibodies, highlighting their potential as a substitute. The robust, low-cost manual protocol developed here enables high-quality multiplex imaging in standard laboratories, expanding access to TSA-based mIF without reliance on proprietary kits or specialized platforms.

6. References

1. Yalow, R.S. and S.A. Berson, *Assay of plasma insulin in human subjects by immunological methods*. Nature, 1959. **184 (Suppl 21)**: p. 1648-9.
2. Ekins, R.P., *The estimation of thyroxine in human plasma by an electrophoretic technique.* Clinica Chimica Acta, 1960. **5**(4): p. 453-459.
3. Hammett-Stabler, C.A., A.J. Pesce, and D.J. Cannon, *Urine drug screening in the medical setting.* Clin Chim Acta, 2002. **315**(1-2): p. 125-35.
4. Marr, K.A., et al., *Detection of galactomannan antigenemia by enzyme immunoassay for the diagnosis of invasive aspergillosis: variables that affect performance*. J Infect Dis, 2004. **190**(3): p. 641-9.
5. Zhou, Y., et al., *Development of a monoclonal antibody-based sandwich-type enzyme-linked immunosorbent assay (ELISA) for detection of abrin in food samples.* Food Chem, 2012. **135**(4): p. 2661-5.
6. Vanderlaan, M., B.E. Watkins, and L. Stanker, *ES Critical Review: Environmental monitoring by immunoassay.* Environ Sci Technol, 1988. **22**(3): p. 247-54.
7. Sakamoto, S., et al., *Enzyme-linked immunosorbent assay for the quantitative/qualitative analysis of plant secondary metabolites*. J Nat Med, 2018. **72**(1): p. 32-42.
8. Ghosh, R., J.E. Gilda, and A.V. Gomes, *The necessity of and strategies for improving confidence in the accuracy of western blots*. Expert Rev Proteomics, 2014. **11**(5): p. 549-60.
9. Bisht, D., et al., *Protocols for Immunofluorescence Techniques*, in *Protocols for the Diagnosis of Pig Viral Diseases*. 2022, Springer. p. 215-229.
10. Nambirajan, A. and D. Jain, *Cell blocks in cytopathology: An update.* Cytopathology, 2018. **29**(6): p. 505-524.
11. Hofman, F., *Immunohistochemistry.* Curr Protoc Immunol, 2002. **Chapter 21**: p. Unit 21 4.
12. Thompson, S.J.T.P.P.H., *Immunoprecipitation and Blotting: The Visualization of Small Amounts of Antigens Using Antibodies and Lectins*. 2009: p. 1845-1858.
13. Blake, C. and B.J. Gould, *Use of enzymes in immunoassay techniques. A review.* Analyst, 1984. **109**(5): p. 533-547.
14. Hicks, J.M., *Fluorescence immunoassay.* Human pathology, 1984. **15**(2): p. 112-116.
15. Liu, G. and Y. Lin, *Nanomaterial labels in electrochemical immunosensors and immunoassays.* Talanta, 2007. **74**(3): p. 308-17.
16. Chard, T., *Introduction to radioimmunoassay and related techniques*. 1978.
17. Padlan, E.A., *X-ray crystallography of antibodies.* Advances in protein chemistry, 1996. **49**: p. 57-134.
18. Morea, V., et al., *Conformations of the third hypervariable region in the VH domain of immunoglobulins*. Journal of molecular biology, 1998. **275**(2): p. 269-294.
19. Leenaars, M. and C.F. Hendriksen, *Critical steps in the production of polyclonal and monoclonal antibodies: evaluation and recommendations.* ILAR J, 2005. **46**(3): p. 269-79.
20. Gorovits, B., et al., *AAPS Perspective on the EURL Recommendation on the use of Non-Animal-Derived Antibodies.* AAPS J, 2021. **23**(2): p. 34.
21. Voskuil, J.J.F., *Commercial antibodies and their validation.* 2014. **3**.
22. Hermanson, G., *Bioconjugate Techniques*. 1996, Academic Press.
23. Chiu, M.L., et al., *Antibody Structure and Function: The Basis for Engineering Therapeutics.* Antibodies (Basel), 2019. **8**(4).

24. Uhlen, M., et al., *A proposal for validation of antibodies.* Nat Methods, 2016. **13**(10): p. 823-7.
25. Coleman, L. and S.M. Mahler, *Purification of Fab fragments from a monoclonal antibody papain digest by Gradiflow electrophoresis.* Protein Expr Purif, 2003. **32**(2): p. 246-51.
26. Li, L., et al., *Single-chain fragment variable produced by phage display technology: Construction, selection, mutation, expression, and recent applications in food safety.* Compr Rev Food Sci Food Saf, 2022. **21**(5): p. 4354-4377.
27. Griffiths, A.D. and A.R. Duncan, *Strategies for selection of antibodies by phage display.* Curr Opin Biotechnol, 1998. **9**(1): p. 102-8.
28. Sompunga, P., et al., *Generation of human and rabbit recombinant antibodies for the detection of Zearalenone by phage display antibody technology.* Talanta, 2019. **201**: p. 397-405.
29. He, J., et al., *One-step immunoassay for the insecticide carbaryl using a chicken single-chain variable fragment (scFv) fused to alkaline phosphatase.* Anal Biochem, 2019. **572**: p. 9-15.
30. Shen, C., et al., *Establishment of monoclonal antibody and scFv immuno-based assay for Cry2Aa toxin in spiked grain samples.* Anal Biochem, 2023. **677**: p. 115270.
31. Baneyx, F., *Recombinant protein expression in Escherichia coli.* Curr Opin Biotechnol, 1999. **10**(5): p. 411-21.
32. Ho, M., S. Nagata, and I. Pastan, *Isolation of anti-CD22 Fv with high affinity by Fv display on human cells.* Proc Natl Acad Sci U S A, 2006. **103**(25): p. 9637-42.
33. Dumoulin, M., et al., *Single-domain antibody fragments with high conformational stability.* Protein Sci, 2002. **11**(3): p. 500-15.
34. Kim, H.J., et al., *Isolation of alpaca anti-hapten heavy chain single domain antibodies for development of sensitive immunoassay.* Anal Chem, 2012. **84**(2): p. 1165-71.
35. Hamers-Casterman, C., et al., *Naturally occurring antibodies devoid of light chains.* Nature, 1993. **363**(6428): p. 446-8.
36. Muyldermans, S., *Nanobodies: natural single-domain antibodies.* Annu Rev Biochem, 2013. **82**: p. 775-97.
37. Greenberg, A.S., et al., *A new antigen receptor gene family that undergoes rearrangement and extensive somatic diversification in sharks.* Nature, 1995. **374**(6518): p. 168-73.
38. Zielonka, S., et al., *Structural insights and biomedical potential of IgNAR scaffolds from sharks.* MAbs, 2015. **7**(1): p. 15-25.
39. Harmsen, M.M. and H.J. De Haard, *Properties, production, and applications of camelid single-domain antibody fragments.* Appl Microbiol Biotechnol, 2007. **77**(1): p. 13-22.
40. Cortez-Retamozo, V., et al., *Efficient cancer therapy with a nanobody-based conjugate.* Cancer Res, 2004. **64**(8): p. 2853-7.
41. Wang, Y., et al., *Nanobody-derived nanobiotechnology tool kits for diverse biomedical and biotechnology applications.* Int J Nanomedicine, 2016. **11**: p. 3287-303.
42. Tanha, J., et al., *Selection by phage display of llama conventional V(H) fragments with heavy chain antibody V(H)H properties.* J Immunol Methods, 2002. **263**(1-2): p. 97-109.
43. Sun, S., et al., *Nanobody: A Small Antibody with Big Implications for Tumor Therapeutic Strategy.* Int J Nanomedicine, 2021. **16**: p. 2337-2356.
44. Decanniere, K., S. Muyldermans, and L. Wyns, *Canonical antigen-binding loop structures in immunoglobulins: more structures, more canonical classes?* J Mol Biol, 2000. **300**(1): p. 83-91.
45. De Genst, E., et al., *Molecular basis for the preferential cleft recognition by dromedary heavy-chain*

antibodies. Proc Natl Acad Sci U S A, 2006. **103**(12): p. 4586-91.
46. Mitchell, L.S. and L.J. Colwell, *Analysis of nanobody paratopes reveals greater diversity than classical antibodies.* Protein Eng Des Sel, 2018. **31**(7-8): p. 267-275.
47. Victora, G.D. and M.C. Nussenzweig, *Germinal centers.* Annu Rev Immunol, 2012. **30**: p. 429-57.
48. Decanniere, K., et al., *A single-domain antibody fragment in complex with RNase A: non-canonical loop structures and nanomolar affinity using two CDR loops.* Structure, 1999. **7**(4): p. 361-70.
49. Liu, M., et al., *Nanobody-A versatile tool for cancer diagnosis and therapeutics.* Wiley Interdiscip Rev Nanomed Nanobiotechnol, 2021. **13**(4): p. e1697.
50. Mitchell, L.S. and L.J. Colwell, *Comparative analysis of nanobody sequence and structure data.* Proteins, 2018. **86**(7): p. 697-706.
51. Hussack, G., C.R. Mackenzie, and J. Tanha, *Characterization of single-domain antibodies with an engineered disulfide bond.* Methods Mol Biol, 2012. **911**: p. 417-29.
52. Van Audenhove, I. and J. Gettemans, *Nanobodies as Versatile Tools to Understand, Diagnose, Visualize and Treat Cancer.* Ebiomedicine, 2016. **8**: p. 40-48.
53. Saerens, D., et al., *Disulfide bond introduction for general stabilization of immunoglobulin heavy-chain variable domains.* Journal of molecular biology, 2008. **377**(2): p. 478-488.
54. Hermeling, S., et al., *Structure-immunogenicity relationships of therapeutic proteins.* Pharm Res, 2004. **21**(6): p. 897-903.
55. Muyldermans, S., C. Cambillau, and L. Wyns, *Recognition of antigens by single domain antibody fragments: the superfluous luxury of paired domains.* Trends in Biochemical Sciences, 2001. **26**(4): p. 230-235.
56. Kijanka, M., et al., *Nanobody-based cancer therapy of solid tumors.* Nanomedicine (Lond), 2015. **10**(1): p. 161-74.
57. Ackaert, C., et al., *Immunogenicity Risk Profile of Nanobodies.* Front Immunol, 2021. **12**: p. 632687.
58. Vincke, C., et al., *General strategy to humanize a camelid single-domain antibody and identification of a universal humanized nanobody scaffold.* J Biol Chem, 2009. **284**(5): p. 3273-3284.
59. Muyldermans, S., *A guide to: generation and design of nanobodies.* FEBS J, 2021. **288**(7): p. 2084-2102.
60. Koch-Nolte, F., et al., *Single domain antibodies from llama effectively and specifically block T cell ecto-ADP-ribosyltransferase ART2.2 in vivo.* FASEB J, 2007. **21**(13): p. 3490-8.
61. Peyrassol, X., et al., *Development by Genetic Immunization of Monovalent Antibodies (Nanobodies) Behaving as Antagonists of the Human ChemR23 Receptor.* J Immunol, 2016. **196**(6): p. 2893-901.
62. Janssens, R., et al., *Generation of heavy-chain-only antibodies in mice.* Proc Natl Acad Sci U S A, 2006. **103**(41): p. 15130-5.
63. Teng, Y., et al., *Diverse human V(H) antibody fragments with bio-therapeutic properties from the Crescendo Mouse.* N Biotechnol, 2020. **55**: p. 65-76.
64. Hoogenboom, H.R., *Selecting and screening recombinant antibody libraries.* Nat Biotechnol, 2005. **23**(9): p. 1105-16.
65. Smith, G.P., *Filamentous fusion phage: novel expression vectors that display cloned antigens on the virion surface.* Science, 1985. **228**(4705): p. 1315-7.
66. McCafferty, J., et al., *Phage antibodies: filamentous phage displaying antibody variable domains.* Nature, 1990. **348**(6301): p. 552-4.
67. Rossotti, M.A., et al., *Method for Sorting and Pairwise Selection of Nanobodies for the Development of Highly Sensitive Sandwich Immunoassays.* Anal Chem, 2015. **87**(23): p. 11907-14.

68. Egloff, P., et al., *Engineered peptide barcodes for in-depth analyses of binding protein libraries.* Nat Methods, 2019. **16**(5): p. 421-428.
69. Muyldermans, S., *Single domain camel antibodies: current status.* J Biotechnol, 2001. **74**(4): p. 277-302.
70. Liu, Y. and H. Huang, *Expression of single-domain antibody in different systems.* Appl Microbiol Biotechnol, 2018. **102**(2): p. 539-551.
71. Virdi, V., et al., *Orally fed seeds producing designer IgAs protect weaned piglets against enterotoxigenic Escherichia coli infection.* Proc Natl Acad Sci U S A, 2013. **110**(29): p. 11809-14.
72. Lentz, E.M., et al., *Translational fusion and redirection to thylakoid lumen as strategies to improve the accumulation of a camelid antibody fragment in transplastomic tobacco.* Planta, 2012. **236**(2): p. 703-14.
73. Bazl, M.R., et al., *Production of chimeric recombinant single domain antibody-green fluorescent fusion protein in Chinese hamster ovary cells.* Hybridoma (Larchmt), 2007. **26**(1): p. 1-9.
74. Kooijmans, S.A.A., et al., *Recombinant phosphatidylserine-binding nanobodies for targeting of extracellular vesicles to tumor cells: a plug-and-play approach.* Nanoscale, 2018. **10**(5): p. 2413-2426.
75. Nguyen, V.K., et al., *Heavy-chain only antibodies derived from dromedary are secreted and displayed by mouse B cells.* Immunology, 2003. **109**(1): p. 93-101.
76. Pardon, E., et al., *A general protocol for the generation of Nanobodies for structural biology.* Nat Protoc, 2014. **9**(3): p. 674-93.
77. Kariuki, C.K. and S. Magez, *Improving the yield of recalcitrant Nanobodies(R) by simple modifications to the standard protocol.* Protein Expr Purif, 2021. **185**: p. 105906.
78. Crauwels, M., et al., *Reshaping nanobodies for affinity purification on protein a.* N Biotechnol, 2020. **57**: p. 20-28.
79. Li, X., et al., *Capture and purification of an untagged nanobody by mixed weak cation chromatography and cation exchange chromatography.* Protein Expr Purif, 2022. **192**: p. 106030.
80. Tsien, R.Y., *The green fluorescent protein.* Annu Rev Biochem, 1998. **67**: p. 509-44.
81. Chalfie, M., et al., *Green fluorescent protein as a marker for gene expression.* Science, 1994. **263**(5148): p. 802-805.
82. Shaner, N.C., P.A. Steinbach, and R.Y. Tsien, *A guide to choosing fluorescent proteins.* Nat Methods, 2005. **2**(12): p. 905-9.
83. Bindels, D.S., et al., *mScarlet: a bright monomeric red fluorescent protein for cellular imaging.* Nat Methods, 2017. **14**(1): p. 53-56.
84. Kommidi, S.S.R., K.M. Atkinson, and B.D. Smith, *Steric protection of near-infrared fluorescent dyes for enhanced bioimaging.* J Mater Chem B, 2024. **12**(34): p. 8310-8320.
85. Montecinos-Franjola, F., et al., *GFP fluorescence tagging alters dynamin-related protein 1 oligomerization dynamics and creates disassembly-refractory puncta to mediate mitochondrial fission.* Sci Rep, 2020. **10**(1): p. 14777.
86. Budiarta, M., M. Streit, and G. Beliu, *Site-specific protein labeling strategies for super-resolution microscopy.* Curr Opin Chem Biol, 2024. **80**: p. 102445.
87. Grimm, J.B., et al., *A general method to fine-tune fluorophores for live-cell and in vivo imaging.* Nat Methods, 2017. **14**(10): p. 987-994.
88. Marx, V., *Probes: paths to photostability.* Nat Methods, 2015. **12**(3): p. 187-90.
89. Nanda, J.S. and J.R. Lorsch, *Labeling a protein with fluorophores using NHS ester derivitization.* Methods Enzymol, 2014. **536**: p. 87-94.

90. Hermanson, G.T., *Bioconjugate techniques*. 2013: Academic press.
91. Partis, M.D., et al., *Cross-linking of protein by ω-maleimido alkanoylN-hydroxysuccinimido esters.* Journal of Protein Chemistry, 1983. **2**(3): p. 263-277.
92. Pickens, C.J., et al., *Practical Considerations, Challenges, and Limitations of Bioconjugation via Azide-Alkyne Cycloaddition.* Bioconjug Chem, 2018. **29**(3): p. 686-701.
93. Choe, W., T.A. Durgannavar, and S.J. Chung, *Fc-Binding Ligands of Immunoglobulin G: An Overview of High Affinity Proteins and Peptides*. Materials (Basel), 2016. **9**(12).
94. Diamandis, E.P. and T.K. Christopoulos, *The biotin-(strept)avidin system: principles and applications in biotechnology.* Clin Chem, 1991. **37**(5): p. 625-36.
95. Cole, N.B., *Site-specific protein labeling with SNAP-tags.* Curr Protoc Protein Sci, 2013. **73**: p. 30 1 1-30 1 16.
96. England, C.G., H. Luo, and W. Cai, *HaloTag technology: a versatile platform for biomedical applications.* Bioconjug Chem, 2015. **26**(6): p. 975-86.
97. Gautier, A., et al., *An engineered protein tag for multiprotein labeling in living cells*. Chem Biol, 2008. **15**(2): p. 128-36.
98. Theile, C.S., et al., *Site-specific N-terminal labeling of proteins using sortase-mediated reactions.* Nat Protoc, 2013. **8**(9): p. 1800-7.
99. Keppler, A., et al., *A general method for the covalent labeling of fusion proteins with small molecules in vivo.* Nat Biotechnol, 2003. **21**(1): p. 86-9.
100. Los, G.V., et al., *HaloTag: a novel protein labeling technology for cell imaging and protein analysis.* ACS Chem Biol, 2008. **3**(6): p. 373-82.
101. Pegg, A.E., *Repair of O6-alkylguanine by alkyltransferases.* Mutation Research/Reviews in Mutation Research, 2000. **462**(2-3): p. 83-100.
102. Keppler, A., et al., *Labeling of fusion proteins of O6-alkylguanine-DNA alkyltransferase with small molecules in vivo and in vitro.* Methods, 2004. **32**(4): p. 437-44.
103. Keppler, A., et al., *Labeling of fusion proteins with synthetic fluorophores in live cells.* Proc Natl Acad Sci U S A, 2004. **101**(27): p. 9955-9.
104. Srikun, D., et al., *Organelle-targetable fluorescent probes for imaging hydrogen peroxide in living cells via SNAP-Tag protein labeling.* J Am Chem Soc, 2010. **132**(12): p. 4455-65.
105. Hein, B., et al., *Stimulated emission depletion nanoscopy of living cells using SNAP-tag fusion proteins.* Biophys J, 2010. **98**(1): p. 158-63.
106. Maurel, D., et al., *Cell-surface protein-protein interaction analysis with time-resolved FRET and snap-tag technologies: application to GPCR oligomerization.* Nat Methods, 2008. **5**(6): p. 561-7.
107. Hussain, A.F., et al., *One-step site-specific antibody fragment auto-conjugation using SNAP-tag technology.* Nat Protoc, 2019. **14**(11): p. 3101-3125.
108. Bodor, D.L., et al., *Analysis of protein turnover by quantitative SNAP-based pulse-chase imaging.* Curr Protoc Cell Biol, 2012. **Chapter 8**: p. Unit8 8.
109. Bosch, P.J., et al., *Evaluation of fluorophores to label SNAP-tag fused proteins for multicolor single-molecule tracking microscopy in live cells.* Biophys J, 2014. **107**(4): p. 803-14.
110. Bobrow, M.N., K.J. Shaughnessy, and G.J. Litt, *Catalyzed reporter deposition, a novel method of signal amplification. II. Application to membrane immunoassays.* J Immunol Methods, 1991. **137**(1): p. 103-12.
111. Faget, L. and T.S. Hnasko, *Tyramide Signal Amplification for Immunofluorescent Enhancement.* Methods

Mol Biol, 2015. **1318**: p. 161-72.
112. Stack, E.C., et al., *Multiplexed immunohistochemistry, imaging, and quantitation: a review, with an assessment of Tyramide signal amplification, multispectral imaging and multiplex analysis.* Methods, 2014. **70**(1): p. 46-58.
113. Parra, E.R., et al., *Procedural Requirements and Recommendations for Multiplex Immunofluorescence Tyramide Signal Amplification Assays to Support Translational Oncology Studies.* Cancers (Basel), 2020. **12**(2).
114. Hernandez, S., et al., *Multiplex Immunofluorescence Tyramide Signal Amplification for Immune Cell Profiling of Paraffin-Embedded Tumor Tissues.* Front Mol Biosci, 2021. **8**: p. 667067.
115. Anyaegbu, C.C., et al., *Optimisation of multiplex immunofluorescence for a non-spectral fluorescence scanning system.* J Immunol Methods, 2019. **472**: p. 25-34.
116. Stocker, M., et al., *Secretion of functional anti-CD30-angiogenin immunotoxins into the supernatant of transfected 293T-cells.* Protein Expr Purif, 2003. **28**(2): p. 211-9.
117. Pleiner, T., M. Bates, and D. Gorlich, *A toolbox of anti-mouse and anti-rabbit IgG secondary nanobodies.* J Cell Biol, 2018. **217**(3): p. 1143-1154.
118. Elegheert, J., et al., *Lentiviral transduction of mammalian cells for fast, scalable and high-level production of soluble and membrane proteins.* Nat Protoc, 2018. **13**(12): p. 2991-3017.
119. Varghese, F., et al., *IHC Profiler: an open source plugin for the quantitative evaluation and automated scoring of immunohistochemistry images of human tissue samples.* PLoS One, 2014. **9**(5): p. e96801.
120. Hartmann, C. and P.R. Ortiz de Montellano, *Baculovirus expression and characterization of catalytically active horseradish peroxidase.* Arch Biochem Biophys, 1992. **297**(1): p. 61-72.
121. Bedaiwy, M.A., et al., *Abundance and Localization of Progesterone Receptor Isoforms in Endometrium in Women With and Without Endometriosis and in Peritoneal and Ovarian Endometriotic Implants.* Reprod Sci, 2015. **22**(9): p. 1153-61.
122. Hudelist, G., et al., *Estrogen receptor beta and matrix metalloproteinase 1 are coexpressed in uterine endometrium and endometriotic lesions of patients with endometriosis.* Fertil Steril, 2005. **84 Suppl 2**: p. 1249-56.
123. Al-Rifai, R., et al., *In vivo efficacy of endothelial growth medium stimulated mesenchymal stem cells derived from patients with critical limb ischemia.* J Transl Med, 2019. **17**(1): p. 261.
124. Bankhead, P., et al., *QuPath: Open source software for digital pathology image analysis.* Sci Rep, 2017. **7**(1): p. 16878.
125. Odell, I.D. and D. Cook, *Immunofluorescence techniques.* J Invest Dermatol, 2013. **133**(1): p. e4.
126. Gray, A.C., et al., *Reproducibility: bypass animals for antibody production.* Nature, 2020. **581**(7808): p. 262.
127. Sograte-Idrissi, S., et al., *Correction: Circumvention of common labelling artefacts using secondary nanobodies.* Nanoscale, 2020. **12**(48): p. 24543.
128. EC, *Directive 2010/63/EU of the European Parliament and of the Council of 22 September 2010 on the protection of animals used for scientific purposes.* Official Journal of the European Union, 2010. **50**.
129. Kunert, R. and D. Reinhart, *Advances in recombinant antibody manufacturing.* Appl Microbiol Biotechnol, 2016. **100**(8): p. 3451-61.
130. Frenzel, A., M. Hust, and T. Schirrmann, *Expression of recombinant antibodies.* Front Immunol, 2013. **4**: p. 217.
131. Ooi, A., et al., *A Guide to Transient Expression of Membrane Proteins in HEK-293 Cells for Functional*

Characterization. Front Physiol, 2016. **7**: p. 300.
132. Li, F., et al., *Cell culture processes for monoclonal antibody production.* MAbs, 2010. **2**(5): p. 466-79.
133. Tan, E., et al., *HEK293 Cell Line as a Platform to Produce Recombinant Proteins and Viral Vectors.* Front Bioeng Biotechnol, 2021. **9**: p. 796991.
134. Dhara, V.G., et al., *Recombinant Antibody Production in CHO and NS0 Cells: Differences and Similarities.* BioDrugs, 2018. **32**(6): p. 571-584.
135. Dalton, A.C. and W.A. Barton, *Over-expression of secreted proteins from mammalian cell lines.* Protein Sci, 2014. **23**(5): p. 517-25.
136. Faravelli, S., et al., *Optimized Recombinant Production of Secreted Proteins Using Human Embryonic Kidney (HEK293) Cells Grown in Suspension.* Bio Protoc, 2021. **11**(8): p. e3998.
137. Subedi, G.P., et al., *High Yield Expression of Recombinant Human Proteins with the Transient Transfection of HEK293 Cells in Suspension.* J Vis Exp, 2015(106): p. e53568.
138. Zhang, C., et al., *EpCAM- and EGFR-Specific Antibody Drug Conjugates for Triple-Negative Breast Cancer Treatment.* Int J Mol Sci, 2022. **23**(11).
139. Khan, K.H., *Gene expression in Mammalian cells and its applications.* Adv Pharm Bull, 2013. **3**(2): p. 257-63.
140. Leander Johansen, J., et al., *A new versatile and compact lentiviral vector.* Mol Biotechnol, 2005. **29**(1): p. 47-56.
141. Bao, G., et al., *Nanobody: a promising toolkit for molecular imaging and disease therapy.* EJNMMI Res, 2021. **11**(1): p. 6.
142. Park, K.S., et al., *Aptamers and Nanobodies as New Bioprobes for SARS-CoV-2 Diagnostic and Therapeutic System Applications.* Biosensors (Basel), 2024. **14**(3).
143. Alexander, E. and K.W. Leong, *Discovery of nanobodies: a comprehensive review of their applications and potential over the past five years.* J Nanobiotechnology, 2024. **22**(1): p. 661.
144. Jullien, D., et al., *Chromatibody, a novel non-invasive molecular tool to explore and manipulate chromatin in living cells.* J Cell Sci, 2016. **129**(13): p. 2673-83.
145. de Bruin, R.C.G., et al., *Highly specific and potently activating Vgamma9Vdelta2-T cell specific nanobodies for diagnostic and therapeutic applications.* Clin Immunol, 2016. **169**: p. 128-138.
146. Holmes, K.L. and L.M. Lantz, *Protein labeling with fluorescent probes.* Methods Cell Biol, 2001. **63**: p. 185-204.
147. De Rosa, L., et al., *Exploiting Protein N-Terminus for Site-Specific Bioconjugation.* Molecules, 2021. **26**(12).
148. Fung, H.Y.J., et al., *Structural Characterization of Tau in Fuzzy Tau:Tubulin Complexes.* Structure, 2020. **28**(3): p. 378-384 e4.
149. Popp, M.W. and H.L. Ploegh, *Making and breaking peptide bonds: protein engineering using sortase.* Angew Chem Int Ed Engl, 2011. **50**(22): p. 5024-32.
150. Williamson, D.J., et al., *Efficient N-terminal labeling of proteins by use of sortase.* Angew Chem Int Ed Engl, 2012. **51**(37): p. 9377-80.
151. Shaner, N.C., G.H. Patterson, and M.W. Davidson, *Advances in fluorescent protein technology.* J Cell Sci, 2007. **120**(Pt 24): p. 4247-60.
152. Block, H., et al., *Immobilized-metal affinity chromatography (IMAC): a review.* Methods Enzymol, 2009. **463**: p. 439-73.
153. Bause, E., *Structural requirements of N-glycosylation of proteins. Studies with proline peptides as conformational probes.* Biochem J, 1983. **209**(2): p. 331-6.

154. Hossler, P., S.F. Khattak, and Z.J. Li, *Optimal and consistent protein glycosylation in mammalian cell culture.* Glycobiology, 2009. **19**(9): p. 936-49.
155. Spadiut, O. and C. Herwig, *Production and purification of the multifunctional enzyme horseradish peroxidase.* Pharm Bioprocess, 2013. **1**(3): p. 283-295.
156. Labome. *Rabbit Antibody Production*. 2021; Available from: https://www.labome.com/method/Rabbit-Antibody.html.
157. Labome. *Mouse Antibody*. 2022; Available from: https://www.labome.com/method/Mouse-Antibody.html.
158. Janeway Jr, C.A., et al., *The structure of a typical antibody molecule*, in *Immunobiology: The Immune System in Health and Disease. 5th edition*. 2001, Garland Science.
159. Brown, M. and C. Wittwer, *Flow cytometry: principles and clinical applications in hematology.* Clin Chem, 2000. **46**(8 Pt 2): p. 1221-9.
160. Gostner, J.M., et al., *Effects of EpCAM overexpression on human breast cancer cell lines.* BMC Cancer, 2011. **11**: p. 45.
161. Wang, X., et al., *CSPG4 protein as a new target for the antibody-based immunotherapy of triple-negative breast cancer.* J Natl Cancer Inst, 2010. **102**(19): p. 1496-512.
162. Jin, L.L., et al., *Relevance and mechanism of STAT3/miR-221-3p/Fascin-1 axis in EGFR TKI resistance of triple-negative breast cancer.* Mol Cell Biochem, 2024. **479**(11): p. 3037-3047.
163. McKnight, B.N., et al., *Cetuximab PET delineated changes in cellular distribution of EGFR upon dasatinib treatment in triple negative breast cancer.* Breast Cancer Res, 2020. **22**(1): p. 37.
164. (n.d.)., T.H.P.A. *ANK3 in cancer*. Retrieved November 22, 2024; Available from: https://www.proteinatlas.org/ENSG00000151150-ANK3/cancer.
165. Kurozumi, S., et al., *Utility of ankyrin 3 as a prognostic marker in androgen-receptor-positive breast cancer.* Breast Cancer Res Treat, 2019. **176**(1): p. 63-73.
166. Alkaraki, A., et al., *Enhancing chemosensitivity of wild-type and drug-resistant MDA-MB-231 triple-negative breast cancer cell line to doxorubicin by silencing of STAT 3, Notch-1, and beta-catenin genes.* Breast Cancer, 2020. **27**(5): p. 989-998.
167. Jia, T., et al., *The differential susceptibilities of MCF-7 and MDA-MB-231 cells to the cytotoxic effects of curcumin are associated with the PI3K/Akt-SKP2-Cip/Kips pathway.* Cancer Cell Int, 2014. **14**(1): p. 126.
168. Vess, A., et al., *A dual phenotype of MDA-MB-468 cancer cells reveals mutual regulation of tensin3 and adhesion plasticity.* J Cell Sci, 2017. **130**(13): p. 2172-2184.
169. Albitar, L., et al., *EGFR isoforms and gene regulation in human endometrial cancer cells.* Mol Cancer, 2010. **9**: p. 166.
170. Gellersen, B., et al., *Human endometrial stromal cell-trophoblast interactions: mutual stimulation of chemotactic migration and promigratory roles of cell surface molecules CD82 and CEACAM1.* Biol Reprod, 2013. **88**(3): p. 80.
171. Grimm, A., et al., *Development and evaluation of antibody-fluorophore-conjugates to detect endometrial tissue.* Geburtshilfe und Frauenheilkunde, 2022. **82**(10): p. 107.
172. O'Shannessy, D.J., et al., *Expression of folate receptor-alpha (FRA) in gynecologic malignancies and its relationship to the tumor type.* Int J Gynecol Pathol, 2013. **32**(3): p. 258-68.
173. Wen, K.C., et al., *The role of EpCAM in tumor progression and the clinical prognosis of endometrial carcinoma.* Gynecol Oncol, 2018. **148**(2): p. 383-392.
174. Kirkwood, P.M., et al., *Single-cell RNA sequencing and lineage tracing confirm mesenchyme to epithelial*

transformation (MET) contributes to repair of the endometrium at menstruation. Elife, 2022. **11**.
175. Gronemeyer, T., G. Godin, and K. Johnsson, *Adding value to fusion proteins through covalent labelling.* Curr Opin Biotechnol, 2005. **16**(4): p. 453-8.
176. Zhou, Q., et al., *Molecular imaging of a fluorescent antibody against epidermal growth factor receptor detects high-grade glioma.* Sci Rep, 2021. **11**(1): p. 5710.
177. Jeong, J., et al., *HER2 signaling regulates HER2 localization and membrane retention.* PLoS One, 2017. **12**(4): p. e0174849.
178. Schneck, H., et al., *EpCAM-Independent Enrichment of Circulating Tumor Cells in Metastatic Breast Cancer.* PLoS One, 2015. **10**(12): p. e0144535.
179. Grapp, M., et al., *Choroid plexus transcytosis and exosome shuttling deliver folate into brain parenchyma.* Nat Commun, 2013. **4**: p. 2123.
180. Hu, D., et al., *New advances of NG2-expressing cell subset in marrow mesenchymal stem cells as novel therapeutic tools for liver fibrosis/cirrhosis.* Stem Cell Res Ther, 2024. **15**(1): p. 199.
181. Zeng, C., et al., *Genetic Alterations in Papillary Thyroid Carcinoma With Hashimoto(')s Thyroiditis: ANK3, an Indolent Maintainer of Papillary Thyroid Carcinoma.* Front Oncol, 2022. **12**: p. 894786.
182. Tiwari, A., et al., *Early insights into the function of KIAA1199, a markedly overexpressed protein in human colorectal tumors.* PLoS One, 2013. **8**(7): p. e69473.
183. Marjanovic, I., et al., *Comparison of flow cytometry, fluorescence microscopy and spectrofluorometry for analysis of gene electrotransfer efficiency.* J Membr Biol, 2014. **247**(12): p. 1259-67.
184. Bales, C.J.K.s.d.c. and i.h. bases, *Laboratory techniques*. 2006: p. 1569-1634.
185. Jung, K.H., et al., *A Fluorogenic AggTag Method Based on Halo- and SNAP-Tags to Simultaneously Detect Aggregation of Two Proteins in Live Cells.* Chembiochem, 2019. **20**(8): p. 1078-1087.
186. Gautier, A., et al., *Selective cross-linking of interacting proteins using self-labeling tags.* J Am Chem Soc, 2009. **131**(49): p. 17954-62.
187. Pellett, P.A., et al., *Two-color STED microscopy in living cells.* Biomed Opt Express, 2011. **2**(8): p. 2364-71.
188. Woitok, M., et al., *Using the SNAP-Tag technology to easily measure and demonstrate apoptotic changes in cancer and blood cells with different dyes.* PLoS One, 2020. **15**(12): p. e0243286.
189. Gu, K., et al., *Development of nanobody-horseradish peroxidase-based sandwich ELISA to detect Salmonella Enteritidis in milk and in vivo colonization in chicken.* J Nanobiotechnology, 2022. **20**(1): p. 167.
190. Sheng, Y., et al., *Nanobody-horseradish peroxidase fusion protein as an ultrasensitive probe to detect antibodies against Newcastle disease virus in the immunoassay.* J Nanobiotechnology, 2019. **17**(1): p. 35.
191. Zhang, W.T., et al., *Development of a nanobody-based immunoassay for the sensitive detection of fibrinogen-like protein 1.* Acta Pharmacol Sin, 2021. **42**(11): p. 1921-1929.
192. Kurien, B.T. and R.H. Scofield, *Western blotting.* Methods, 2006. **38**(4): p. 283-93.
193. Li, C.W., et al., *Glycosylation and stabilization of programmed death ligand-1 suppresses T-cell activity.* Nat Commun, 2016. **7**: p. 12632.
194. Bae, Y., et al., *HRP-conjugated plug-and-playable IgG-binding nanobodies as secondary antibody mimics in immunoassays.* Sensors Actuators B: Chemical, 2020. **320**: p. 128312.
195. Lim, J.C.T., et al., *An automated staining protocol for seven-colour immunofluorescence of human tissue sections for diagnostic and prognostic use.* Pathology, 2018. **50**(3): p. 333-341.
196. Sheng, W., et al., *Multiplex Immunofluorescence: A Powerful Tool in Cancer Immunotherapy.* Int J Mol Sci, 2023. **24**(4).

197. Parra, E.R., et al., *Validation of multiplex immunofluorescence panels using multispectral microscopy for immune-profiling of formalin-fixed and paraffin-embedded human tumor tissues.* Sci Rep, 2017. **7**(1): p. 13380.
198. Viratham Pulsawatdi, A., et al., *A robust multiplex immunofluorescence and digital pathology workflow for the characterisation of the tumour immune microenvironment.* Mol Oncol, 2020. **14**(10): p. 2384-2402.
199. Gorris, M.A.J., et al., *Eight-Color Multiplex Immunohistochemistry for Simultaneous Detection of Multiple Immune Checkpoint Molecules within the Tumor Microenvironment.* J Immunol, 2018. **200**(1): p. 347-354.
200. Ehrenberg, A.J., et al., *A manual multiplex immunofluorescence method for investigating neurodegenerative diseases.* J Neurosci Methods, 2020. **339**: p. 108708.
201. Bulun, S.E., et al., *Estrogen receptor-beta, estrogen receptor-alpha, and progesterone resistance in endometriosis.* Semin Reprod Med, 2010. **28**(1): p. 36-43.
202. Chen, H., et al., *Epigenetics of Estrogen and Progesterone Receptors in Endometriosis.* Reprod Sci, 2020. **27**(11): p. 1967-1974.
203. Powell, S.G., et al., *Vascularisation in Deep Endometriosis: A Systematic Review with Narrative Outcomes.* Cells, 2023. **12**(9).
204. Scheerer, C., et al., *Characterization of endometriosis-associated immune cell infiltrates (EMaICI).* Arch Gynecol Obstet, 2016. **294**(3): p. 657-64.
205. Trukhacheva, E., et al., *Estrogen receptor (ER) beta regulates ERalpha expression in stromal cells derived from ovarian endometriosis.* J Clin Endocrinol Metab, 2009. **94**(2): p. 615-22.
206. Mori, H., et al., *Characterizing the tumor immune microenvironment with tyramide-based multiplex immunofluorescence.* Journal of mammary gland biology and neoplasia, 2020. **25**: p. 417-432.
207. Quigley, L.T., et al., *Protocol for investigating tertiary lymphoid structures in human and murine fixed tissue sections using Opal-TSA multiplex immunohistochemistry.* STAR Protoc, 2023. **4**(1): p. 101961.
208. Lipman, N.S., et al., *Monoclonal versus polyclonal antibodies: distinguishing characteristics, applications, and information resources.* ILAR J, 2005. **46**(3): p. 258-68.
209. Li, C., et al., *Natural Single-Domain Antibody-Nanobody: A Novel Concept in the Antibody Field.* J Biomed Nanotechnol, 2018. **14**(1): p. 1-19.
210. Wharton, K.A., Jr., et al., *Tissue Multiplex Analyte Detection in Anatomic Pathology - Pathways to Clinical Implementation.* Front Mol Biosci, 2021. **8**: p. 672531.
211. Humphries, M.P., P. Maxwell, and M. Salto-Tellez, *QuPath: The global impact of an open source digital pathology system.* Comput Struct Biotechnol J, 2021. **19**: p. 852-859.
212. Apaolaza, P.S., P.I. Petropoulou, and T. Rodriguez-Calvo, *Whole-Slide Image Analysis of Human Pancreas Samples to Elucidate the Immunopathogenesis of Type 1 Diabetes Using the QuPath Software.* Front Mol Biosci, 2021. **8**: p. 689799.

7. Supplementary materials

7.1 Sequences of open reading frames

7.1.1 Nb anti mouse IgG1 Fab-SNAP

ATGGAGACAGACACACTCCTGCTATGGGTACTGCTGCTCTGGGTTCCAGGTTCCACTGGT
GACGCGGCCCAGCCGGCCCAGGTGCAATTGGTAGAGTGTGGGGGAGGCTTGGTGCAGCC
TGGGGGGTCTCTGAGACTCTCCTGTGCAGCCTCTGGATTCACTTTCGCTAACTACTACATG
AGCTGGGTCCGCCAGGCTCCAGGAAAGGGGCCCGAGTGGGTCTCAGCAATTAATACTCT
TGGTGGTAAAACAAAGTATGCAGACTCCGTGAAGGGCCGATTCACCATCTCCAGAGACA
ACGCCAAGAGCACGCTGTATCTGCAAATGAACAGCCTGAAACCTGAGGATACGGCCCTG
TATTACTGTGCGAGAGAGGTCACATACTATAGTGGTACTTACTACCTATTTGGGACGAAAC
AAGAGTATGACTACAGGGGCCAGGGGACCCAGGTCACAGTCTCATCATGTTCTAGAATGG
ACAAAGACTGCGAAATGAAGCGCACCACCCTGGATAGCCCTCTGGGCAAGCTGGAACTG
TCTGGGTGCGAACAGGGCCTGCACGAGATCAAGCTGCTGGGCAAAGGAACATCTGCCGC
CGACGCCGTGGAAGTGCCTGCCCCAGCCGCCGTGCTGGGCGGACCAGAGCCACTGATGC
AGGCCACCGCCTGGCTCAACGCCTACTTTCACCAGCCTGAGGCCATCGAGGAGTTCCCT
GTGCCAGCCCTGCACCACCCAGTGTTCCAGCAGGAGAGCTTTACCCGCCAGGTGCTGTG
GAAACTGCTGAAAGTGGTGAAGTTCGGAGAGGTCATCAGCTACCAGCAGCTGGCGGCCC
TGGCGGGCAATCCCGCCGCCACCGCCGCCGTGAAAACCGCCCTGAGCGGAAATCCCGTG
CCCATTCTGATCCCCTGCCACCGGGTGGTGTCTAGCTCTGGCGCCGTGGGGGGCTACGAG
GGCGGGCTCGCCGTGAAAGAGTGGCTGCTGGCCCACGAGGGCCACAGACTGGGCAAGC
CTGGGCTGGGCGCTGAGCACGAATTTCGAGGAGGGCCCGAACAAAAACTCATCTCAGAA
GAGGATCTGAATAGCGCCGTCGACCATCATCATCATCATCATTGA

7.1.2 Nb anti mouse IgG1 Fc-SNAP

ATGGAGACAGACACACTCCTGCTATGGGTACTGCTGCTCTGGGTTCCAGGTTCCACTGGT
GACGCGGCCCAGCCGGCCCAGGTGCAATTGGTGGAGTCTGGGGGAGGCTTGGTGCAGC
CTGGGGGGTCTCTGAGGCTCTCCTGTGCAGCCTCTGGATTCACATTCAGTGATACCTGGA
TGAACTGGGTCCGCCAGGCTCCAGGGAAGGGGCTCTATTGGATCTCAGCCATCAATCCGG
ACGGTGGTAACACAGCCTATGCAGACTCCGTCAAGGGCCGGTTCACCATCTCCAGAGAC
AACGCCAAGAACATGGTGTATCTGCAGATGGACAACCTGAGACCTGAGGACACGGCCAT
GTATTACTGCGCAAAGGGTTGGGTTCGCCTTCCAGATCCCGATCTGGTAAGGGGCCAGGG
GACCCAGGTCACAGTCTCCTCCGGTGGATGTTCTAGAATGGACAAAGACTGCGAAATGA
AGCGCACCACCCTGGATAGCCCTCTGGGCAAGCTGGAACTGTCTGGGTGCGAACAGGGC
CTGCACGAGATCAAGCTGCTGGGCAAAGGAACATCTGCCGCCGACGCCGTGGAAGTGCC
TGCCCCAGCCGCCGTGCTGGGCGGACCAGAGCCACTGATGCAGGCCACCGCCTGGCTCA
ACGCCTACTTTCACCAGCCTGAGGCCATCGAGGAGTTCCCTGTGCCAGCCCTGCACCACC
CAGTGTTCCAGCAGGAGAGCTTTACCCGCCAGGTGCTGTGGAAACTGCTGAAAGTGGTG

AAGTTCGGAGAGGTCATCAGCTACCAGCAGCTGGCGGCCCTGGCGGGCAATCCCGCCGC
CACCGCCGCCGTGAAAACCGCCCTGAGCGGAAATCCCGTGCCCATTCTGATCCCCTGCCA
CCGGGTGGTGTCTAGCTCTGGCGCCGTGGGGGGCTACGAGGGCGGGCTCGCCGTGAAAG
AGTGGCTGCTGGCCCACGAGGGCCACAGACTGGGCAAGCCTGGGCTGGGCGCTGAGCA
CGAATTTCGAGGAGGGCCCGAACAAAAACTCATCTCAGAAGAGGATCTGAATAGCGCCG
TCGACCATCATCATCATCATCATTGA

7.1.3 Nb anti mouse IgG2a Fc-SNAP

ATGGAGACAGACACACTCCTGCTATGGGTACTGCTGCTCTGGGTTCCAGGTTCCACTGGT
GACGCGGCCCAGCCGGCCCAGGTGCAATTGGTAGAGTGTGGGGGAGGCTTGGTGCAGCC
TGGGGGGTCTCTGAGACTCTCCTGTGTAGCCTCTGGATTCACCTTCAGTAGCGCCTACAT
GAGCTGGGTCCGCCAGGCTCCAGGAAAGGGGCCCGAGTGGGTCTCAACTATTAGTACAG
GTGGTGGTATCGTAAACTATGCAGACTCCGTGAAGGGCCGATTCGCCATCTCCAGAGACA
ACGCCAAGAACACCCTGTATCTGCAAATGAACAAACTGAAACCTGAGGACACGGCCCTC
TATTACTGTGCGAGCAATAAAGGCCCGCATTACCATAGCGACTATTTTGATTCGAATCTGTA
TGACTTCTGGGGCCAGGGGACCCGGGTCACAGTCTCATCATGTTCTAGAATGGACAAAG
ACTGCGAAATGAAGCGCACCACCCTGGATAGCCCTCTGGGCAAGCTGGAACTGTCTGGG
TGCGAACAGGGCCTGCACGAGATCAAGCTGCTGGGCAAAGGAACATCTGCCGCCGACG
CCGTGGAAGTGCCTGCCCCAGCCGCCGTGCTGGGCGGACCAGAGCCACTGATGCAGGCC
ACCGCCTGGCTCAACGCCTACTTTCACCAGCCTGAGGCCATCGAGGAGTTCCCTGTGCCA
GCCCTGCACCACCCAGTGTTCCAGCAGGAGAGCTTTACCCGCCAGGTGCTGTGGAAACT
GCTGAAAGTGGTGAAGTTCGGAGAGGTCATCAGCTACCAGCAGCTGGCGGCCCTGGCGG
GCAATCCCGCCGCCACCGCCGCCGTGAAAACCGCCCTGAGCGGAAATCCCGTGCCCATT
CTGATCCCCTGCCACCGGGTGGTGTCTAGCTCTGGCGCCGTGGGGGGCTACGAGGGCGG
GCTCGCCGTGAAAGAGTGGCTGCTGGCCCACGAGGGCCACAGACTGGGCAAGCCTGGG
CTGGGCGCTGAGCACGAATTTCGAGGAGGGCCCGAACAAAAACTCATCTCAGAAGAGG
ATCTGAATAGCGCCGTCGACCATCATCATCATCATCATTGA

7.1.4 Nb anti mouse kappa chain-SNAP

ATGGAGACAGACACACTCCTGCTATGGGTACTGCTGCTCTGGGTTCCAGGTTCCACTGGT
GACGCGGCCCAGCCGGCCCAGGTGCAATTGGTAGAGTCTGGGGGAGGCTGGGTGCAGC
CTGGGGGGTCTCTGAGACTCTCCTGTGCAGCCTCTGGATTCACCTTCAGTGACACTGCCA
TGATGTGGGTCCGCCAGGCTCCAGGGAAGGGGCGAGAGTGGGTCGCAGCTATTGATACT
GGTGGTGGATACACATACTATGCAGACTCCGTGAAGGGCCGATTCACCATCTCCAGAGAC
AACGCCAAGAACACGCTGTATCTGCAAATGAACAGCCTGAAACCGGAGGACACGGCCC
GATACTACTGTGCGAAGACCTACTCCGGTAATTACTATAGCAACTACACGGTTGCCAACTA
TGGCACCACGGGCCGGGGGACCCTGGTCACAGTCTCCTCCGGTGGATGTTCTAGAATGG
ACAAAGACTGCGAAATGAAGCGCACCACCCTGGATAGCCCTCTGGGCAAGCTGGAACTG
TCTGGGTGCGAACAGGGCCTGCACGAGATCAAGCTGCTGGGCAAAGGAACATCTGCCGC
CGACGCCGTGGAAGTGCCTGCCCCAGCCGCCGTGCTGGGCGGACCAGAGCCACTGATGC

AGGCCACCGCCTGGCTCAACGCCTACTTTCACCAGCCTGAGGCCATCGAGGAGTTCCCT
GTGCCAGCCCTGCACCACCCAGTGTTCCAGCAGGAGAGCTTTACCCGCCAGGTGCTGTG
GAAACTGCTGAAAGTGGTGAAGTTCGGAGAGGTCATCAGCTACCAGCAGCTGGCGGCCC
TGGCGGGCAATCCCGCCGCCACCGCCGCCGTGAAAACCGCCCTGAGCGGAAATCCCGTG
CCCATTCTGATCCCCTGCCACCGGGTGGTGTCTAGCTCTGGCGCCGTGGGGGGCTACGAG
GGCGGGCTCGCCGTGAAAGAGTGGCTGCTGGCCCACGAGGGCCACAGACTGGGCAAGC
CTGGGCTGGGCGCTGAGCACGAATTTCGAGGAGGGCCCGAACAAAAACTCATCTCAGAA
GAGGATCTGAATAGCGCCGTCGACCATCATCATCATCATTGA

7.1.5 Nb anti rabbit IgG Fc-SNAP

ATGGAGACAGACACACTCCTGCTATGGGTACTGCTGCTCTGGGTTCCAGGTTCCACTGGT
GACGCGGCCCAGCCGGCCCAGGTGCAATTGGTAGAGTCTGGGGGAGGCTTGGTGCAGGC
TGGTGACTCTCTGCGACTCTCCTGTGTAGCCTCTGGGCGCTCCTTGGATGGGGCCACCAT
GCGCTGGTACCGCCAGGCTCCAGGGAAGGAGCGAGAATTTGTTGCAGGCATTTTTTGGG
ATGAGATTGGTACGGAATATGCAGACACTGCGAAGGGCCGATTCACCATCTCCAGAGACA
ATGCCAAGAACACGATATATCTACAAATGACCAACCTGAGGTCCGAAGACACGGCCATGT
ATTATTGTAATGGATTAGTATTCGGGGGTGAATACTGGGGACAGGGGACCCAGGTCACAG
TCTCCTCCGGTGGATGTTCTAGAATGGACAAAGACTGCGAAATGAAGCGCACCACCCTG
GATAGCCCTCTGGGCAAGCTGGAACTGTCTGGGTGCGAACAGGGCCTGCACGAGATCAA
GCTGCTGGGCAAAGGAACATCTGCCGCCGACGCCGTGGAAGTGCCTGCCCCAGCCGCCG
TGCTGGGCGGACCAGAGCCACTGATGCAGGCCACCGCCTGGCTCAACGCCTACTTTCAC
CAGCCTGAGGCCATCGAGGAGTTCCCTGTGCCAGCCCTGCACCACCCAGTGTTCCAGCA
GGAGAGCTTTACCCGCCAGGTGCTGTGGAAACTGCTGAAAGTGGTGAAGTTCGGAGAG
GTCATCAGCTACCAGCAGCTGGCGGCCCTGGCGGGCAATCCCGCCGCCACCGCCGCCGT
GAAAACCGCCCTGAGCGGAAATCCCGTGCCCATTCTGATCCCCTGCCACCGGGTGGTGTC
TAGCTCTGGCGCCGTGGGGGGCTACGAGGGCGGGCTCGCCGTGAAAGAGTGGCTGCTGG
CCCACGAGGGCCACAGACTGGGCAAGCCTGGGCTGGGCGCTGAGCACGAATTTCGAGG
AGGGCCCGAACAAAAACTCATCTCAGAAGAGGATCTGAATAGCGCCGTCGACCATCATC
ATCATCATCATTGA

7.1.6 Nb anti mouse IgG1 Fab-HRP

ATGGAGACAGACACACTCCTGCTATGGGTACTGCTGCTCTGGGTTCCAGGTTCCACTGGT
GACGCGGCCCAGCCGGCCCAGGTGCAATTGGTAGAGTGTGGGGGAGGCTTGGTGCAGCC
TGGGGGGTCTCTGAGACTCTCCTGTGCAGCCTCTGGATTCACTTTCGCTAACTACTACATG
AGCTGGGTCCGCCAGGCTCCAGGAAAGGGGCCCGAGTGGGTCTCAGCAATTAATACTCT
TGGTGGTAAAACAAAGTATGCAGACTCCGTGAAGGGCCGATTCACCATCTCCAGAGACA
ACGCCAAGAGCACGCTGTATCTGCAAATGAACAGCCTGAAACCTGAGGATACGGCCCTG
TATTACTGTGCGAGAGAGGTCACATACTATAGTGGTACTTACTACCTATTTGGGACGAAAC
AAGAGTATGACTACAGGGGCCAGGGGACCCAGGTCACAGTCTCATCATGTTCTAGAATGC
AGTTAACCCCTACATTCTACGACAATAGCTGTCCCAACGTGTCCAACATCGTTCGCGACA

CAATCGTCAACGAGCTCAGATCCGATCCCAGGATCGCTGCTTCAATATTACGTCTGCACTT
CCATGACTGCTTCGTGAATGGTTGCGACGCTAGCATATTACTGGACAACACCACCAGTTT
CCGCACTGAAAAGGATGCATTCGGGAACGCTAACAGCGCCAGGGGCTTTCCAGTGATCG
ATCGCATGAAGGCTGCCGTTGAGTCAGCATGCCCACGAACAGTCAGTTGTGCAGACCTG
CTGACTATAGCTGCGCAACAGAGCGTGACTCTTGCAGGCGGACCGTCCTGGAGAGTGCC
GCTCGGTCGACGTGACTCCCTACAGGCATTCCTAGATCTGGCCAACGCCAACTTGCCTGC
TCCATTCTTCACCCTGCCCCAGCTGAAGGATAGCTTTAGAAACGTGGGTCTGAATCGCTC
GAGTGACCTTGTGGCTCTGTCCGGAGGACACACATTTGGAAAGAACCAGTGTAGGTTCA
TCATGGATAGGCTCTACAATTTCAGCAACACTGGGTTACCTGACCCCACGCTGAACACTA
CGTATCTCCAGACACTGAGAGGCTTGTGCCCACTGAATGGCAACCTCAGTGCACTAGTGG
ACTTTGATCTGCGGACCCCAACCATCTTCGATAACAAGTACTATGTGAATCTAGAGGAGC
AGAAAGGCCTGATACAGAGTGATCAAGAACTGTTTAGCAGTCCAAACGCCACTGACACC
ATCCCACTGGTGAGAAGTTTTGCTAACTCTACTCAAACCTTCTTTAACGCCTTCGTGGAA
GCCATGGACCGTATGGGTAACATTACCCCTCTGACGGGTACCCAAGGCCAGATTCGTCTG
AACTGCAGAGTGGTCAACAGCAACTCTGGCGCTGAGCACGAATTTCGAGGAGGGCCCG
AACAAAAACTCATCTCAGAAGAGGATCTGAATAGCGCCGTCGACCATCATCATCATCATC
ATTGA

7.1.7 Nb anti mouse IgG1 Fc-HRP

ATGGAGACAGACACACTCCTGCTATGGGTACTGCTGCTCTGGGTTCCAGGTTCCACTGGT
GACGCGGCCCAGCCGGCCCAGGTGCAATTGGTGGAGTCTGGGGGAGGCTTGGTGCAGC
CTGGGGGGTCTCTGAGGCTCTCCTGTGCAGCCTCTGGATTCACATTCAGTGATACCTGGA
TGAACTGGGTCCGCCAGGCTCCAGGGAAGGGGCTCTATTGGATCTCAGCCATCAATCCGG
ACGGTGGTAACACAGCCTATGCAGACTCCGTCAAGGGCCGGTTCACCATCTCCAGAGAC
AACGCCAAGAACATGGTGTATCTGCAGATGGACAACCTGAGACCTGAGGACACGGCCAT
GTATTACTGCGCAAAGGGTTGGGTTCGCCTTCCAGATCCCGATCTGGTAAGGGGCCAGGG
GACCCAGGTCACAGTCTCCTCCGGTGGATGTTCTAGAATGCAGTTAACCCCTACATTCTAC
GACAATAGCTGTCCCAACGTGTCCAACATCGTTCGCGACACAATCGTCAACGAGCTCAG
ATCCGATCCCAGGATCGCTGCTTCAATATTACGTCTGCACTTCCATGACTGCTTCGTGAAT
GGTTGCGACGCTAGCATATTACTGGACAACACCACCAGTTTCCGCACTGAAAAGGATGCA
TTCGGGAACGCTAACAGCGCCAGGGGCTTTCCAGTGATCGATCGCATGAAGGCTGCCGTT
GAGTCAGCATGCCCACGAACAGTCAGTTGTGCAGACCTGCTGACTATAGCTGCGCAACA
GAGCGTGACTCTTGCAGGCGGACCGTCCTGGAGAGTGCCGCTCGGTCGACGTGACTCCC
TACAGGCATTCCTAGATCTGGCCAACGCCAACTTGCCTGCTCCATTCTTCACCCTGCCCCA
GCTGAAGGATAGCTTTAGAAACGTGGGTCTGAATCGCTCGAGTGACCTTGTGGCTCTGTC
CGGAGGACACACATTTGGAAAGAACCAGTGTAGGTTCATCATGGATAGGCTCTACAATTT
CAGCAACACTGGGTTACCTGACCCCACGCTGAACACTACGTATCTCCAGACACTGAGAG
GCTTGTGCCCACTGAATGGCAACCTCAGTGCACTAGTGGACTTTGATCTGCGGACCCCAA
CCATCTTCGATAACAAGTACTATGTGAATCTAGAGGAGCAGAAAGGCCTGATACAGAGTG
ATCAAGAACTGTTTAGCAGTCCAAACGCCACTGACACCATCCCACTGGTGAGAAGTTTTG
CTAACTCTACTCAAACCTTCTTTAACGCCTTCGTGGAAGCCATGGACCGTATGGGTAACAT

TACCCCTCTGACGGGTACCCAAGGCCAGATTCGTCTGAACTGCAGAGTGGTCAACAGCA
ACTCTGGCGCTGAGCACGAATTTCGAGGAGGGCCCGAACAAAAACTCATCTCAGAAGAG
GATCTGAATAGCGCCGTCGACCATCATCATCATCATCATTGA

7.1.8 Nb anti mouse IgG2a Fc-HRP

ATGGAGACAGACACACTCCTGCTATGGGTACTGCTGCTCTGGGTTCCAGGTTCCACTGGT
GACGCGGCCCAGCCGGCCCAGGTGCAATTGGTAGAGTGTGGGGGAGGCTTGGTGCAGCC
TGGGGGGTCTCTGAGACTCTCCTGTGTAGCCTCTGGATTCACCTTCAGTAGCGCCTACAT
GAGCTGGGTCCGCCAGGCTCCAGGAAAGGGGCCCGAGTGGGTCTCAACTATTAGTACAG
GTGGTGGTATCGTAAACTATGCAGACTCCGTGAAGGGCCGATTCGCCATCTCCAGAGACA
ACGCCAAGAACACCCTGTATCTGCAAATGAACAAACTGAAACCTGAGGACACGGCCCTC
TATTACTGTGCGAGCAATAAAGGCCCGCATTACCATAGCGACTATTTTGATTCGAATCTGTA
TGACTTCTGGGGCCAGGGGACCCGGGTCACAGTCTCATCATGTTCTAGAATGCAGTTAAC
CCCTACATTCTACGACAATAGCTGTCCCAACGTGTCCAACATCGTTCGCGACACAATCGTC
AACGAGCTCAGATCCGATCCCAGGATCGCTGCTTCAATATTACGTCTGCACTTCCATGACT
GCTTCGTGAATGGTTGCGACGCTAGCATATTACTGGACAACACCACCAGTTTCCGCACTG
AAAAGGATGCATTCGGGAACGCTAACAGCGCCAGGGGCTTTCCAGTGATCGATCGCATG
AAGGCTGCCGTTGAGTCAGCATGCCCACGAACAGTCAGTTGTGCAGACCTGCTGACTAT
AGCTGCGCAACAGAGCGTGACTCTTGCAGGCGGACCGTCCTGGAGAGTGCCGCTCGGTC
GACGTGACTCCCTACAGGCATTCCTAGATCTGGCCAACGCCAACTTGCCTGCTCCATTCTT
CACCCTGCCCCAGCTGAAGGATAGCTTTAGAAACGTGGGTCTGAATCGCTCGAGTGACCT
TGTGGCTCTGTCCGGAGGACACACATTTGGAAAGAACCAGTGTAGGTTCATCATGGATAG
GCTCTACAATTTCAGCAACACTGGGTTACCTGACCCCACGCTGAACACTACGTATCTCCA
GACACTGAGAGGCTTGTGCCCACTGAATGGCAACCTCAGTGCACTAGTGGACTTTGATCT
GCGGACCCCAACCATCTTCGATAACAAGTACTATGTGAATCTAGAGGAGCAGAAAGGCCT
GATACAGAGTGATCAAGAACTGTTTAGCAGTCCAAACGCCACTGACACCATCCCACTGGT
GAGAAGTTTTGCTAACTCTACTCAAACCTTCTTTAACGCCTTCGTGGAAGCCATGGACCG
TATGGGTAACATTACCCCTCTGACGGGTACCCAAGGCCAGATTCGTCTGAACTGCAGAGT
GGTCAACAGCAACTCTGGCGCTGAGCACGAATTTCGAGGAGGGCCCGAACAAAAACTC
ATCTCAGAAGAGGATCTGAATAGCGCCGTCGACCATCATCATCATCATCATTGA

7.1.9 Nb anti mouse kappa chain-HRP

ATGGAGACAGACACACTCCTGCTATGGGTACTGCTGCTCTGGGTTCCAGGTTCCACTGGT
GACGCGGCCCAGCCGGCCCAGGTGCAATTGGTAGAGTCTGGGGGAGGCTGGGTGCAGC
CTGGGGGGTCTCTGAGACTCTCCTGTGCAGCCTCTGGATTCACCTTCAGTGACACTGCCA
TGATGTGGGTCCGCCAGGCTCCAGGGAAGGGGCGAGAGTGGGTCGCAGCTATTGATACT
GGTGGTGGATACACATACTATGCAGACTCCGTGAAGGGCCGATTCACCATCTCCAGAGAC
AACGCCAAGAACACGCTGTATCTGCAAATGAACAGCCTGAAACCGGAGGACACGGCCC
GATACTACTGTGCGAAGACCTACTCCGGTAATTACTATAGCAACTACACGGTTGCCAACTA
TGGCACCACGGGCCGGGGGACCCTGGTCACAGTCTCCTCCGGTGGATGTTCTAGAATGC

AGTTAACCCCTACATTCTACGACAATAGCTGTCCCAACGTGTCCAACATCGTTCGCGACA
CAATCGTCAACGAGCTCAGATCCGATCCCAGGATCGCTGCTTCAATATTACGTCTGCACTT
CCATGACTGCTTCGTGAATGGTTGCGACGCTAGCATATTACTGGACAACACCACCAGTTT
CCGCACTGAAAAGGATGCATTCGGGAACGCTAACAGCGCCAGGGGCTTTCCAGTGATCG
ATCGCATGAAGGCTGCCGTTGAGTCAGCATGCCCACGAACAGTCAGTTGTGCAGACCTG
CTGACTATAGCTGCGCAACAGAGCGTGACTCTTGCAGGCGGACCGTCCTGGAGAGTGCC
GCTCGGTCGACGTGACTCCCTACAGGCATTCCTAGATCTGGCCAACGCCAACTTGCCTGC
TCCATTCTTCACCCTGCCCCAGCTGAAGGATAGCTTTAGAAACGTGGGTCTGAATCGCTC
GAGTGACCTTGTGGCTCTGTCCGGAGGACACACATTTGGAAAGAACCAGTGTAGGTTCA
TCATGGATAGGCTCTACAATTTCAGCAACACTGGGTTACCTGACCCCACGCTGAACACTA
CGTATCTCCAGACACTGAGAGGCTTGTGCCCACTGAATGGCAACCTCAGTGCACTAGTGG
ACTTTGATCTGCGGACCCCAACCATCTTCGATAACAAGTACTATGTGAATCTAGAGGAGC
AGAAAGGCCTGATACAGAGTGATCAAGAACTGTTTAGCAGTCCAAACGCCACTGACACC
ATCCCACTGGTGAGAAGTTTTGCTAACTCTACTCAAACCTTCTTTAACGCCTTCGTGGAA
GCCATGGACCGTATGGGTAACATTACCCCTCTGACGGGTACCCAAGGCCAGATTCGTCTG
AACTGCAGAGTGGTCAACAGCAACTCTGGCGCTGAGCACGAATTTCGAGGAGGGCCCG
AACAAAAACTCATCTCAGAAGAGGATCTGAATAGCGCCGTCGACCATCATCATCATCATC
ATTGA

7.1.10 Nb anti rabbit IgG Fc-HRP

ATGGAGACAGACACACTCCTGCTATGGGTACTGCTGCTCTGGGTTCCAGGTTCCACTGGT
GACGCGGCCCAGCCGGCCCAGGTGCAATTGGTAGAGTCTGGGGGAGGCTTGGTGCAGGC
TGGTGACTCTCTGCGACTCTCCTGTGTAGCCTCTGGGCGCTCCTTGGATGGGGCCACCAT
GCGCTGGTACCGCCAGGCTCCAGGGAAGGAGCGAGAATTTGTTGCAGGCATTTTTTGGG
ATGAGATTGGTACGGAATATGCAGACACTGCGAAGGGCCGATTCACCATCTCCAGAGACA
ATGCCAAGAACACGATATATCTACAAATGACCAACCTGAGGTCCGAAGACACGGCCATGT
ATTATTGTAATGGATTAGTATTCGGGGGTGAATACTGGGGACAGGGGACCCAGGTCACAG
TCTCCTCCGGTGGATGTTCTAGAATGCAGTTAACCCCTACATTCTACGACAATAGCTGTCC
CAACGTGTCCAACATCGTTCGCGACACAATCGTCAACGAGCTCAGATCCGATCCCAGGAT
CGCTGCTTCAATATTACGTCTGCACTTCCATGACTGCTTCGTGAATGGTTGCGACGCTAGC
ATATTACTGGACAACACCACCAGTTTCCGCACTGAAAAGGATGCATTCGGGAACGCTAAC
AGCGCCAGGGGCTTTCCAGTGATCGATCGCATGAAGGCTGCCGTTGAGTCAGCATGCCC
ACGAACAGTCAGTTGTGCAGACCTGCTGACTATAGCTGCGCAACAGAGCGTGACTCTTG
CAGGCGGACCGTCCTGGAGAGTGCCGCTCGGTCGACGTGACTCCCTACAGGCATTCCTA
GATCTGGCCAACGCCAACTTGCCTGCTCCATTCTTCACCCTGCCCCAGCTGAAGGATAGC
TTTAGAAACGTGGGTCTGAATCGCTCGAGTGACCTTGTGGCTCTGTCCGGAGGACACAC
ATTTGGAAAGAACCAGTGTAGGTTCATCATGGATAGGCTCTACAATTTCAGCAACACTGG
GTTACCTGACCCCACGCTGAACACTACGTATCTCCAGACACTGAGAGGCTTGTGCCCACT
GAATGGCAACCTCAGTGCACTAGTGGACTTTGATCTGCGGACCCCAACCATCTTCGATAA
CAAGTACTATGTGAATCTAGAGGAGCAGAAAGGCCTGATACAGAGTGATCAAGAACTGT
TTAGCAGTCCAAACGCCACTGACACCATCCCACTGGTGAGAAGTTTTGCTAACTCTACTC

AAACCTTCTTTAACGCCTTCGTGGAAGCCATGGACCGTATGGGTAACATTACCCCTCTGA
CGGGTACCCAAGGCCAGATTCGTCTGAACTGCAGAGTGGTCAACAGCAACTCTGGCGCT
GAGCACGAATTTCGAGGAGGGCCCGAACAAAAACTCATCTCAGAAGAGGATCTGAATAG
CGCCGTCGACCATCATCATCATCATCATTGA

7.2 Supplementary figures

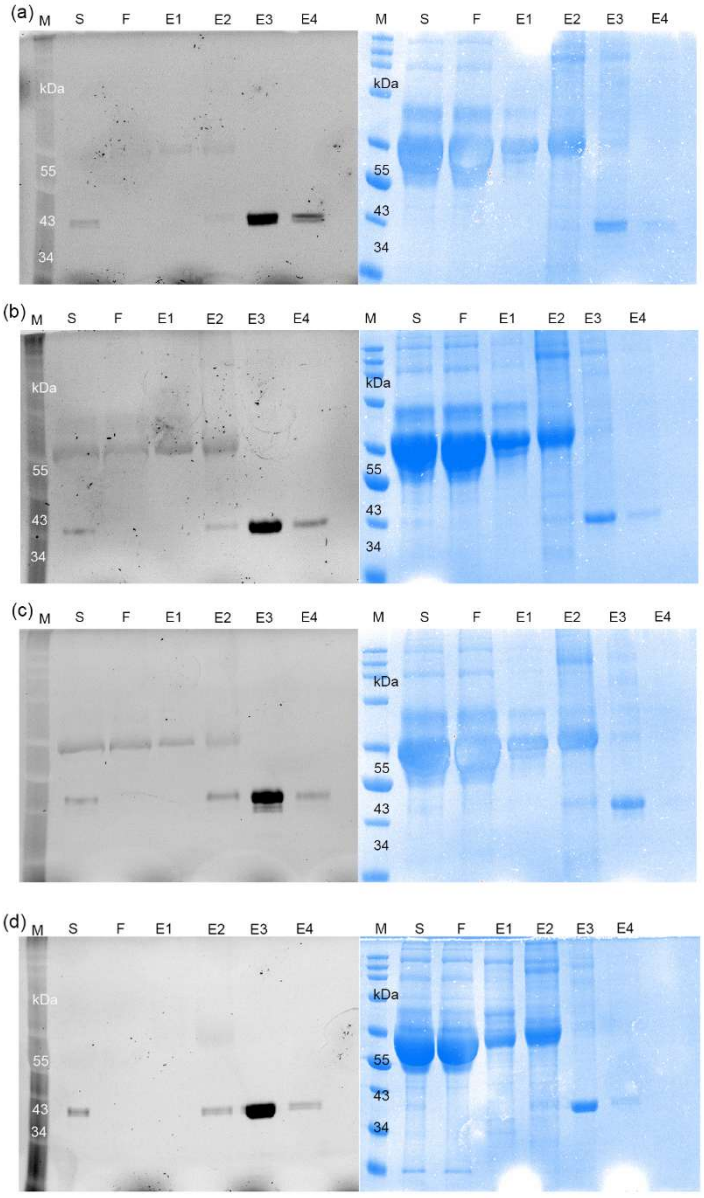

Supplementary Figure 1 Nbs anti-IgG-SNAP fusion proteins enrichment. (a) Enrichment of Nb anti-mouse IgG1 Fab-SNAP. (b) Enrichment of Nb anti-mouse IgG2a Fc-SNAP. (c) Enrichment of Nb anti-mouse kappa chain-SNAP. (d) Enrichment of Nb anti-rabbit IgG Fc-SNAP. All fractions were collected during enrichment, and conjugated to SNAP-Surface® Alexa Fluor® 488 followed SDS-PAGE running. The SDS-PAGE gels were subsequently stained

with Coomassie brilliant blue. SDS gel was imaged by ChemiDoc XRS+ System. M: Blue prestained protein standard broad range (11-250 kDa). S: filtered supernatant. F: flowthrough. E1: protein eluted in 10 mM imidazole. E2: protein eluted in 40 mM imidazole. E3 and E4: protein eluted in 250 mM imidazole.

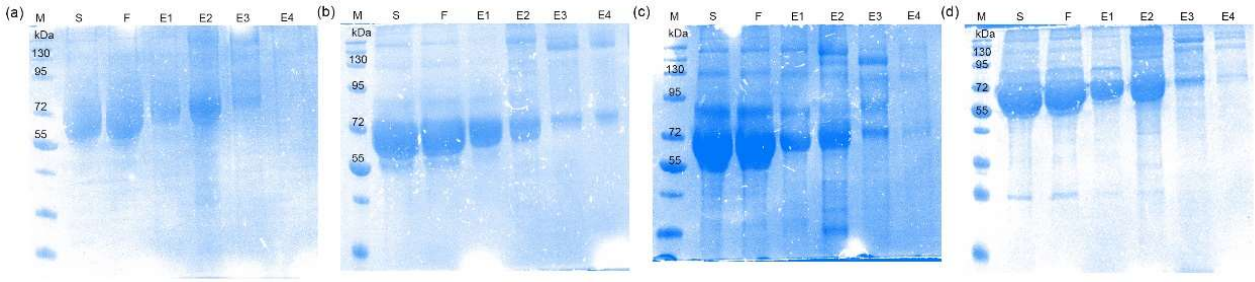

Supplementary Figure 2 Nbs anti-IgG-HRP fusion proteins enrichment. (a) Enrichment of Nb anti-mouse IgG1 Fab-HRP. (b) Enrichment of Nb anti-mouse IgG2a Fc-HRP. (c) Enrichment of Nb anti-mouse kappa chain-HRP. (d) Enrichment of Nb anti-rabbit IgG Fc-HRP. All fractions were collected during enrichment, after running SDS-PAGE, the gel was stained with Coomassie brilliant blue, then imaged by ChemiDoc XRS+ System. M: Blue prestained protein standard broad range (17-250 kDa). S: filtered supernatant. F: flowthrough. E1: protein eluted in 10 mM imidazole. E2: protein eluted in 40 mM imidazole. E3 and E4: protein eluted in 250 mM imidazole.

Supplementary Figure 3 The setting of TSA-based mIF on Axio Scan.Z1 slide scanner. ERα （yellow, 430 channel）, αSMA （green, 488 channel）, PR (orange, 546 channel), CD20 (red, 647 channel) and CD31 (magenta, 750 channel). ERα: estrogen receptor alpha; αSMA: alpha smooth muscle actin; PR: progesterone receptor.

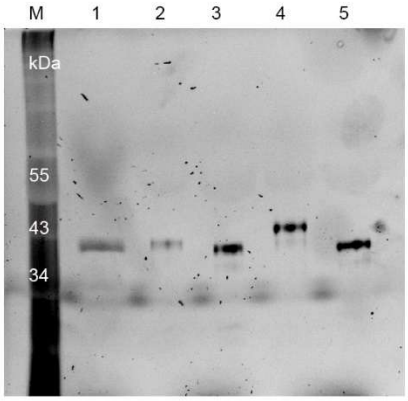

Supplementary Figure 4 The expression of Nbs anti-IgG-SNAP fusion proteins in the supernatant. The supernatants from transfected HEK293T cells of Nbs anti-IgG-SNAP were conjugated to SNAP-Surface® Alexa Fluor® 488 followed SDS-PAGE running. SDS gel was imaged by ChemiDoc XRS+ System. M: Blue prestained protein standard broad range (11-250 kDa). Lane1: The supernatant of Nb anti-mouse IgG1 Fab-SNAP. Lane 2: The supernatant of Nb anti-mouse IgG1 Fc-SNAP. Lane 3: The supernatant of Nb anti-mouse IgG2a Fc-SNAP. Lane 4: The supernatant of Nb anti-mouse kappa chain-SNAP. Lane 5: The supernatant of Nb anti-rabbit IgG Fc-SNAP.

Abbreviations

Ig	Immunoglobulin
Nb	Nanobody
BG	Benzylguanine
HRP	Horseradish peroxidase
WB	Western blot
TSA	Tyramide signal amplification
mIF	Multiplex immunofluorescence
ELISA	Enzyme-linked immunosorbent assay
IF	Immunofluorescence
ICC	Immunocytochemistry
IHC	Immunohistochemistry
IP	Immunoprecipitation
MW	Molecular weight
VH	Variable heavy chain
CH	Constant heavy chain
VL	Variable light chain
CL	Constant light chain
FAE	Fab-arm exchange
Fab	Fragment of antigen binding
Fc	Fragment crystallizable
CDR	Complementarity-determining region
FR	Frame region
mAb	Monoclonal antibody
pAb	Polyclonal antibody
HCAb	Heavy chain antibody
scFv	Single-chain variable fragment

Fv	Variable fragment
VHH	Variable domain of the heavy chain of heavy-chain antibody
IgNAR	Immunoglobulin new antigen receptor
PCR	Polymerase chain reaction
SPR	Surface plasmon resonance
PTM	Post-translational modification
CHO	Chinese hamster ovary
HEK	Human embryonic kidney
His	Histidine
IMAC	Immobilized metal affinity chromatography
FP	Fluorescent protein
GFP	Green fluorescent protein
POI	Protein of interest
NHS	N-hydroxysuccinimide
hAGT	Human repair protein *O*6-alkylguanine-DNA alkyltransferase
TMR	Tetramethylrhodamine
STED	Simulated emission depletion
FRET	Fluorescence resonance energy transfer
CARD	Catalytic reporter deposit
ABC	Avidin-biotin complex
FFPE	Formalin-fixed paraffin-embedded
TME	Tumor microenvironment
EGFR	Epidermal growth factor receptor
HER-2	Human epidermal growth factor receptor 2
PR	Progesterone receptor
ERα	Estrogen receptor alpha
GAPDH	Glyceraldehyde-3-phosphate
NG2	Nerve/glial-antigen 2

FOLR1	Folate receptor alpha
EpCAM	Epithelial cell adhesion molecule
CTNNB1	beta Catenin 1
ANK3	Ankyrin 3
αSMA	α Smooth Muscle Actin
FBS	Fetal calf serum
NEAA	Non-essential amino acids
SDS-PAGE	sodium dodecyl-sulfate polyacrylamide gel electrophoresis
BSA	Bovine serum albumin
PVDF	Polyvinylidene difluoride
DAPI	4’,6-Diamidino-2-phenylindole
HIER	Heat-induced epitope retrieval
IRES	Internal ribosome entry site
EGFP	Enhanced green fluorescent protein
CMV	Cytomegalovirus
IFA	Indirect immunofluorescence assay
cPPT/CST	Central polypurine tract and central termination sequence
RRE	Rev response element
AmpR	Ampicillin resistance
EmGFP	Emerald green fluorescent protein
LTR	Long terminal repeat
TME	Tumor microenvironment
TIME	Tumor immune microenvironment
TMA	Tissue microarray
HIER	Heat-induced epitope retrieval
cDNA	Complementary DNA

Publications

Sheng W, Zhang C, Mohiuddin T M, Al-Rawe M, Zeppernick F, Falcone FH, Meinhold-Heerlein I, Hussain AF. Multiplex immunofluorescence: a powerful tool in cancer immunotherapy[J]. **International Journal of Molecular Sciences**, 2023, 24(4): 3086.

Sheng W, Zhang C, Mohiuddin T M, l-Rawe M, Schmitz R, Niebert M, Konrad L, Wagner S, Zeppernick F, Meinhold-Heerlein I, Hussain AF. Development of SNAP-Tag Based Nanobodies as Secondary Antibody Mimics for Indirect Immunofluorescence Assays[J]. **Cells**, 2025, 14, 691.

Zhang C, **Sheng W,** Mohiuddin T M, Al-Rawe M, Schmitz R, Niebert M, Zeppernick F, Meinhold-Heerlein I, Hussain AF. A coiled coil-based pre-targeting drug delivery system for precise treatment of breast cancer[J]. **European Journal of Pharmaceutics and Biopharmaceutics**, 2025 Sep;214:114794.

Zhang C, **Sheng W**, Al-Rawe M, Mohiuddin TM, Niebert M, Zeppernick F, Meihold-Heerlein I, Hussain AF. EpCAM-and EGFR-specific antibody drug conjugates for triple-negative breast cancer treatment[J]. **International Journal of Molecular Sciences**, 2022, 23(11): 6122.

Mohiuddin T M, Zhang C, **Sheng W**, Al-Rawe M, Zeppernick F, Meinhold-Heerlein I, Hussain AF. Near infrared photoimmunotherapy: a review of recent progress and their target molecules for cancer therapy[J]. **International journal of molecular sciences**, 2023, 24(3): 2655.

Hussain A F, Grimm A, **Sheng W**, Zhang C, Al-Rawe M, Bräutigam K, Abu Mraheil M, Zeppernick F, Meinhold-Heerlein I. Toward homogenous antibody drug conjugates using enzyme-based conjugation approaches[J]. **Pharmaceuticals**, 2021, 14(4): 343.

Acknowledgement

From the bottom of my heart, I am truly grateful to these people who supported and guided me in Germany. Because of you, I felt a sense of warmth and belong here, and I will cherish these memories for the rest of my life.

First and foremost, I would like to express my sincere gratitude to my supervisor, Prof. Dr. Ivo Meinhold-Heerlein who offered me the precious opportunity to further my studies, for his valuable guidance and continuous encouragement throughout my reasearch. Along the same lines, I am also deeply thankful to Dr. Ahmad Fawzi Hussain, for his mentorship and generously passing on knowledge to me. His patient guidance has been instrumental in both my academic growth and personal development. I would also like to extend my gratitude to my co-supervisor, Prof. Dr. Franco Harald Falcone, for his constructive advice and support. His expertise and thoughtful insights have greatly contributed to the development of my research.

Furthermore, I am grateful to my colleagues and friends in our university. Thanks to Chaoyu, Mohiuddin, and all the colleagues, thank you for staying with me and helping me, whether it was overcoming challenges in experiments or difficulties in daily life. Thanks to Taoli, Xuesong and Yuxi, you have brought optimism and energy to me.

Finally, special thanks go to my family, whose steadfast love and support have been my greatest source of strength. Even though we are thousands of miles apart, the familial affection has always been with me and a constant motivation throughout these years, and it can last a lifetime.

This thesis represents not only my academic endeavor but also the collective efforts of those who supported me along the way and helped me achieve my medical dream, they are precious gifts that life has given me.